

**SISSA**

Scuola  
Internazionale  
Superiore di  
Studi Avanzati

Neuroscience Area – PhD course in  
Joint PhD Program in Molecular Biology

# Glycopeptide analysis of different prion strains

Candidate:  
Natali Nakić

Advisor:  
Prof. Giuseppe Legname  
Co-advisor:  
Prof. Gordan Lauc

Academic Year 2019-2020





Neuroscience Area – PhD course in  
Joint PhD Program in Molecular Biology

# Glycopeptide analysis of different prion strains

Candidate:  
Natali Nakić

Advisor:  
Prof. Giuseppe Legname  
Co-advisor:  
Prof. Gordan Lauc

Academic Year 2019-2020



---

## Abstract

Prion diseases or transmissible spongiform encephalopathies (TSEs) are a group of infectious neurodegenerative diseases. They are caused by a conformational change of the cellular prion protein (PrP<sup>C</sup>) to the misfolded form (PrP<sup>Sc</sup>). TSEs differ from one another in incubation time, clinical signs, and biochemical properties. These differences are a result of multiple conformationally different PrP<sup>Sc</sup> states, called strains. One of the main ways to characterize strains is by immunoblotting, since each strain has a specific pattern where different glycoforms can be distinguished. This is due to the fact the prion protein has two N-glycosylation sites, however, the knowledge regarding exact N-glycan structures on different prion strains has not been researched so far. The phenomenon of prion strains still remains to be explained; therefore, the aim of this study was to, for the first time, differentiate individual N-glycan structures on different glycosylation sites.

The first part of the project included optimization of the protocol for isolation of large-scale PrP<sup>Sc</sup>. Isolation of the prion protein was shown to be somewhat challenging. Two different approaches were tested, immunopurification and the density medium approach. After performing all of the experiments, the prion protein was successfully isolated from sheep brain tissue, infected with three different prion strains, by using the density medium approach. To analyze the glycan structures, site-specific analysis was performed. The isolated PrP<sup>Sc</sup> was loaded on SDS-PAGE, and after staining the gel with Coomassie, the bands corresponding to PrP<sup>Sc</sup> glycoforms were cut from it and the protein was digested with trypsin. A mixture of peptides and glycopeptides was obtained. To minimize suppression of glycopeptide ionization, an enrichment procedure was performed. Tryptic digests before and after the enrichment procedure were analyzed using reverse phase liquid chromatography coupled with electrospray mass spectrometry (LC-ESI-MS).

Glycan structures detected on sheep PrP<sup>Sc</sup> were identified as “brain-specific” N-glycans, which are usually rich in sialic acid, fucose residues, and have the presence of bisecting *N*-acetylglucosamine (GlcNAc). The analysis on different strains showed that there are no major differences in the glycan composition, leading to the conclusion that the N-glycan composition does not contribute to prion strain diversities, but rather that the differences come from the protein’s conformation, therefore confirming the “protein-only” hypothesis.



---

## List of abbreviations

2-AB:	2-aminobenzamide
4R $\beta$ S:	4-rung $\beta$ -solenoid
$\alpha$ -syn:	$\alpha$ -synuclein protein
A $\beta$ :	amyloid- $\beta$ protein
ACN:	acetonitrile
AD:	Alzheimer's disease
ALS:	amyotrophic lateral sclerosis
Asn:	asparagine
Asp:	aspartic acid
BCA:	bicinchoninic acid
BH:	brain homogenate
BPC:	base peak chromatogram
CDG:	congenital disorders of glycosylation
CE:	capillary electrophoresis
CHO:	Chinese Hamster Ovary
CJD:	Creutzfeldt-Jakob disease
CNS:	central nervous system
CWD:	chronic wasting disease
DMEM:	Dulbecco's Modified Eagle Medium
Dol:	dolichol
DTT:	dithiothreitol
EDEM:	ER degradation-enhancing $\alpha$ -mannosidase I-like
EIC:	extracted ion chromatogram
EM:	electron microscopy
Endo H:	endoglycosidase H
ER:	endoplasmic reticulum
ESI-MS:	electrospray ionization-mass spectrometry
FBS:	fetal bovine serum
FFI:	fatal familial insomnia
FTIR:	Fourier transform infrared spectroscopy
Fuc:	fucose
GAG:	glycosaminoglycan
Gal:	galactose
GalNAc:	<i>N</i> -acetylgalactosamine
GBP:	glycan-binding protein
GDP:	guanosine-5'-diphosphate
Glc:	glucose
GlcNAc:	<i>N</i> -acetylglucosamine
GlcNAc-TI:	<i>N</i> -acetylglucosaminyltransferase I
GPI:	glycosylphosphatidylinositol
GSS:	Gerstmann-Sträussler-Scheinker
GT1:	mouse hypothalamic cell line
HD:	Huntington's diseases
Hex:	hexose

---

HexNAc:	<i>N</i> -acetylhexoseamine
HILIC:	hydrophilic interaction liquid chromatography
HPLC:	high-pressure liquid chromatography
HRP:	horseradish peroxidase
i:	iatrogenic
IAA:	iodoacetamide
LacNAc:	<i>N</i> -acetylactosamine
LC-MS:	liquid chromatography-mass spectrometry
mAb:	monoclonal antibody
MALDI:	matrix-assisted laser desorption ionization
Man:	mannose
MEM:	Minimal Essential Medium
Mo:	mouse
MS:	mass spectrometry
N2a:	mouse neuroblastoma cell line
NEAA:	non-essential amino acids
NeuAc:	<i>N</i> -acetylneuraminic acid
NeuGc:	<i>N</i> -glycolylneuraminic acid
NFTs:	neurofibrillary tangles
NMDA:	<i>N</i> -methyl-D-aspartate
NMR:	nuclear magnetic resonance
OR:	octapeptide-repeat region
OST:	oligosaccharyltransferase
P:	phosphate
PA:	2-aminopyridine
PBS:	phosphate-buffered saline
PD:	Parkinson's disease
PIRBS:	parallel in-register $\beta$ -sheet
PK:	proteinase K
PMCA:	protein misfolding cyclic amplification
PMSF:	phenylmethylsulphonyl fluoride
PNGase A:	peptide-N-glycosidase A
PNGase F:	peptide-N-glycosidase F
PNS:	peripheral nervous system
<i>Prnp</i> :	prion protein gene in non-human species
PrP:	prion protein
PrP <sup>C</sup> :	physiological cellular form of PrP
PrP <sup>Sc</sup> :	misfolded, pathogenic form of the prion protein
C <sup>tmp</sup> PrP:	C-terminal transmembrane PrP form
N <sup>tmp</sup> PrP:	N-terminal transmembrane PrP form
PTA:	sodium phosphotungstic acid
PTM:	post-translational modification
recPrP:	recombinant prion protein
RML:	Rocky Mountain Laboratory
RT:	room temperature
RT-QuIC:	real-time quaking induced conversion
s:	sporadic
SAMP:	self-associated molecular pattern



---

ScGT1:	mouse hypothalamic cell line chronically infected with PrP <sup>Sc</sup>
ScN2a:	mouse neuroblastoma cell line chronically infected with PrP <sup>Sc</sup>
SDS:	sodium dodecyl sulfate
SDS-PAGE:	sodium dodecyl sulfate-polyacrylamide gel electrophoresis
SN:	supernatant
SOD-1:	Superoxide dismutase
TDP-43:	TAR DNA-binding protein 43
TFA:	trifluoroacetic acid
TME:	transmissible mink encephalopathy
TSEs:	transmissible spongiform encephalopathies
UDP:	uridine-5'-diphosphate
UPLC:	ultra-performance liquid chromatography
v:	variant
WHO:	world health organization
WT:	wild type



## Table of Contents

<b>Abstract</b> .....	<b>5</b>
<b>List of abbreviations</b> .....	<b>7</b>
<b>1 INTRODUCTION</b> .....	<b>15</b>
1.1 Neurodegenerative diseases .....	15
1.1.1 Prion diseases .....	16
1.1.1.1 Scrapie .....	17
1.2 The prion protein (PrP) .....	18
1.2.1 Structure and biosynthesis of the ovine cellular prion protein (ovPrP <sup>C</sup> ).....	18
1.2.2 Trafficking and processing of PrP <sup>C</sup> .....	20
1.2.3 Functions of PrP <sup>C</sup> .....	21
1.3 The scrapie prion protein (PrP <sup>Sc</sup> ) .....	22
1.3.1 The “protein-only” hypothesis .....	23
1.3.2 Prion strains and the species barrier.....	25
1.4 Glycosylation of proteins .....	27
1.4.1 Functions of glycosylation.....	28
1.4.2 Types of glycosylation .....	29
1.5 N-linked glycosylation.....	29
1.5.1 Structure and diversity of N-linked glycans .....	29
1.5.2 Biosynthesis of N-linked glycans .....	31
1.5.2.1 Initial synthesis and processing of N-glycans in the ER .....	32
1.5.2.2 Processing and final maturation of N-glycans in the Golgi complex.....	33
1.5.3 Methods for analyzing N-linked glycans .....	35
1.6 Glycosylation of the prion protein and prion infection.....	37
1.6.1 Prion protein sialylation.....	38
1.7 Aims of the research .....	39
<b>2 MATERIALS AND METHODS</b> .....	<b>41</b>
2.1 Samples used for PrP isolation .....	41
2.1.1 Cell lines .....	41
2.1.2 Mice brains.....	41

---

2.1.3	PMCA material .....	42
2.1.4	Sheep brains .....	42
2.2	Protocols used for PrP <sup>Sc</sup> isolation and purification.....	42
2.2.1	Sodium phosphotungstic acid (PTA) precipitation.....	42
2.2.2	PK digestion.....	43
2.2.3	Thermolysin digestion .....	43
2.2.4	Use of a density medium (iodixanol).....	43
2.2.5	Immunopurification .....	44
2.2.5.1	Incubation of mAb with the protein .....	44
2.2.5.2	Pre-immobilizing mAb to Protein G beads .....	45
2.3	Detection of PrP <sup>Sc</sup> .....	45
2.3.1	SDS polyacrylamide gel electrophoresis (SDS-PAGE) .....	45
2.3.2	Coomassie staining of gels.....	46
2.3.3	Silver staining of gels.....	46
2.3.4	Western blot .....	46
2.4	Isolation and purification of PrP <sup>Sc</sup> glycopeptides .....	47
2.4.1	In-gel trypsin digestion .....	47
2.4.1.1	Excising PrP <sup>Sc</sup> bands from Coomassie stained gels .....	47
2.4.1.2	Reduction and alkylation of PrP <sup>Sc</sup> .....	47
2.4.1.3	Destaining gel pieces from Coomassie stained gels .....	47
2.4.1.4	Trypsin digestion .....	48
2.4.1.5	Extraction and drying of glycopeptide digests .....	48
2.4.2	In-solution trypsin digestion .....	48
2.4.3	Glycopeptide HILIC enrichment .....	49
2.5	Glycopeptide detection and analysis.....	49
2.5.1	LC-MS/MS analysis of PrP <sup>Sc</sup> glycopeptides from sheep brains .....	49
2.5.2	Data processing.....	50
2.5.2.1	Analysis at the proteomic level .....	50
2.5.2.2	Analysis at the glycopeptide level.....	50

---

<b>3</b>	<b>RESULTS .....</b>	<b>52</b>
3.1	Analysis of MoPrP <sup>Sc</sup> .....	52
3.1.1	Optimizing isolation protocol of MoPrP <sup>Sc</sup> .....	52
3.1.1.1	Initial testing with cell lines.....	52
3.1.1.2	Using PMCA amplified material .....	55
3.1.1.3	Protocols based on the use of density medium approach .....	58
3.2	Optimizing isolation protocol of ovPrP <sup>Sc</sup> .....	63
3.2.1	Immunopurification approach.....	64
3.2.2	Use of a density medium approach.....	70
3.3	LC-MS/MS analysis of different ovPrP <sup>Sc</sup> strains.....	73
3.3.1	Analysis of N-184 glycosylation site.....	75
3.3.1.1	Quantitative analysis of N-184 glycosylation site from different prion strains ..	82
3.3.2	Analysis of N-200 glycosylation site.....	86
3.3.2.1	Quantitative analysis of N-200 glycosylation site from different prion strains ..	95
<b>4</b>	<b>DISCUSSION .....</b>	<b>100</b>
4.1	Developing a protocol for large-scale isolation and purification of PrP <sup>Sc</sup> .....	100
4.2	Determining the glycan composition of different prion strains .....	102
	<b>BIBLIOGRAPHY .....</b>	<b>107</b>



---

# CHAPTER I

## 1 INTRODUCTION

### 1.1 Neurodegenerative diseases

Neurodegenerative diseases represent a major threat to human health and their prevalence has been increasing in recent years. Some of the examples of neurodegenerative diseases include Alzheimer's disease (AD), Parkinson's disease (PD), Huntington's disease (HD), amyotrophic lateral sclerosis (ALS), frontotemporal dementia and transmissible spongiform encephalopathies (TSEs) [1].

These diseases have a wide range of symptoms, causing disruptions in cognitive, social and emotional behavior. Developing effective treatments is desperately needed but quite challenging, since molecular mechanisms involved in neurodegeneration are not completely known. They involve multiple processes operating simultaneously in the brain, including spongiform degeneration, synaptic alterations, brain inflammation, neuronal death and the accumulation of protein aggregates, which are the result of abnormalities in protein processing of one or more specific neuronal proteins. The mechanism of abnormal processing can involve misfolding of a protein, altered post-translational modifications of newly synthesized proteins, abnormal proteolytic cleavage or diminished clearance of degraded proteins [2, 3]. Different neurodegenerative diseases are caused by aggregation of one or more distinct proteins: amyloid- $\beta$  ( $A\beta$ ) and tau as neurofibrillary tangles (NFTs) in AD [4, 5],  $\alpha$ -synuclein ( $\alpha$ -syn) in PD [6], huntingtin in HD [7], Cu/Zn superoxide dismutase (SOD1) and TAR DNA-binding protein 43 (TDP-43) in ALS [8, 9], prions (PrP<sup>Sc</sup>) in TSEs [10], and others.

Of all the studies on neurodegenerative diseases agents, the discovery of prions has led to the most unexpected findings and served as a model for explaining the pathogenesis of many other neurodegenerative diseases. The concept that a protein can act as an infectious agent and cause

degeneration in the central nervous system was accepted in the 1980s with the research of Stanley B. Prusiner [1, 10].

Neurodegenerative diseases represent a fast-growing group of disorders and the World Health Organization (WHO) states that today's 44 million cases will only continue to increase and could even become the second most common cause of death, right after cardiovascular diseases [11]. Even though prion diseases occur at a low rate, affecting approximately 3–6 people per million annually, they represent a prototype of different proteinopathies, thus it is important to focus on finding an answer these types of disorders impose [12].

### **1.1.1 Prion diseases**

Prion diseases are also known as transmissible spongiform encephalopathies (TSEs) and they represent a group of infectious and fatal neurodegenerative diseases. The first prion disease described, back in the 18<sup>th</sup> century, was scrapie in sheep, but it was not until the 1930s that it was defined as a transmissible disease. The following decades discovered some unusual properties of the causative agent, such as resistance to inactivation by heat and ionizing radiation, which led scientists to believe no nucleic acids were present, or that it was, which was believed for a long time, a “slow virus” [13].

Prion diseases affect humans and various animal species. They can be sporadic (85%), genetic (10–15%) or acquired by infection (less than 1%) [14]; in humans they include kuru [15], Creutzfeldt-Jakob disease (CJD) [16], Gerstmann-Sträussler-Scheinker syndrome (GSS) [17] and fatal familial insomnia [18]. In animals they include bovine spongiform encephalopathy (BSE) in cattle [19], scrapie in sheep and goats [20], chronic wasting disease (CWD) in cervids [21] and transmissible mink encephalopathy (TME) [22]. Neuropathological features of prion diseases include spongiform change, neuronal loss and gliosis (of both astroglia and microglia). Incubation times and clinical symptoms are quite heterogeneous within different syndromes. However, one thing is common for all prion diseases, after the onset of clinical signs, the progression of the diseases is fast, inevitably causing death [3].

Prion diseases are usually definitely confirmed by post-mortem histopathological brain tissue analysis or brain biopsy, since currently there is no standard diagnostic tool to diagnose them pre-symptomatically. Nowadays, assays for detecting prions are being improved, one of the most



---

important ones being real-time quaking induced conversion (RT-QuIC) which has had a considerable impact in diagnosing prion diseases clinically [23-25].

It is of great importance to overcome the difficulty of diagnosing prion diseases, in order to develop appropriate treatments. Ever since the discovery of TSEs, a lot of effort has been put into curing or at least modifying the course of the diseases, unfortunately so far without success. There is still a lot of work to be done, and understanding the basics, like the structure of the prion protein and the molecular mechanism behind the disease, are fundamental in the fight against these disorders [26].

#### ***1.1.1.1 Scrapie***

Scrapie is considered a prototype of the TSEs, as it was the first one described and the first to be shown as both infectious and transmissible. The name scrapie derives from a common clinical sign of the disease, where animals compulsively scrape off their fleece against fences and other objects [27].

Several polymorphisms in the gene encoding for the sheep prion protein (*Prnp*) have been associated to scrapie susceptibility. Polymorphisms at codons 136, 154, and 171 are significant in determining resistance or susceptibility to scrapie. The polymorphisms V<sub>136</sub>R<sub>154</sub>Q<sub>171</sub> and A<sub>136</sub>R<sub>154</sub>Q<sub>171</sub> are correlated with a higher susceptibility to scrapie; whereas A<sub>136</sub>R<sub>154</sub>R<sub>171</sub> and A<sub>136</sub>H<sub>154</sub>Q<sub>171</sub> are associated with resistance to scrapie [27, 28], even though some cases of scrapie with the latter one have been reported [29].

Scrapie occurs naturally in sheep and emerges in two forms, classical and atypical. Atypical scrapie was first described in 1998, Norway and since then has been identified in other countries. It appears mainly in older sheep and interestingly, with genotypes ARR/ARR, resistant to classical scrapie [30, 31]. These two forms differ in their clinical symptoms; however, confirmation of the diseases is challenging since the same symptoms can occur also in other conditions. Therefore, clinical diagnosis should be validated together with neuropathological and biochemical analysis [32].

Even though there is still no strong evidence for zoonotic risk of scrapie in humans, studies have shown that classical scrapie can be directly transmitted to cynomolgus macaques, an important model for human prion disease [33, 34], but also in transgenic mice overexpressing human PrP [35]. Additional experimental studies should be performed in order to fully understand the potential risk of scrapie for public health.

---

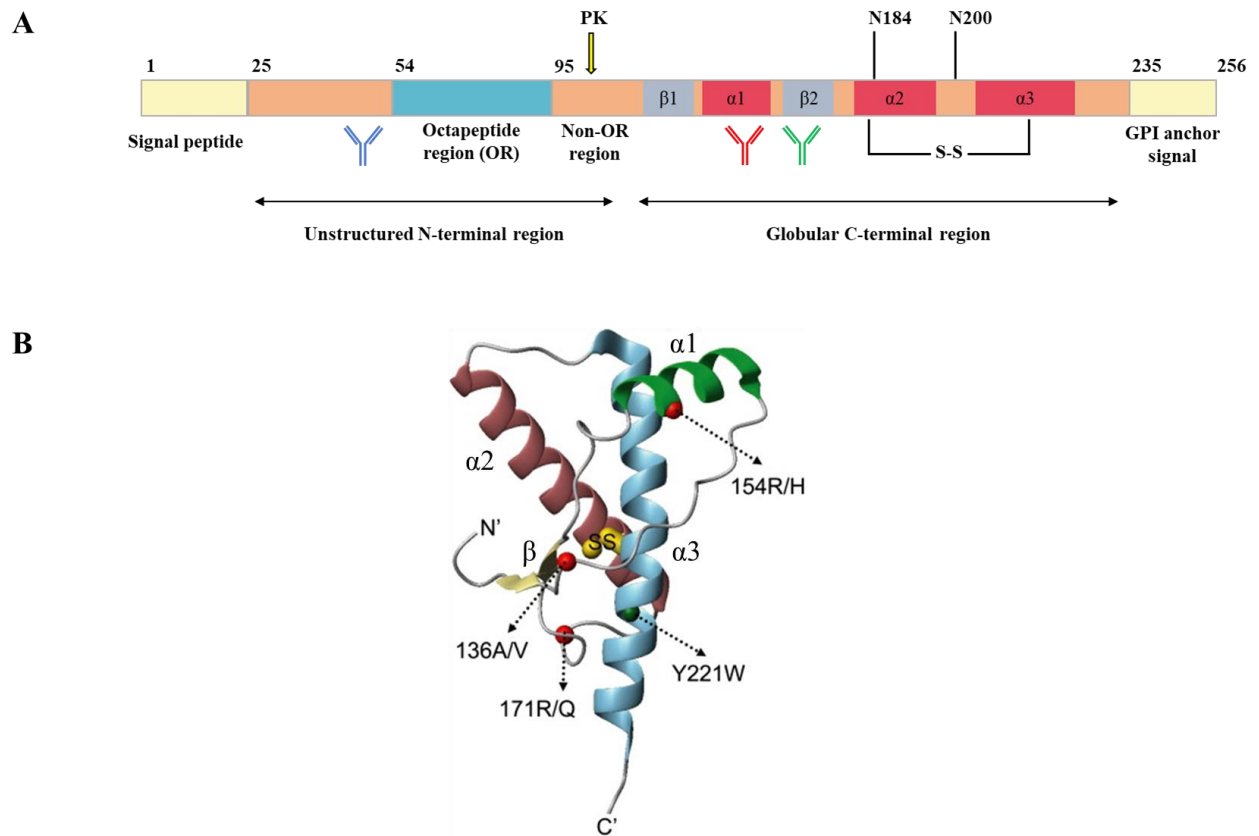
## 1.2 The prion protein (PrP)

The term prion was proposed in 1982 by Stanley B. Prusiner, an acronym that stands for “proteinaceous infectious particle” [10]. The prion protein exists in multiple forms, mainly the physiological form (PrP<sup>C</sup>) and the pathogenic form (PrP<sup>Sc</sup>). It has high expression levels in the central nervous system (CNS), however, it can also be found in other peripheral tissues [36]. The expression of PrP<sup>C</sup> differs from cell to cell and also in different brain regions [37].

### 1.2.1 Structure and biosynthesis of the ovine cellular prion protein (ovPrP<sup>C</sup>)

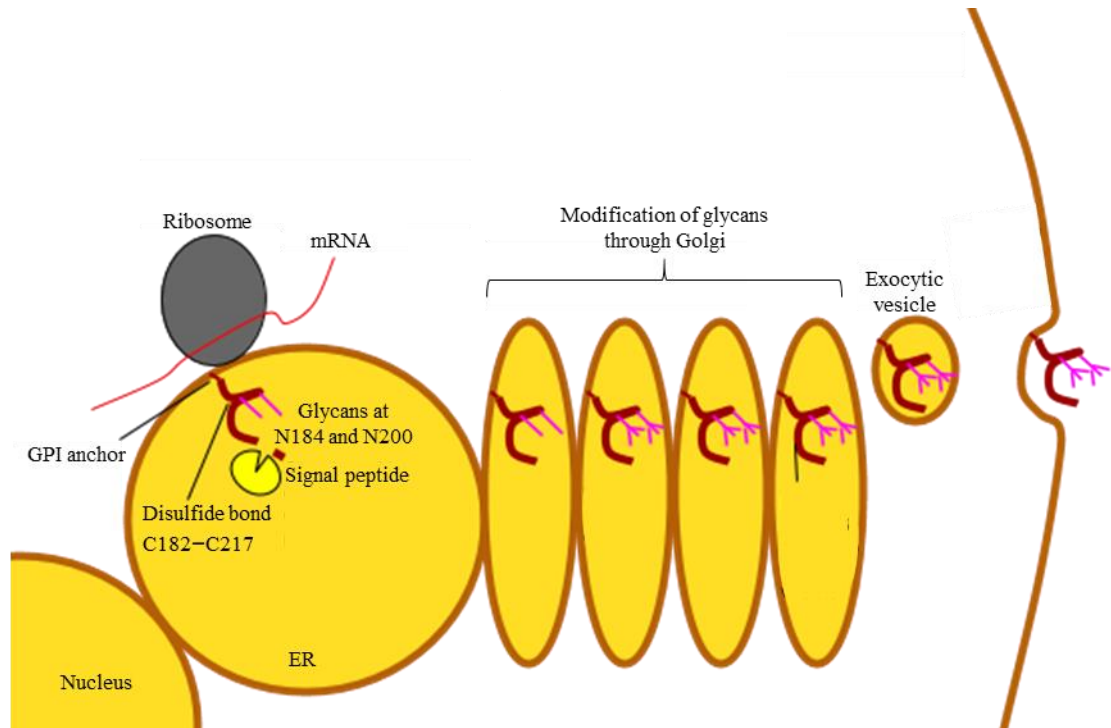
The *Prnp* gene in sheep encodes for the cellular prion protein (ovPrP<sup>C</sup>), which is 256 amino acids long. It is composed of an unstructured N-terminal domain (25–120) which contains the evolutionary conserved octapeptide region (OR) that binds copper, followed by a non-octapeptide region (non-OR) and a globular C-terminal domain (126–234), that has a defined structure. It is consisted of a short two-stranded antiparallel  $\beta$ -sheet, three  $\alpha$ -helices, and a disulfide bond (C182–C217) linking  $\alpha$ 2 and  $\alpha$ 3 helices. The globular domain contains two N-glycosylation sites at asparagine residues 184 and 200 (**Figure 1**) [38]. Structural analysis of PrP<sup>C</sup> was performed on the bacterially expressed PrP and even though this recombinant PrP (recPrP) is not submitted to post-translational modifications, from a structural point of view it is equivalent to the physiological form of PrP<sup>C</sup>.

The primary signal that regulates trafficking of PrP<sup>C</sup> is the signal peptide, composed of 24 amino acid residues (1–24). It causes a co-translational translocation of the complex mRNA and ribosome to the endoplasmic reticulum (ER). After the cleavage of the signal peptide, the prion protein is further translated directly to the ER. N-linked glycans can be co-translationally added to the protein at two asparagine residues (N-184 and N-200), leading to the existence of the di-, mono- and unglycosylated forms of PrP (two, one or none of the glycosylation sites are occupied). The last 22 amino acid residues at the C-terminus are also cleaved off and replaced by a glycosylphosphatidylinositol (GPI) anchor, which attaches the prion protein to the plasma membrane [39]. PrP<sup>C</sup> is then transported to the Golgi where the glycans are further modified and matured, leading to complex and heterogeneous structures and at this point, the protein is considered mature (**Figure 2**) [40].



**Figure 1.** Structure of sheep PrP<sup>C</sup>. Schematic illustration of primary PrP<sup>C</sup> structure. The unprocessed form contains the signal peptide (1–25), octapeptide region (OR, 54–95), two short  $\beta$ -strands and three  $\alpha$ -helices and a GPI anchor signal at the C-terminus. The approximate PK cutting site is marked with an arrow and the epitopes recognized by antibodies used in this thesis are shown, EF2 (in blue), SAF 61 (in red) and SAF 84 (in green) (A). Secondary structure of the globular domain of PrP<sup>C</sup> (B). Modified from [41].

PrP<sup>C</sup> can exist in three different topological forms. The majority is secreted to the cell surface by the exocytic pathway where it remains attached with the GPI anchor, but it can also adopt two transmembrane forms, where the central hydrophobic region is integrated into the membrane. The N<sup>tm</sup>PrP integrates into the membrane with the N-terminus located into the ER lumen and the C-terminus remains in the cytosol, while the C<sup>tm</sup>PrP integrates in the opposite direction [42].



**Figure 2.** Schematic of the biosynthesis of sheep PrP<sup>C</sup>. Modified from [43].

### 1.2.2 Trafficking and processing of PrP<sup>C</sup>

After transporting PrP<sup>C</sup> to the cell surface, the protein can be submitted to cycles of endocytosis. The process is quite complex and has been explained by clathrin-dependent and independent pathways. Before entering the clathrin-dependent endocytic pathway, PrP<sup>C</sup> leaves the lipid rafts to the non-raft membranes, from where it goes to coated pits. It has been suggested that basic residues KKRPKP in the N-terminal domain are important for the clathrin-mediated endocytosis [44]. This type of endocytosis is surprising for a GPI anchored protein, since PrP<sup>C</sup> lacks amino acid residues responsible for interacting with proteins necessary for clathrin-dependent endocytosis. However, this is enabled because of the copper binding in the OR region [45].

It has been shown in CHO (Chinese Hamster Ovary) cells that PrP<sup>C</sup> is internalized by caveolae, one of the most common clathrin-independent endocytosis pathways [46]. Since nonneuronal cells were used, the question remains whether this can be applied for PrP<sup>C</sup> trafficking in neurons.

During the cycling of PrP<sup>C</sup> between the endocytic compartment and the plasma membrane, a fraction of the protein is subjected to proteolytic cleavage through PrP processing. Three main types of cleavage are named  $\alpha$ -cleavage,  $\beta$ -cleavage and ectodomain shedding. The  $\alpha$ -cleavage leads to the creation of N1 and C1 fragments;  $\beta$ -cleavage of N2 and C2 while the shedding results in the release of an almost full-length PrP from the cell surface. Research shows that proteolytic cleavage of PrP could have a role in the pathology of prion diseases [47].

### 1.2.3 Functions of PrP<sup>C</sup>

Since establishing the connection between prion diseases and PrP<sup>C</sup>, the prion protein has been extensively studied and the goal has been to fully understand the biological functions of the prion protein. Even though the function is still not clear, many efforts have been made towards this.

PrP<sup>C</sup> is highly expressed in the CNS where it is involved in many processes, such as synaptic transmission and plasticity [48], memory formation [49], neurite outgrowth [50, 51], neuroprotection [52] and myelin maintenance [53]. The amount of PrP is different from cell to cell and from one brain region to the other, however, it has been revealed that it is mostly localized in the synaptic region [54]. It has also been shown that PrP from astrocytes promotes neuronal differentiation and survival [55], has a protective role under oxidative stress [56], and has an effect on lactate metabolism [57].

The neuronal functions of PrP<sup>C</sup> are related to its ability to bind divalent cations, such as Cu<sup>2+</sup> [58], Fe<sup>2+</sup> [59] and Zn<sup>2+</sup> [60] in the N-terminal domain. The highest affinity is, however, for copper binding, both in the OR region and the non-OR region. Although it was long thought that copper binding in general is not directly involved in prion infectivity (because it appears to be so for the OR region), it has been shown that the non-OR region could be related to prion conversion [61].

The neuroprotective role of PrP<sup>C</sup> has been established through modulation of *N*-methyl-D-aspartate (NMDA) receptors. By binding copper to PrP<sup>C</sup>, S-nitrosylation of NMDA receptors is promoted, inhibiting the ion channel and limiting its excessive activity. It has been suggested that this mechanism is possibly not active in prion diseases, which then leads to neuronal death [62].

### 1.3 The scrapie prion protein (PrP<sup>Sc</sup>)

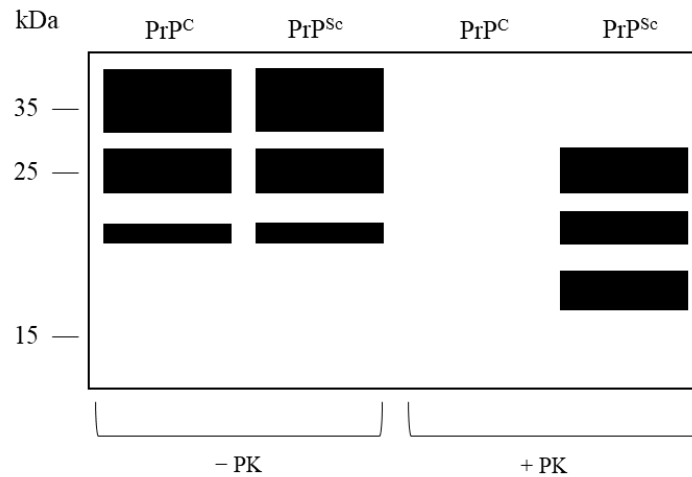
The scrapie prion protein (PrP<sup>Sc</sup>) is the pathological form of the prion protein. It shares the same primary amino acid sequence as PrP<sup>C</sup> however, they differ in their secondary structure. Over the years many information have emerged regarding PrP<sup>C</sup> structure, confirming its composition of 45% of  $\alpha$ -helices and only few  $\beta$ -sheets. Difficulties concerning the structure of PrP<sup>Sc</sup> remain to be solved, mainly because of its insolubility and the tendency to aggregate. However, by using techniques such as circular dichroism and Fourier transform infrared spectroscopy (FTIR), the increased proportion of  $\beta$ -sheets in PrP<sup>Sc</sup> has been confirmed, in contrast to PrP<sup>C</sup> [63]. Several models of PrP<sup>Sc</sup> structure have been suggested, such as  $\beta$ -spiral model [64],  $\beta$ -helix model [65], and parallel in-register  $\beta$ -sheet (PIRBS) model [66], shown to be the model corresponding to most of other misfolding proteins [67]. Recent X-ray diffraction studies and cryo-electron microscopy have actually indicated the structure to be in agreement with the 4-rung  $\beta$ -solenoid (4R $\beta$ S) model [68].

**Table 1.** Characteristics and differences between PrP<sup>C</sup> and PrP<sup>Sc</sup>.

<b>PrP<sup>C</sup></b>	<b>PrP<sup>Sc</sup></b>
Monomer	Forms aggregates
Attached to the cell surface	Intra- or extracellular located
Soluble	Insoluble
PK sensitive	Partially PK resistant
Mostly $\alpha$ -helices	Mostly $\beta$ -sheets
Non-infectious	Infectious

Other main differences are listed in **Table 1**. Unlike PrP<sup>C</sup>, which is a monomeric protein, PrP<sup>Sc</sup> tends to form aggregates, causing neuronal apoptosis and brain vacuolation within the CNS, and eventually causing death. Because of the high content of  $\beta$ -sheets, PrP<sup>Sc</sup> is partially resistant to proteinase K (PK), leaving a PK-resistant core, noted PrP<sup>27-30</sup>, leading to the formation of amyloid fibrils. This biochemical feature is the most common way in which PrP<sup>C</sup> and PrP<sup>Sc</sup> are distinguished. By digesting an uninfected and infected sample with PK and performing an immunoblot, there is a

clear difference in these two samples. PrP<sup>C</sup> is completely degraded, while for PrP<sup>Sc</sup> samples there is a shift towards lower molecular weight because of the N-terminus cleavage of the prion protein. The Western blot of PrP<sup>Sc</sup> is characterized by a typical three-band pattern, corresponding to different site occupancies of the prion protein (di-, mono- and unglycosylated, listed from highest molecular weight to lowest) (**Figure 3**) [69].



**Figure 3.** Schematic of an immunoblot of PrP<sup>C</sup> and PrP<sup>Sc</sup> without or with PK treatment.

Even though this technique has been widely used and accepted as a way of characterizing prions, it has become apparent that some PrP<sup>Sc</sup> forms are sensitive to PK digestion [70-72]. Therefore, it is necessary to develop new diagnostic tools in order to detect these prion forms. Digestion by thermolysin has been proven as an alternative enzymatic digestion. Thermolysin, as PK, completely digests PrP<sup>C</sup>, but interestingly, leaves both the PK-sensitive and resistant PrP<sup>Sc</sup> in their full-length form. The fact that the N-terminal domain of PrP<sup>Sc</sup> is left intact allows for possible improvements in diagnosis of prion diseases or strain definition [73, 74].

### 1.3.1 The “protein-only” hypothesis

The main event of prion diseases is the conversion of PrP<sup>C</sup> to PrP<sup>Sc</sup>. It was long believed that prion diseases were caused by parasites or viruses. It was first proposed by Griffith [75], that the agent causing the disease could be a self-replicating protein. Prusiner later proposed, what is today the most widely accepted model, although still controversial, the “protein-only” hypothesis. It states that

---

the prion protein can replicate without nucleic acids and that it is the main, and possibly only, agent causing prion diseases [76].

To this date, many evidences strongly support this hypothesis. It has been demonstrated, since linking familial cases of TSE with mutations in the gene encoding for PrP, how a genetic disorder propagates in an infectious manner [77]. Also, by discovering that both PrP<sup>C</sup> and PrP<sup>Sc</sup> are encoded by the same gene and as no differences were found between their mRNAs and the primary amino acid sequence, it was an indication that the difference could be due to conformation [78]. Further strong evidence was the fact that PrP<sup>C</sup> knockout (KO) transgenic mice were resistant to prion infection, showing that the prion protein is necessary for the disease to occur [79]. An important finding was also the ability to maintain infectivity in mouse neuroblastoma cell line (N2a) after chronically infecting them with brain homogenate containing PrP<sup>Sc</sup> [80].

The final proof for this hypothesis was the production of synthetic prions in 2004. Misfolding of recombinant mouse prion protein (recMoPrP) was succeeded *in vitro*, after which transgenic mice were inoculated intracerebrally with the formed amyloid fibrils. Followed by a long incubation time, the mice developed clinical signs of the disease and the presence of prions was confirmed by Western blot. Prions from brain homogenates from these animals were further transmitted to both wild type (WT) and transgenic mice; PrP<sup>Sc</sup> was found also in their brains [81]. Synthetic prions can also be generated in large quantities *in vitro* by performing protein misfolding cyclic amplification (PMCA). PMCA is a method in which brain homogenates from healthy animals are mixed with a seed (containing PrP<sup>Sc</sup>), causing the conversion of PrP<sup>C</sup> to PrP<sup>Sc</sup> and the formation of aggregates, which are then broken up into smaller fragments by rounds of sonication cycles. The smaller fragments act as seeds that continue the conversion and synthesis of new PrP<sup>Sc</sup> molecules [82]. The fact that there is cell-free conversion of PrP<sup>C</sup> to PrP<sup>Sc</sup>, proves that synthetic prions are able to cause the disease and therefore support the given hypothesis [83].

There are two different models explaining the conversion of PrP<sup>C</sup> to PrP<sup>Sc</sup> (**Figure 4**):

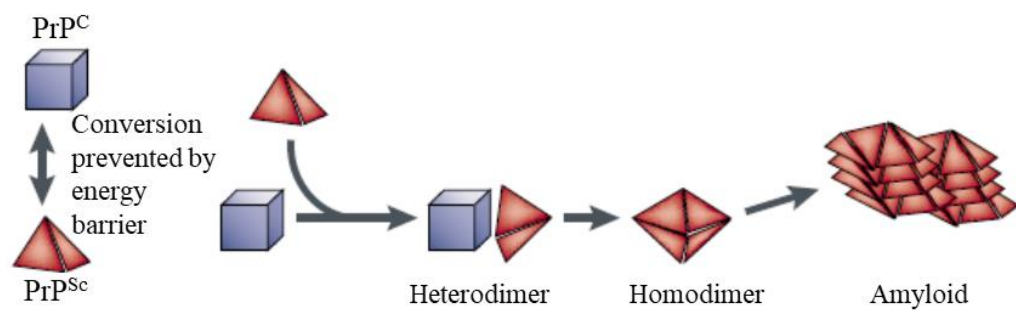
- The template-assisted conversion model was proposed by Stanley B. Prusiner [76]. It states that the conversion is not spontaneous, since it is prevented by an energy barrier. However, a direct interaction of PrP<sup>Sc</sup> with PrP<sup>C</sup> leads to a formation of a heterodimer, which assists the conformational change of PrP<sup>C</sup>. At this point, there are two molecules that can serve as a template for the next PrP<sup>C</sup> molecule, leading to an exponential growth of PrP<sup>Sc</sup> molecules



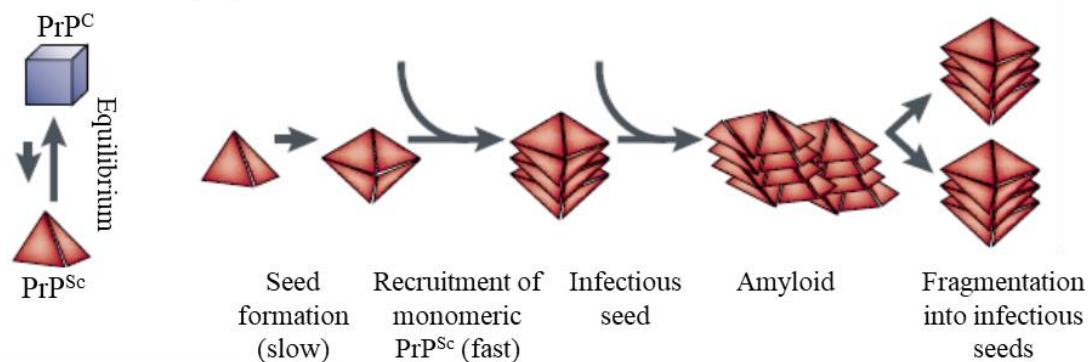
and the formation of amyloid fibrils. It has also been proposed that an intermediate structure ( $\text{PrP}^*$ ) of the conversion could exist, however, its presence has not been proven yet [84].

- The nucleation-polymerization model was proposed by Jarret and Lansbury [85]. It states that even though  $\text{PrP}^{\text{Sc}}$  and  $\text{PrP}^{\text{C}}$  are in equilibrium,  $\text{PrP}^{\text{C}}$  is the favored form. The formation of the seed is thermodynamically an unfavorable process and a rate determining step in this mechanism. However, after formation of the nucleus, the fast step is the recruitment of more and more  $\text{PrP}^{\text{C}}$  molecules which change their conformation to  $\text{PrP}^{\text{Sc}}$ , adding to the seed and further forming amyloids.

#### A Template-assisted conversion model



#### B Nucleation-polymerization model

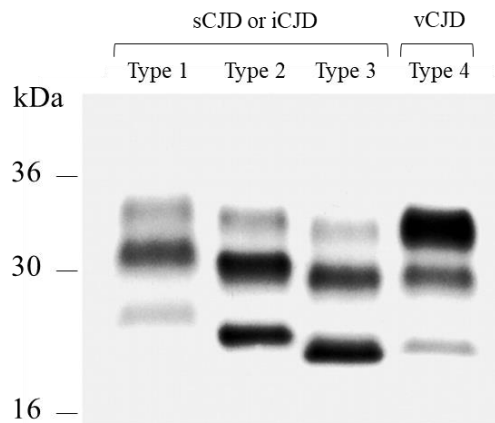


**Figure 4.** Two models explaining the conformational conversion of  $\text{PrP}^{\text{C}}$  to  $\text{PrP}^{\text{Sc}}$ . The template-assisted model (A) and the nucleation-polymerization model (B). Modified from [86].

### 1.3.2 Prion strains and the species barrier

Another surprising feature of prions is the existence of strains. Even though this concept was difficult to accept, evidences kept growing. It was first proposed by Pattison and Millson [87] after confirming different phenotypic traits in goats. Further experiments revealed how each strain has a specific

signature. After transmitting different prion strains to mice and serially passaging them, experiments continuously resulted in the characteristic pattern of both clinical signs and incubation periods [88, 89]. Strains differ from one another in clinical symptoms, incubation time, lesion profile and biochemical properties, such as PK-resistance, and electrophoretic mobility [90-92]. These biochemical properties are the ones most often used for characterizing and differing prion strains (**Figure 5**). The phenomenon of prion strains is still not completely understood. The presence of different phenotypic properties in organisms with the same genotype leads to the conclusion that differences in strains are not due to genetic variability, but rather in their conformational states [93]. Strains also differ in their immunoblot patterns, caused by variability in glycan site occupancy (di-, mono- and unglycosylated states). Differences in the actual glycosylation patterns remain to be investigated, since number of evidences claim glycans are not responsible for the existence of strains, however, some researchers believe they could have a role in defining their properties [81].



**Figure 5.** Immunoblot of different human prion strains after PK digestion, sporadic CJD (sCJD), iatrogenic CJD (iCJD) and variant CJD (vCJD). There is an obvious difference in their electrophoretic mobility, depending on the size of the PK-resistant core and a difference in their glycan site occupancy, where for each strain a different glycoform is more dominant than the others. Modified from [94].

One of the explanations of strain diversity is the fact that prions can be transmitted between species and this is another major point in differing prion diseases from other neurodegenerative disorders. Luckily, a phenomenon known as the “species barrier” limits the transmission and can lead to a prolonged incubation time [95]. Prions are, however, known to adapt, meaning that after the initial infection and by serial passages to the same species, the incubation time can decrease [96]. Variations in the primary protein sequence of PrP in different species could cause the conformation

diversity in prions and could explain both the strain diversity and the species barrier [97, 98]. Some animals, for example rabbits, horses and dogs, show a reduced susceptibility to prion diseases [99].

The only example of interspecies prion transmission to humans was from BSE in cattle, causing a new form of CJD, called variant CJD (vCJD). The epidemic of BSE started in United Kingdom and was first identified in 1986. Consumption of material infected with BSE caused a public health crisis and it was not until 1996 that it was linked to the newly formed TSE (vCJD) [100]. Since then, 229 cases have been reported worldwide, 177 of those in the UK. After introducing new control measures, there has been a decline in the emergence of the disease. This epidemic pointed out that people should be more aware regarding prion diseases [101]. Currently there is no way to predict a generation of new prion strains and which impact it could have on other species. For this reason, the most recent epidemic of CWD in cervids is causing a concern amongst scientists. Even though experiments have indicated that the species barrier is greater than the one between humans and cattle; CWD transmission to other species could cause an intermediary strain, with a potential to infect humans [102, 103].

## **1.4 Glycosylation of proteins**

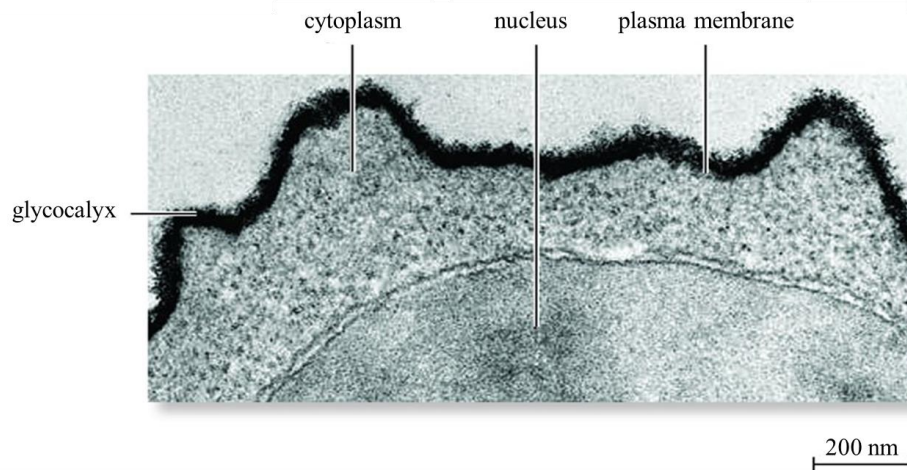
Glycosylation is one of the most common and most important co- and post-translational modifications (PTM). It is a process in which glycans, composed of monosaccharide units, are attached to proteins or lipids. Attachment of glycan structures contribute significantly to the mass, structure and stability of proteins [104]. Unlike proteins, glycans are not encoded in the genome, but their attachment to the peptide backbone is regulated through a complex network of several hundred enzymes, transcription factors, transporters, and other proteins. Glycans can be composed from only 2 and even up to 20 monosaccharide units, which can be linked in numerous ways (depending on the glycosidic linkages, which is more complex than the peptide bond), leading to the phenomenon of heterogeneity and creation of branched structures, unlike the linear polymers such as DNA and proteins. A glycoprotein can have from one to couple of glycosylation sites, where each site can carry many different glycan structures, causing an immensely complex glycoproteome, much more complicated than the proteome [105]. Vertebrates have a highly evolved glycome, which differs from that of lower eukaryotes and prokaryotes. Glycans in mammals are specifically well conserved, although with variations between species [106].

### 1.4.1 Functions of glycosylation

It is not surprising that, due to their complexity, functions of many glycans are still unknown. However, throughout the years many efforts have been put into understanding this and many answers have emerged. Glycans have an important role regarding the structure, accelerating the folding and stability of proteins [107, 108]. It has been shown that due to glycosylation, the proteins can become more resistant to proteases [109].

Eukaryotic cells usually have a thick layer of glycan structures (called glycocalyx, **Figure 6**) surrounding them and it represents an obvious physical barrier that needs to be overpassed in order for an interaction with the cell to occur. Glycans can act as ligands for cell-cell or cell-microbe interaction [110]. An important feature related to glycans is their specific recognition by glycan-binding proteins (GBPs), which are divided into two main groups: lectins and sulfated glycosaminoglycan (GAG)-binding proteins. Lectins are typically very selective for certain glycan structures and for this reason have been used as a tool for studying them [111].

The important role of glycans has been noted in conditions where glycosylation is disrupted in some way; either in the formation of glycans before their transfer to the protein or altered expression of proteins involved in the formation and/or branching of glycans during their biosynthesis, leading to congenital disorders of glycosylation (CDG), shown to be lethal [112].



**Figure 6.** The electron micrograph of a cell surface, showing a thick layer of glycans on it. Modified from [113].

## 1.4.2 Types of glycosylation

Glycans are divided according to the type of linkage to the protein or lipid. The two most common and most studied types are:

1. N-glycosylation – the glycan is covalently attached to the protein through *N*-acetylglucosamine (GlcNAc) to the nitrogen atom of an asparagine (Asn) by  $\beta$ -linkage (GlcNAc $\beta$ 1-Asn). This type of glycosylation occurs at a conserved tripeptide sequence Asn – X – Ser/Thr (where X can be any amino acid except Pro), but if there are conformational constraints around these sites, it is possible that glycosylation will not occur. N-glycans have also been found at Asn– X – Cys, under the condition that the cysteine is in its reduced form (Cys<sub>red</sub>).
2. O-glycosylation – the glycan is attached to the oxygen atom of an amino acid containing a functional hydroxyl group (Ser or Thr), possibly through GlcNAc, but more often *N*-acetylgalactosamine (GalNAc) by  $\alpha$ -linkage. Glycans linked through GalNAc are often referred to as mucin-type O-glycans [112].

Other, less common, types of glycosylation include:

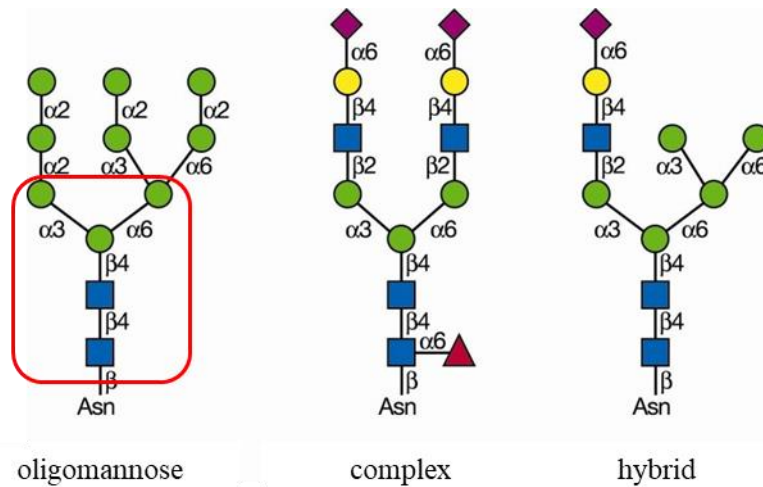
3. C-glycosylation – a carbon atom from a mannose (Man) is attached by  $\alpha$ -linkage to a carbon atom of the indole ring of the first tryptophan (W) in the sequence W – X – X – W (where X can be any amino acid).
4. Glypiation – the addition of the GPI anchor to the C-terminus of a protein, linking it to the lipids in the membrane, thus embedding the protein in the cell surface [111].
5. Glycosaminoglycans (GAGs) – long linear repeating disaccharide units, composing polysaccharide sugar chains; when attached to a protein (at the Ser residue) they are called proteoglycans [114].

## 1.5 N-linked glycosylation

### 1.5.1 Structure and diversity of N-linked glycans

All of the N-linked glycans have the same core structure, consisting of two GlcNAc and three mannose residues: Man $\alpha$ 1–6(Man $\alpha$ 1–3)Man $\beta$ 1–4GlcNAc $\beta$ 1–4GlcNAc $\beta$ 1–Asn. There are three general types of N-linked glycans (**Figure 7**):

- high mannose (or oligomannose) – only mannose residues are attached to the core;
- complex – each “antennae” on the core structure is elongated by attaching a GlcNAc to the mannose residue;
- hybrid structures – one or two antennae are attached to the Man $\alpha$ 1–3 arm, while only mannose residues are attached to the Man  $\alpha$ 1–6 arm [115].



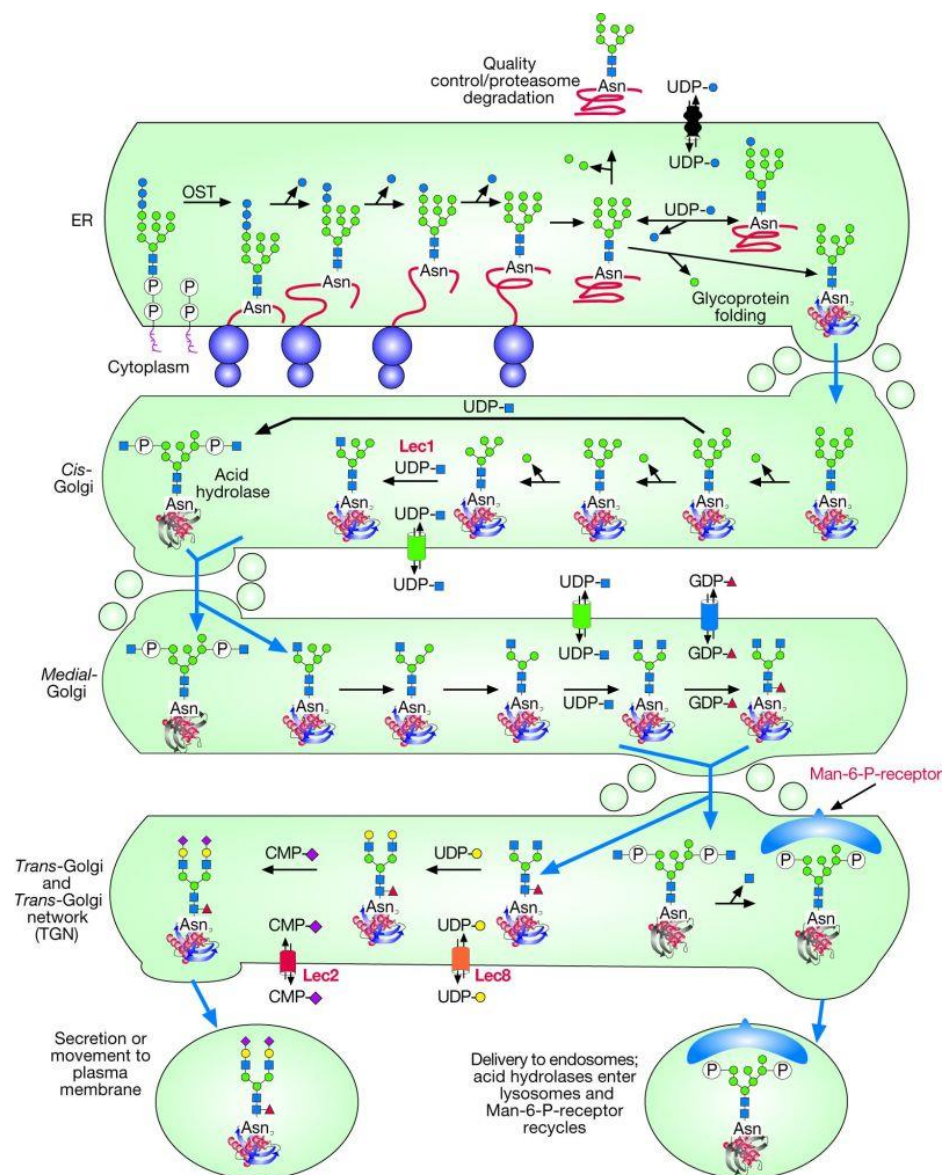
**Figure 7.** Three general types of N-linked glycans, sharing the same core structure (marked in the red rectangle). Blue square – *N*-acetylglucosamine (GlcNAc), green circle – mannose, red triangle – fucose, yellow circle – galactose, purple diamond – *N*-acetylneuraminic acid (Neu5Ac). Modified from [115].

The diversity of N-glycans, as seen in **Figure 7**, comes not only from the type of monosaccharide unit, but also from the type of glycosidic bond, where an anomeric carbon from one monosaccharide is linked to the hydroxyl group of another C-atom. The anomeric carbon of each monosaccharide has a hydroxyl group that can adopt two orientations, named  $\alpha$  and  $\beta$ . In addition to this, monosaccharides also have multiple hydroxyl group, meaning there are various possibilities for their linkages. Another important characteristic leading to the diversity of glycan structures is branching; glycans can have two (called biantennary), or can be even more complex, with three (triantennary), four (tetraantennary) or even more branches [111].

The complexity of glycosylation on a protein (or even a single glycosylation site) comes from the fact that the biosynthetic pathway of glycans is under the influence of numerous factors, such as the localization and abundance of certain enzymes, the accessibility of glycans to the enzymes and the availability of sugar donors in different cell compartments [116]./

### 1.5.2 Biosynthesis of N-linked glycans

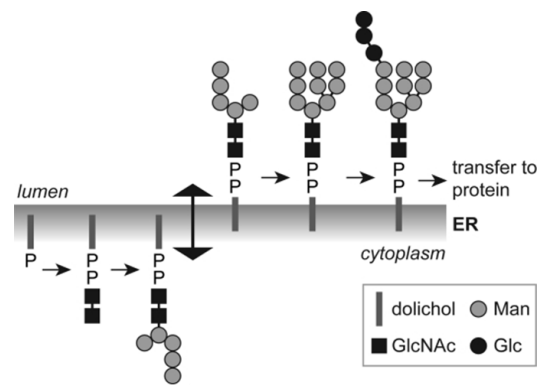
The biosynthesis of all N-glycans in eukaryotic cells first starts at the cytosolic side of the ER membrane, then moving to the Golgi (**Figure 8**). The synthesis in general occurs first by forming an oligosaccharide precursor linked to a lipid carrier, then transferring the oligosaccharide to the Asn in the protein. The N-glycans are partially processed in the ER lumen by glycosidases (enzymes cutting monosaccharides) and glycosyltransferases (enzymes adding new monosaccharides), but the final processing steps and maturation of the glycoprotein occur in the Golgi [117]. The biosynthesis will be discussed in detail in the next sections.



**Figure 8.** Biosynthesis of N-linked glycans starting in the ER, followed by the maturation in the Golgi [115].

### 1.5.2.1 Initial synthesis and processing of N-glycans in the ER

Dolichol is a polyisoprenol lipid carrier and depending on the cell type and organism, the number of isoprene units varies, in yeast it can be comprised of 14–18 units [118], while in mammals of 18–20 units [119]. The oligosaccharide precursor is synthesized on a dolichol phosphate (Dol-P), which in the beginning is located at the cytoplasmic side of the ER membrane. The first step includes the transfer of GlcNAc-1-P from UDP-GlcNAc (UDP, uridine diphosphate) to Dol-P, leading to the formation of Dol-P-P-GlcNAc; this reaction is catalyzed by the enzyme GlcNAc-1-phosphotransferase. Another GlcNAc and other five mannose residues are added from UDP-GlcNAc and GDP-Man (GDP, guanosine diphosphate), respectively, now forming  $\text{Man}_5\text{GlcNAc}_2\text{-P-P-Dol}$ . Glycosyltransferases catalyzing these reactions, transfer only the monosaccharide unit, unlike the GlcNAc-1-phosphotransferase [120]. Precursor  $\text{Man}_5\text{GlcNAc}_2\text{-P-P-Dol}$  is then translocated to the ER lumen by a flippase [121], followed by an extension with four mannose units from Dol-P-Man and three glucose units from Dol-P-Glc, generating a 14-sugar N-glycan precursor  $\text{Glc}_3\text{Man}_9\text{GlcNAc}_2\text{-P-P-Dol}$  [120].



**Figure 9.** Synthesis of the dolichol-linked oligosaccharide precursor. GlcNAc – *N*-acetylglucosamine, Man – mannose, Glc – glucose [121].

Following the formation of the mature high-mannose N-glycan precursor, an enzyme oligosaccharyltransferase (OST) catalyzes the transfer of the glycan from Dol-P-P to the nascent protein, specifically to Asn in the Asn-X-Ser/Thr sequon. OST is a transmembrane protein complex and in mammals it is composed of seven or eight different subunits [122]. Although functions of all these subunits are not completely clear, it is evident that OST interacts with ribosomes and the translocon complex, allowing the co-translational transfer of the glycan to the protein [123].



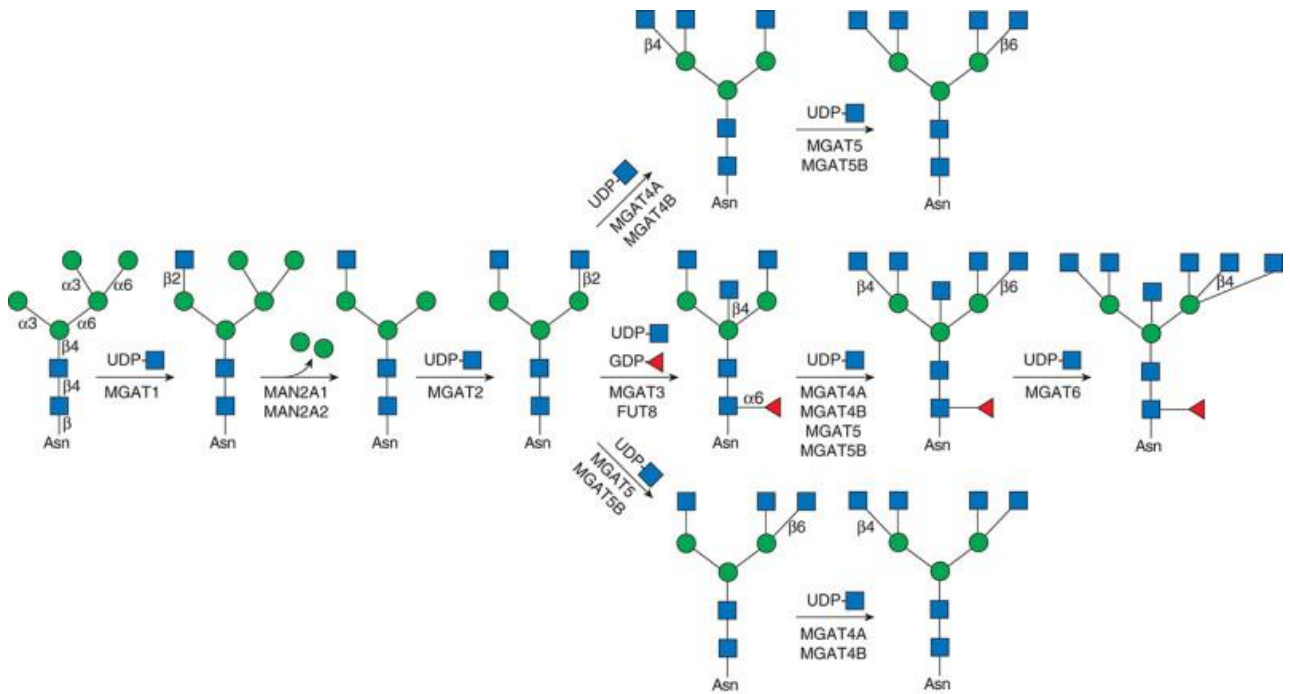
---

After the transfer to the protein, the 14-sugar  $\text{Glc}_3\text{Man}_9\text{GlcNAc}_2$  is further processed in the ER by “trimming” steps, which include the cleavage of three glucose and one mannose residue. The three glucose residues are removed by different enzymes,  $\alpha$ -glucosidase I removes the terminal glucose ( $\alpha$ 1,2-linked) [124], while  $\alpha$ -glucosidase II removes the other two glucose residues ( $\alpha$ 1,3-linked) [125]. This step is important in order to allow further processing and folding, the glycoprotein goes through a quality control pathway by interacting to calnexin and calreticulin (ER chaperons) [126]. If the glycoprotein leaves this step properly folded,  $\alpha$ -mannosidase I removes the terminal mannose ( $\alpha$ 1,2-linked), leaving  $\text{Man}_8\text{GlcNAc}_2$  which is then moved to the Golgi [127]. If the glycoprotein is not properly folded, it is recognized by ER degradation-enhancing  $\alpha$ -mannosidase I-like (EDEEM) protein, causing the degradation of the protein [128].

#### ***1.5.2.2 Processing and final maturation of N-glycans in the Golgi complex***

It is, however, possible for not completely processed glycans, still carrying a glucose residue, to enter the Golgi. If this happens, endo- $\alpha$ -mannosidase in the *cis*-Golgi cleaves a glucose and mannose unit in  $\text{GlcMan}_9\text{GlcNAc}_2$ , leaving an isomer of  $\text{Man}_8\text{GlcNAc}_2$ , which is different from the one produced in the ER. Further trimming of mannose residues is catalyzed by  $\alpha$ -mannosidases IA and IB, generating  $\text{Man}_5\text{GlcNAc}_2$ , the intermediate structure leading to the synthesis of hybrid and complex N-glycans. This structure or the ones with eight or nine mannose units can remain unprocessed and get secreted to the plasma membrane and are called high mannose N-glycans [111].

Further synthesis of hybrid and complex N-glycans starts in the *medial*-Golgi by adding a GlcNAc residue with the help of a glycosyltransferase called *N*-acetylglucosaminyltransferase I (GlcNAc-TI or MGAT1), to the  $\alpha$ 1-3Man in  $\text{Man}_5\text{GlcNAc}_2$ . Major part of N-glycans get trimmed by  $\alpha$ -mannosidase II (MAN2AI and MAN2A2, **Figure 10**), which cleaves two terminal mannose residues, forming  $\text{GlcNAcMan}_3\text{GlcNAc}_2$ . Only after the removal of both mannose units can another GlcNAc be added with GlcNAc-TII (MGAT2) to the other mannose in the core structure ( $\alpha$ 1-6Man), the base for all biantennary N-glycans. If  $\alpha$ -mannosidase II does not cleave off the second mannose unit, hybrid structures are formed. Other branches can be added to the biantennary structure, yielding tri- and tetraantennary structures (with three and four branches, respectively). Both hybrid and complex N-glycans can also have a “bisecting” GlcNAc unit, under the influence of GlcNAc-TIII (MGAT3), but only after the two GlcNAc residues are already added [111, 129].



**Figure 10.** Schematic of the N-glycan branching in the Golgi. Adding and trimming of each monosaccharide is under influence of a specific glycosyltransferase or glycosidase, shown in the figure. Blue square – *N*-acetylglucosamine (GlcNAc), green circle – mannose, red triangle – fucose [111].

The final processing and maturation of complex N-glycans occurs in the *trans*-Golgi and the reactions can be divided into three parts:

1. Addition of monosaccharides to the N-glycan core: the most common modification is the addition of a fucose. In vertebrates the fucose is attached to the GlcNAc linked directly to the Asn in  $\alpha$ 1-6 linkage, while in plants only in  $\alpha$ 1-3 linkage. In invertebrates, both of GlcNAc residues in the core can have a fucose, either in  $\alpha$ 1-3 or  $\alpha$ 1-6 linkage.
2. Elongation of the branches: most of the hybrid and complex N-glycans have a galactose (Gal) unit attached to the GlcNAc, producing Gal $\beta$ 1-4GlcNAc, also called *N*-acetyllactosamine or simply LacNAc. The branch can be further elongated by repeating the disaccharide motive, forming poly-LacNAc. The addition of GalNAc instead of Gal is also possible, forming a branch with GalNAc $\beta$ 1-4GlcNAc, named LacdiNAc.
3. “Capping” of the branches: the addition of sialic acids, fucose, galactose, GlcNAc and sulfates. The capping monosaccharides are usually  $\alpha$ -linked, guiding them away from the  $\beta$ -linked branches, enabling them to interact with lectins and antibodies [111].

---

### 1.5.3 Methods for analyzing N-linked glycans

Glycans contribute greatly to a protein's conformation and folding and given the many important roles they have in the cell, there is an increased need to analyze them. Because of the structural complexity and variability that glycosylation brings, this microheterogeneity leads to a decreased concentration of each analyte (each glycan structure), therefore analysis of glycans is one of the most challenging amongst all post-translational modifications. Methods usually used in glycosylation analysis are [130]:

- a) separation techniques such as gel electrophoresis or capillary gel electrophoresis (CGE);
- b) separation methods based on chromatography, strong or weak anion exchange chromatography, size exclusion chromatography, and lectin affinity chromatography.
- c) mass spectrometry (MS) techniques, usually matrix-assisted laser desorption ionization (MALDI) and electrospray ionization mass spectrometry (ESI-MS). MS techniques are commonly coupled to other techniques, such as high-pressure liquid chromatography (HPLC) or gas chromatography (GC).
- d) nuclear magnetic resonance (NMR) or X-ray crystallography for 3D structure analysis.

None of these methods alone can give all the required information (detailed glycan structure, site-specific and linkage analysis) and for this reason they are usually used in combination with each other. Specifically, MS techniques have become an important tool in glycan analysis because of their high sensitivity, the possibility of directly coupling them to chromatographic separation methods and additionally, sequencing glycan structures can be achieved with fragmentation by tandem mass spectrometry (MS<sub>n</sub>) [130, 131]. MS can also be combined with exoglycosidases, enzymes cleaving monosaccharides in a highly specific and accurate way, leading to information regarding the exact sequence and linkage of the monosaccharides [132, 133]. Three main strategies in proteomics include bottom-up, middle down, and top-down approaches. Bottom-up is a strategy where proteins are enzymatically digested into peptides [134], the most commonly used method for identification and quantification of proteins [135, 136], but also for studying post-translational modifications [137-141].

Glycosylation can be analyzed at three different levels: glycoprotein, glycopeptide and released glycans. Glycans can be analyzed from intact glycoproteins, under native conditions [142] or denaturing by separation with sodium dodecyl sulfate-polyacrylamide gel electrophoresis (SDS-

---

PAGE) or 2D gel electrophoresis. Due to the microheterogeneity of glycan structures, bands corresponding to glycoproteins are usually diffused, making it difficult to separate glycoforms. Nevertheless, SDS-PAGE can be used as a detection tool, together in combination with lectins [143] and specific enzymes, exoglycosidases [132] (cleaving terminal monosaccharide units) and endoglycosidases (releasing complete glycans).

Glycopeptides are obtained by digesting the glycoprotein with specific proteinases, most commonly with trypsin, chymotrypsin, Glu-C and Lys-C. After digestion, there is a mixture of glycopeptides, and peptides present in the sample. Glycopeptides are difficult to detect, since their abundance in this mixture is usually quite low, the signal of the peptide is dispersed across number of glycoforms and the glycopeptide ionization is suppressed [137]. Therefore, it is usually necessary to use enrichment techniques which can selectively separate glycopeptides from peptides. Enrichment techniques usually include hydrophilic interaction liquid chromatography (HILIC) or size exclusion. Glycopeptides are usually analyzed by coupling techniques; first by separating them chromatographically (using LC or GC), then selective detection by ESI-MS, MSn (LC-ESI-MS/MS) or MALDI. The biggest advantage of analyzing glycans at the glycopeptide level is the fact that site-specific glycosylation can be identified [130, 144].

Glycans can also be analyzed by releasing them from proteins using enzymes. Both peptide-N-glycosidase F (PNGase F) and PNGase A digest all types of N-linked glycans, by cleaving GlcNAc from Asn, converting it to Asp (aspartic acid). PNGase F, however, is unable to digest GlcNAc if the fucose on it is  $\alpha$ 1-3 linked – in this case PNGase A is used [145]. Endoglycosidase H (Endo H) is an enzyme which digests between the two GlcNAc residues. Endo H is specific for high mannose and hybrid N-glycans but cannot digest complex structures [146]. After glycan release, they are fluorescently labelled, either with 2-aminobenzamide (2-AB) [147], 2-aminobenzoic acid (2-AA) [148], 2-aminopyridine (PA) [149], procainamide [150], and 1-aminopyrene-3,6,8-trisulfonic acid (APTS), usually used for CGE analysis [151]. After a cleaning step from the excess of fluorescent dye, released glycans can be analyzed by chromatographic methods, CE or MS techniques.

Although many improvements have been made in the last years, structural glycan analysis remains quite a challenging task. There is no standard technique that could provide all of the information regarding the structures of glycans, thus, combining different approaches is necessary to obtain a clearer image.

---

## 1.6 Glycosylation of the prion protein and prion infection

The prion protein is a sialoglycoprotein, with two N-glycosylation sites. As mentioned before, the occupation of these glycosylation sites leads to the existence of four different glycoforms: di-, mono- (when either one or the other site is occupied, hence counting as two glycoforms) and unglycosylated. This has been confirmed both on PrP<sup>C</sup> and PrP<sup>Sc</sup>, after treating the protein with PNGase F, there is a shift in their molecular weight towards the unglycosylated form [152, 153].

Throughout the years, many efforts have been put into understanding the importance of glycosylation of the prion protein. Studies usually included introducing different point mutations in the *Prnp* gene, and the use of different constructs and different cell lines often leads to contradictory results. Cell constructs where mutations were introduced in threonine in the tripeptide sequon (T183A and T199A in hamster) produced unglycosylated PrP, which led to the intracellular accumulation of PrP, instead of trafficking it to the cell surface [153]. Another study, using the same construct, showed that PrP<sup>C</sup> cannot be converted to PrP<sup>Sc</sup>, presumably because of the intracellular localization of the protein [154]. This suggested that glycans are necessary for correct localization of the prion protein. However, Korth et al. and Neuendorf et al. showed, by using different constructs, but still generating unglycosylated mutants (N180Q and N196Q; T182N and T198A in mice), that PrP<sup>C</sup> was actually correctly localized on the cell surface and that unglycosylated PrP<sup>C</sup> was readily converted to PrP<sup>Sc</sup>, indicating that glycans are in fact not necessary for prion infection [155, 156]. This suggested that it is not the lack of glycans which prevents the trafficking of PrP to the cell surface, but rather the mutation itself, by changing the properties of the protein [157]. Finally, Cancellotti et al. confirmed that the level of unglycosylated PrP in the mutated constructs is comparable to the one in wild type PrP and in fact mainly localized intracellularly. In contrast, the di- and monoglycosylated PrP is translocated to the cell surface, suggesting that glycans do have an impact in determining the cellular localization of PrP. They also claim that glycans do not influence the maturation and stability of the protein, therefore the PrP is only partially dependent on glycosylation [158, 159].

As mentioned before, the immunoblot of PrP<sup>Sc</sup> resulting in the typical three band pattern is the main way of differing PrP<sup>Sc</sup> from PrP<sup>C</sup>, but also PrP<sup>Sc</sup> strains from one another. So far, only few studies have performed structural analysis of PrP N-glycans. In a study from 1989 [160], PrP<sup>Sc</sup> was isolated from Syrian hamster brains and in combination with exoglycosidases, MS analysis revealed

---

the presence of complex N-glycans (bi-, tri- and tetraantennary). Next, a study from 1999 compared released and labelled N-glycans from both PrP<sup>C</sup> and PrP<sup>Sc</sup> and detected more than 50 N-glycan structures. Researchers found that the two forms share the same set of N-glycans, however, they differ in the relative proportion of each structure. It was hypothesized that this could be due to changes in the activity of a specific enzyme in the infected brain [161]. The first detailed, site-specific analysis of N-glycans was performed on mouse PrP<sup>Sc</sup> (glycosylation sites at N-180 and N-196). Analysis was done at the glycopeptide level, using LC-MS. Around 60 complex N-glycan structures were found, characterized as bi-, tri- and tetraantennary, sialylated and fucosylated (both core fucose and outer arm fucose were found). The analysis also revealed the differences in N-glycan composition between the sites; N-glycans at N-180 were mainly bi- and triantennary, while at N-196 there was an increased proportion of tri- and tetraantennary structures, which were sialylated to a higher degree than on N-180 [162].

### 1.6.1 Prion protein sialylation

Even though sialylation of PrP has been known for more than 20 years [161], it was not until recently that its role in prions has started to be explored [163]. Sialic acid is a terminal monosaccharide on N-glycan structures and because of this has an important role in cellular functions [164]. The term sialic acid is related to two major derivatives, *N*-acetylneuraminic acid (NeuAc) and *N*-glycolylneuraminic acid (NeuGc). Since humans carry an irreversible mutation in the gene encoding for *N*-acetylneuraminic acid hydroxylase, only NeuAc is produced, while other mammals produce both NeuAc and NeuGc [165]. However, the situation in brain tissue is different, in species where NeuGc is synthesized, its expression is suppressed in neural tissue. Also, NeuAc can be found in higher concentrations in mammalian brains (rat, mouse, pig, bovine, sheep, etc.) [166] and spleen, than in other organs [167].

The effect glycans have on a protein has long been neglected and they have been considered as mere cell decorations; also due to the fact that there were, and still are, many challenges regarding glycan analysis [131]. Resolving the PrP<sup>Sc</sup> structure has also imposed many problems throughout the years, because of its insolubility and aggregation [168]. In order to have a realistic model of any protein, glycans should be taken into consideration. Molecular models have been able to reveal that the N-glycans are directed outwards and that sialylation results in quite a dense and negative charge on the surface of PrP<sup>Sc</sup>. Because of the electrostatic repulsion from sialic acid residues, the PrP<sup>Sc</sup>

---

replication rate is affected [169]. Using an exoglycosidase, neuraminidase, which cleaves sialic acid and thus removes the electrostatic repulsions, researchers found an increase in desialylated prions' replication rate, which also turned out to be strain-specific, suggesting sialylation of PrP<sup>Sc</sup> is strain-specific. One of the main ways to distinguish prion strains is the difference in their immunoblot pattern. The same group of scientists were able to show that desialylation of different PrP<sup>Sc</sup> strains also controls the glycoform ratio, meaning that prions lose their specific ratio when exposed to desialylated substrates [163, 169, 170].

The involvement of sialic acids in prions has been displayed in determining their fate. Sialic acids contribute to the self-associated molecular pattern (SAMP) [171, 172], meaning that by removing them from the cell surface, galactose becomes the exposed monosaccharide residue, sending an “eat me” signal to macrophages [173] or leading to phagocytosis of neurons [174]. Regarding prion fate, experiments have demonstrated that desialylated PrP<sup>Sc</sup> is not able to induce prion disease in wild type animals, indicating that sialic acid has a protective role for prions, preventing their clearance from the immune system [169, 175, 176].

## 1.7 Aims of the research

PrP<sup>Sc</sup> is considered as the main agent in prion diseases and its structure remains to be elucidated in order to comprehend the mechanism leading to these disorders. It is known that PrP<sup>Sc</sup> and PrP<sup>C</sup> share the same primary amino acid sequence, meaning that the two glycosylation sites are conserved in both forms. Glycosylation of PrP results in the existence of di-, mono- and unglycosylated forms of the protein, clearly seen on the immunoblot of PrP<sup>Sc</sup>.

The finding that synthetic prions are infectious, regardless of the method of their formation, leads to the conclusion that PrP is necessary for infection. This was, however, also an indication that glycosylation is not necessary for the infectivity of prions, since synthetic prions do not carry N-linked glycans nor the GPI anchor [81]. It has also been pointed out that PrP glycosylation is not required for the existence of prion strains, since experiments show that unglycosylated PrP<sup>C</sup> preserves strain information [177, 178]. However, despite many confirmations, the “protein-only” hypothesis is still under debate and some other theories have even been proposed, such as the responsibility of glycans for the existence of different strains and their contribution in defining certain strain properties [179, 180].

Even though a lot of progress has been made in the glycobiology field, trying to emphasize the importance of glycomics, and in resolving the puzzle prion diseases impose, many problems are still unresolved. This PhD thesis aimed to contribute to the long-lasting question regarding prion strains.

The main goals in this work were:

- First and foremost, to develop a protocol for isolating different strains of prions. Any structural analysis involving glycans requires a large amount of the starting material, in order to obtain a pure and homogeneous isolate [181] (in this case the prion protein). There is no standard and straightforward protocol for isolating prions, especially in large-scale, therefore, different starting materials and different protocols were tested for this point. Large-scale in this project refers to obtaining of at least a couple of micrograms of the prion protein, the aim being around 10  $\mu\text{g}$  (or less).
- The second part involved the analysis of PrP<sup>Sc</sup> N-glycans on a glycopeptide level, by using LC-MS/MS as an analytical tool; to receive information about the structures in a site-specific manner. The aim was to observe whether there are differences in glycan structures occupying the two glycosylation sites, as has been shown previously [162], but the final goal was to conclude if different prion strains differ in their N-glycan composition and if this could be the reason for strain diversity.



---

## CHAPTER II

## 2 MATERIALS AND METHODS

### 2.1 Samples used for PrP isolation

#### 2.1.1 Cell lines

Mouse hypothalamic cell line (GT1) chronically infected either with Rocky Mountain Laboratory (RML) or 22L prion strains (ScGT1) were cultured in Dulbecco's Modified Eagle Medium (DMEM) (Gibco), supplemented with 10% fetal bovine serum (FBS, Gibco) and 1% penicillin-streptomycin.

Mouse neuroblastoma cell line (N2a) chronically infected with RML or 22L prion strain (ScN2a) were cultured in Minimal Essential Medium (Mem) (Gibco), supplemented with 10% FBS, 1% penicillin-streptomycin and 1% non-essential amino acids (NEAA).

All the cell lines were incubated in 10 cm Petri dishes (or at some point in 150 cm<sup>2</sup> cell culture flasks) at 37 °C, in a humidified incubator, under 5% CO<sub>2</sub>. After reaching 80–90% confluence, a smaller part of cells was sub-cultured, the majority were harvested in cold lysis buffer (10 mM Tris-HCl pH 8.0, 150 mM NaCl, 0.5% Nonidet P-40 substitute, 0.5% sodium deoxycholate). The cell lysates were collected, and the cell debris was removed by centrifugation at 2,000 rpm for 10 min at 4 °C in a bench microfuge (Eppendorf). The total amount of the protein in a sample was measured by bicinchoninic acid (BCA) protein assay (Pierce) and the supernatant was frozen at -80 °C until further use.

#### 2.1.2 Mice brains

Brains from CD1 mice strains, chronically infected with RML were kindly provided by dr. Fabio Moda (IRCCS Istituto Neurologico Carlo Besta, Milano). 10% (w/v) brain homogenates (BHs) were prepared in lysis buffer (same one used for preparing cell lysates) after which the samples were

---

centrifuged at 2,000 g for 5 minutes at room temperature (RT) in a bench microfuge (Eppendorf) to remove cell debris. The samples were either stored at -20 °C or used immediately for PrP<sup>Sc</sup> isolation.

### **2.1.3 PMCA material**

PMCA material was kindly provided by dr. Fabio Moda (IRCCS Istituto Neurologico Carlo Besta, Milano) and was performed as described previously [82]. Briefly, 10% brain homogenates of CD1 mice, which were prepared in conversion buffer (150 mM sodium chloride, 1% Triton X-100 in PBS 1X), supplemented with complete protease inhibitor cocktail (cOmplete, EDTA-free Protease Inhibitor Cocktail, Roche), were used as PMCA substrates. Ten µL of RML brain homogenate was added to 90 µL of PMCA substrate and subjected to PMCA analysis performed by alternating cycles of sonication (20 sec, 250–260W) to cycles of incubation (29 min and 40 sec) at 37–40°C, using a micro-sonicator (Misonix, S3000). To increase the efficiency of amplification, 3 teflon beads were added to each sample. After 96 cycles (referred to as PMCA round), 20 µL of the amplified products was subjected to Western blot analysis.

### **2.1.4 Sheep brains**

Sheep brains with VRQ/VRQ genotype infected with 21K fast, 21K slow or 19K prion strain were kindly provided by Prof. Olivier Andréoletti (Ecole Nationale Vétérinaire de Toulouse, Toulouse). Using a glass tissue homogenizer grinder, 20% (w/v) brain homogenates were prepared either just in 1X phosphate-buffered saline (PBS, pH 7.4) or in 1X PBS containing protease inhibitor cocktail and 4% N-lauroylsarcosine sodium salt (sarkosyl). The homogenates were centrifuged at 1,000 g for 10 minutes at RT in a bench centrifuge (Eppendorf); the supernatants (SNs) were transferred to clean 50 mL tubes (Falcon) and stored at -80 °C until further use.

## **2.2 Protocols used for PrP<sup>Sc</sup> isolation and purification**

### **2.2.1 Sodium phosphotungstic acid (PTA) precipitation**

After preparation of cell lysates, 1X PBS containing 4% sarkosyl was added to the samples (so that the final concentration of sarkosyl reaches 2%), complete protease inhibitor (Roche) and PTA (to reach the final concentration of 0.5%). Samples were incubated at 37 °C with constant shaking at 350 rpm for 1 h, after which they were centrifuged at 14,000 g for 30 min at RT in a bench microfuge.

---

The pellet was washed with 500  $\mu\text{L}$  of 2% sarkosyl and centrifuged again under same conditions. The pellet was then resuspended in sterile distilled water and stored at  $-80\text{ }^{\circ}\text{C}$  until use.

### **2.2.2 PK digestion**

The protein obtained either from cell lysates or brain tissues was digested with PK (Roche) in a range of 10-40  $\mu\text{g}/\text{mL}$  of PK (depending on the protocol used, will be mentioned in the Results) for 45-60 min at  $37\text{ }^{\circ}\text{C}$ . The reaction was stopped with the addition of 1–2 mM phenylmethylsulphonyl fluoride (PMSF, Sigma) and the samples were centrifuged at 186,000 g for 1 h at  $6\text{ }^{\circ}\text{C}$  in an ultracentrifuge (Beckman Coulter). After obtaining the pellet, the supernatants were discarded, and the pellets were further used for isolation or resuspended in 2X or 5X sample loading buffer (125 mM Tris-HCl pH 6.8, 200 mM dithiothreitol (DTT), 20% glycerol, 10% 2-mercaptoethanol, 4% SDS, and 0.2% bromphenol blue), boiled at  $100\text{ }^{\circ}\text{C}$  for 10 minutes and used for immunoblotting.

### **2.2.3 Thermolysin digestion**

Protein obtained from sheep brains and used for further immunopurification with EF2 antibody was digested with thermolysin (Sigma) with 25  $\mu\text{g}/\text{mL}$  for 30 min at  $37\text{ }^{\circ}\text{C}$ . The reaction was stopped with the addition of 2 mM EDTA and the samples were centrifuged at 186,000 g for 1 h at  $6\text{ }^{\circ}\text{C}$  in an ultracentrifuge. The supernatant was discarded, the pellet sonicated in PBS and incubated with antibody-beads complex (will be explained in one of the next sections).

### **2.2.4 Use of a density medium (iodixanol)**

The protocol was based on two publications [182, 183] where pronase E and PTA were used to isolate  $\text{PrP}^{\text{Sc}}$  of high purity. Brain homogenates or cell lysates containing 4% sarkosyl were treated with 100  $\mu\text{g}/\text{mL}$  of pronase E (Sigma) and incubated for 30 min at  $37\text{ }^{\circ}\text{C}$  (all further incubations were performed at this temperature, with constant shaking at 800 rpm). The reaction was stopped with 10 mM EDTA. Samples were incubated with benzonase (Merck Millipore) for 10 min, after which 0.3% of PTA pH 7.4 was added to the sample and the sarkosyl was diluted until a concentration of 2% (w/v) was reached. Samples were further incubated for another 30 min, and a solution of 60% iodixanol (OptiPrep Density Gradient Medium, Sigma) was added to the sample, in order to have a final concentration of 35% (w/v). Samples were centrifuged at 16,100 g for 90 min and the first supernatant (SN1) was transferred to a clean 1.5 mL tube.

---

The SN1 was diluted in a ratio 1:1 with 2% sarkosyl containing 0.3% PTA and after a 10-minute incubation the samples were centrifuged at 16,100 g for 90 min. The second supernatant (SN2) was discarded and the pellet (P2) was resuspended in a wash buffer (PBS containing 17.5% (w/v) iodixanol and 0.1% (w/v) sarkosyl). Pellets from two samples were pooled together and PK was performed as described in the previous section (10 µg/ml of PK and 1 mM of PMSF was used).

After PK digestion, the samples were mixed with 180 µL of the wash buffer and 0.3% PTA and centrifuged at 16,100 g for 30 min. The supernatant (SN3) was discarded and the wash was repeated with the pellet (P3). The final pellet (P4) was resuspended in PBS containing 0.1% sarkosyl and used further for silver staining or immunoblotting.

The described protocol was tested on all the samples, however, many variations to the protocol were tested and the exact protocols will be mentioned in the Results section, shown together with corresponding immunoblots and/or silver stained gels.

## **2.2.5 Immunopurification**

### ***2.2.5.1 Incubation of mAb with the protein***

PrP<sup>Sc</sup> from sheep brains was partially isolated with the density medium protocol. After PK digestion, 10-20 µg of SAF 61 (concentration of stock solution was 1 mg/mL) was added to the sample containing the protein. The protein-mAb complex was incubated for 2 h at 4 °C on a rotation wheel, and 20 µL of Protein A magnetic beads (Thermo Scientific, 10 mg/mL beads concentration) were washed twice with the binding buffer (PBS). The buffer was removed from the beads using a magnetic rack and discarded, after which the protein-mAb complex was added to the beads and incubated for 1 h on the rotation wheel at 4 °C. The sample was washed twice with the binding buffer, and the protein was eluted by adding 0.1 M glycine HCl, pH 2.5. Before elution, Tris-HCl, pH 8.8 was added to the elution tube, in order to neutralize the low pH solution. In this way the PrP<sup>Sc</sup> remained insoluble and can be collected by centrifugation. The tube was sonicated in a sonication bath 3x30 sec and the sample was centrifuged at 186,000 g for 30 min at 6 °C in an ultracentrifuge, washed with H<sub>2</sub>O and centrifuged again.

### **2.2.5.2 Pre-immobilizing mAb to Protein G beads**

In the case of using SAF 61 as the mAb, the samples were previously treated with PK. The samples incubated with EF2 were treated with thermolysin instead of PK, since PK digests the prion protein at its N-terminus, therefore removing the epitope for EF2. Instead, thermolysin digests PrP<sup>C</sup> and leaves PrP<sup>Sc</sup> in its full-length form [73].

Co-Immunoprecipitation Kit (Pierce) was used to prepare the mAb-beads complex. Spin column (Pierce) was usually used to couple 40-75 µg of mAb in a 1:1 ratio with the beads. The sample containing PrP<sup>Sc</sup> was added to the mAb-beads complex and incubated overnight (O.N.) at 4 °C on a rotation wheel. After the incubation, the column was spun in a bench microfuge and the flow-through (F.T.) was collected. The mAb-beads complex was washed twice with 1X PBS and two types of elution were tested:

1. Elution with low pH – Tris-HCl, pH 8.8 was added to the elution tube before elution, in order to neutralize the elution buffer. Solution of glycine HCl, pH 2.5 was added to the column, after which it was sonicated in a sonication bath for 3x30 sec, the elute was spun down, collected and then centrifuged in an ultracentrifuge at 186,000 g. The pellet was collected and resuspended in 2X sample loading buffer.
2. Elution with SDS together with acetone precipitation – 250 µL of Tris-HCl (50 mM, pH 8.0) containing 2.5% SDS was added to the column and the spin column was incubated with shaking at 1,000 rpm, 37 °C for 20 min. The elution buffer was spun down in a 1.5 mL tube, after adding 1 mL of cold acetone to it, the sample was vortexed and incubated for 1 h at -80 °C and 15 min at -20 °C. The sample was centrifuged at 16,100 g for 30 min at RT in a bench centrifuge. The supernatant was removed, and the tubes were left under the hood briefly to allow the acetone to evaporate completely. The pellet was resuspended in 2X sample loading buffer.

## **2.3 Detection of PrP<sup>Sc</sup>**

### **2.3.1 SDS polyacrylamide gel electrophoresis (SDS-PAGE)**

After isolation procedure, the pellets containing PrP<sup>Sc</sup> were resuspended in 2X or 5X sample loading buffer and boiled at 100 °C for 10 minutes. Before loading them onto a 12% Tris-Glycine SDS-

PAGE gel, the samples were spun down. PageRuler Plus Prestained Protein Ladder (Thermo Fisher Scientific) was used as a molecular weight marker. The gel electrophoresis was performed at 90 V for approximately 30 min, after which at 120 V for 90 min, or until the dye front ran off the end of the gel.

### **2.3.2 Coomassie staining of gels**

As a detection and isolation tool, after electrophoresis, gels were stained in GelCode Blue Safe Protein Stain (Thermo Fisher Scientific) by gently shaking for 1 h. Gels were destained overnight in ultrapure water.

### **2.3.3 Silver staining of gels**

Gels were also stained with PlusOne Protein Silver Staining Kit (GE Healthcare) according to the manufacturer's instructions. Briefly, proteins were fixed in a 30% ethanol solution for 45–60 min. The gels were then incubated in a sensitizing solution (containing ethanol, sodium thiosulfate, sodium acetate, and glutardialdehyde) for 45–60 min, to increase the contrast of the staining. After 3–4 washing steps in ultrapure water, gels were incubated in a silver nitrate solution for 45 min. The gels were rinsed another two times in ultrapure water, before image development with a solution containing sodium carbonate and formaldehyde. The developing was stopped with EDTA solution when the desired intensity of the bands was achieved.

### **2.3.4 Western blot**

After electrophoresis, proteins were transferred onto nitrocellulose membranes (GE Healthcare) for 120 min at 250 mA by Criterion Blotter (Bio-Rad). The membranes were blocked with 5% non-fat milk in TBS-T (200 mM Tris, 1.5 mM NaCl, and 0.05% Tween-20) for 1 h, after which they were incubated overnight at 4 °C with a primary antibody: 1:1000 anti-PrP W226 antibody (for mouse PrP<sup>Sc</sup>), 1:1000 or 1:500 anti-PrP SAF 61 antibody or anti-PrP SAF 84 antibody (for sheep PrP<sup>Sc</sup>), diluted in blocking solution. Membranes were washed three times with TBS-T, after which they were incubated with horseradish peroxidase (HRP)-conjugated secondary antibody goat anti-mouse, diluted 1:1000 in blocking solution. After three washes, the membranes were developed using enhanced chemiluminescence (GE Healthcare) and the band intensity was acquired using the UVI Soft software (Uvitec Alliance, Cambridge).

---

## 2.4 Isolation and purification of PrP<sup>Sc</sup> glycopeptides

### 2.4.1 In-gel trypsin digestion

Protocol for MS analysis of proteins from silver stained gels, published by Shevchenko et al. [184], was optimized to improve the sensitivity of the analysis and to speed up the procedure. The in-gel digestion protocol is used for silver stained or Coomassie stained gels and is compatible with bottom-up MS approaches [185].

#### 2.4.1.1 Excising PrP<sup>Sc</sup> bands from Coomassie stained gels

After overnight rinsing with ultrapure water (Millipore Milli-Q), the Coomassie stained gel was transferred onto a glass tray and the diglycosylated band of PrP<sup>Sc</sup> from different strains was excised with a clean scalpel. Each band was cut into small cubes (approximately 1 x 1 mm); the gel pieces were transferred into a 1.5 mL microcentrifuge tube and spun down in a bench microcentrifuge.

#### 2.4.1.2 Reduction and alkylation of PrP<sup>Sc</sup>

Bottom-up workflow for MS analysis includes the reduction of disulfide bonds with DTT and alkylation of sulfhydryl groups of cysteines with iodoacetamide (IAA) [186, 187]. Before the reduction step, gel pieces were incubated for 10 minutes with acetonitrile (ACN) in order to dehydrate them. After removing ACN, a solution of 10 mM DTT prepared in 100 mM ammonium bicarbonate was added and gel pieces were incubated for 30 minutes at 56 °C. Samples were cooled down to RT and the incubation with ACN was repeated. After 10 minutes, ACN was removed and the samples were incubated with 55 mM IAA in 100 mM ammonium bicarbonate at RT in the dark for 20 minutes. ACN was added again and removed after a 10 minute-incubation.

#### 2.4.1.3 Destaining gel pieces from Coomassie stained gels

Gel pieces were incubated and left shaking for 30 minutes at RT, with a solution of 100 mM ammonium bicarbonate / ACN (1:1, v/v). Neat ACN was added and shaking was continued for 15–20 minutes. The two steps were repeated until the gel pieces were destained.

#### **2.4.1.4 Trypsin digestion**

Twenty  $\mu\text{g}$  of lyophilized trypsin (Promega) was resuspended in 10 mM ammonium bicarbonate containing 10% ACN (v/v) in order to prepare a solution of 13  $\text{ng}/\mu\text{L}$  (this concentration was used for cell cultures, while for sheep brains 5–6.5  $\text{ng}/\mu\text{L}$  was used). Trypsin buffer was added to the destained gel pieces so that they were covered completely. Samples were left for 30 min in an ice bucket in the fridge, and if it was necessary, more trypsin buffer was added. To saturate them enough with trypsin buffer, gel pieces were left in the fridge for another 90 minutes. After this, the tubes containing gel pieces were transferred into an air thermostat and incubated overnight at 37 °C.

#### **2.4.1.5 Extraction and drying of glycopeptide digests**

Extraction buffer, a solution of 5% formic acid / ACN (1:2, v/v) was added to each sample so that the ratio of the volumes of digests and extraction buffer was 1:2. Samples were incubated for 30 minutes in a shaker, at 37 °C. The supernatant was removed slowly with a pipette and moved to a clean 1.5 mL microcentrifuge tube, after which the sample was dried in a vacuum centrifuge. The extraction procedure was usually repeated two times, to be sure that the glycopeptides are extracted. Dried extracts were either resuspended in ultrapure water after which they were loaded directly to the LC-MS or were frozen at -20 °C to use for HILIC enrichment.

#### **2.4.2 In-solution trypsin digestion**

This protocol was based on a paper published by Stimson et al. [162], but with some adjustments [188]. After PK digestion, the total amount of the protein was quantified with BCA protein assay and the sample was reconstituted in 10  $\mu\text{L}$  of 6 M guanidine HCl (GndHCl), 150 mM ammonium bicarbonate ( $\text{NH}_4\text{HCO}_3$ ), pH 8.0. After this, 1  $\mu\text{L}$  of 200 mM DTT / 150 mM ammonium bicarbonate pH 8.0 was added to the sample and it was incubated for 1 h at RT. The alkylation step was performed by adding 10  $\mu\text{L}$  of 200 mM iodoacetamide / 150 mM ammonium bicarbonate and the sample was incubated for 1 h at room temperature, in the dark.

Another 77.5  $\mu\text{L}$  of 150 mM ammonium bicarbonate was added to the sample, in order to dilute the GndHCl until the concentration of 0.6 M. Trypsin solution was added in a ratio of 1:20 (w/w, trypsin:protein) and the samples were incubated overnight (~18 h) at 37 °C.



---

After the incubation with trypsin, formic acid was added to the sample, so that the pH reached 3–4. The sample was dried until 10  $\mu\text{L}$  in a vacuum centrifuge and stored at  $-20\text{ }^{\circ}\text{C}$  until analysis.

### **2.4.3 Glycopeptide HILIC enrichment**

A suspension of 50 mg/mL Chromabond HILIC beads in 0.1% trifluoroacetic acid (TFA) was prepared for glycopeptide enrichment. Hundred  $\mu\text{L}$  of the suspension was added to a well of the filter plate (Orochem). The HILIC beads were washed two times with 0.1% TFA and equilibrated with three washes of 80% ACN containing 0.1% TFA (v/v). All the washes were removed by vacuum filtration (Pall).

Dried glycopeptides were resuspended in ultrapure water and diluted with 100% ACN / 0.1% TFA to reach the final concentration of 80% of ACN. Diluted glycopeptides were added to the well of the filter plate, incubated for 1 min and the solution vacuumed to waste. The glycopeptides were washed two times with a solution of 80% ACN / 0.1% TFA to remove any remained impurities. After the washes, the filter plate was placed on a clean PCR plate in which the glycopeptides were eluted with 0.1% TFA by centrifugation for 5 minutes. The samples were then dried in a vacuum centrifuge and reconstituted in ultrapure water (ready for the LC-MS/MS analysis) or stored at  $-20\text{ }^{\circ}\text{C}$  until use.

## **2.5 Glycopeptide detection and analysis**

### **2.5.1 LC-MS/MS analysis of PrP<sup>Sc</sup> glycopeptides from sheep brains**

Digested glycopeptides were separated on Acquity M Class UPLC system (Waters) coupled to Compact mass spectrometer (Bruker) with an electrospray ionization (ESI) source. Samples were used either directly after the trypsin digestion (1–2  $\mu\text{L}$  from 20  $\mu\text{L}$ ) or after the enrichment procedure (18  $\mu\text{L}$  from 20  $\mu\text{L}$ ). They were loaded onto a PepMap 100 C18 trap column (5 mm x 300  $\mu\text{m}$ , Thermo Fisher Scientific) at a flow rate of 40  $\mu\text{L}/\text{min}$  of solvent A (0.1% formic acid) to wash off impurities and salts. Glycopeptides were separated on C18 analytical column (150 mm x 100  $\mu\text{m}$ , 100  $\text{\AA}$ , Advanced Materials Technology) using a linear gradient from 0% to 80% of solvent B (80% ACN) in solvent A, at a flow rate of 1  $\mu\text{L}/\text{min}$  in a 90-minute analytical run.

Acquity UPLC was coupled to the mass spectrometer and the glycopeptides were fragmented by tandem MS/MS using CaptiveSpray interface, where nanoBooster was used to introduce gaseous

---

acetonitrile into nitrogen flow. The mass spectrometer operated in a positive ion mode; capillary voltage was set to 1300 V, nitrogen pressure was set to 0.2 bar and the drying gas to 4.0 l/min at 150 °C. Auto MS/MS method was used by selecting three precursor ions and exclusion criteria after three MS/MS spectra. Mass range was from 50 m/z to 4000 m/z, with spectra rate of 1 Hz. Transfer time was from 70  $\mu$ s to 150  $\mu$ s and pre-pulse storage was 12  $\mu$ s.

## 2.5.2 Data processing

### 2.5.2.1 Analysis at the proteomic level

The accession numbers of amino acid sequences for both mouse PrP (P04925) and sheep PrP with VRQ/VRQ polymorphism (Q712V9) were obtained from UniProt database and used in PeptideMass [189], a software tool located at the ExPASy server [190], which theoretically cleaves the protein with a chosen enzyme (in this thesis trypsin was used) and calculates the theoretical masses of the peptides. After tandem MS (MS/MS) analysis, the obtained raw file was analyzed using MaxQuant [191], to identify and quantify peptides from all proteins of an assigned proteome.

### 2.5.2.2 Analysis at the glycopeptide level

Glycan identification and quantification was performed by using DataAnalysis software (version 4.4, Bruker). Extracted ion chromatogram (EIC) corresponding to [HexNAcHex + H]<sup>+</sup>, one of the most common glycan-specific marker ions, with an m/z value of 366.13<sup>+</sup> was created and each sample was searched for the presence of glycan fragments. If the amino acid sequence confirming the PrP peptide was found in the MS/MS spectrum, it was searched for other glycan-specific ions, such as 204.08<sup>+</sup> [HexNAc + H]<sup>+</sup> and in case of sialylation m/z value of 292.09<sup>+</sup> [NeuAc + H]<sup>+</sup> [192]. Fragmentation spectra were analyzed by using GlycoWorkbench [193], a visual editor used not only for displaying glycan structures, but also for interpretation and annotation of glycan MS data. Glycan structures can be easily assembled, their mass (or that of glycopeptides) calculated rapidly, together with theoretical fragments obtained after MS<sub>n</sub> analysis.

After finding and confirming the presence of at least one glycopeptide at a given retention time, the base peak chromatogram (BPC) was searched for other m/z values corresponding to potential glycopeptides. A list of masses, corresponding to all multiple-charged ions of PrP glycopeptides detected for each structure, was created and characterized in GlycoMod [194], a computational tool that proposes all the possible glycan and glycopeptide structures from experimentally determined

mass values. GlyConnect database [195] was used to search for glycan structures of biological relevance, previously reported in one or more published articles. Even though some structures were not found in GlyConnect, they were still taken into consideration for further analysis, since not much is known about PrP glycan structures, therefore, we were not sure which structures we could expect to find. After determining which of the potential masses correspond to PrP glycopeptides, EIC was created for each structure, including  $m/z$  values of all the multiple charged states detected for each analyte.

Finally, by confirming the glycopeptides and choosing their corresponding EICs, all the chromatograms were integrated using DataAnalysis software (version 4.4), and relative areas were normalized by total area and calculated for each glycan structure in each prion strain.

## CHAPTER III

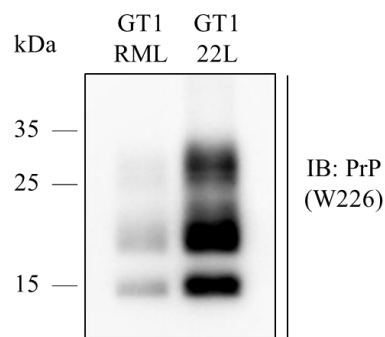
### 3 RESULTS

#### 3.1 Analysis of MoPrP<sup>Sc</sup>

##### 3.1.1 Optimizing isolation protocol of MoPrP<sup>Sc</sup>

###### 3.1.1.1 Initial testing with cell lines

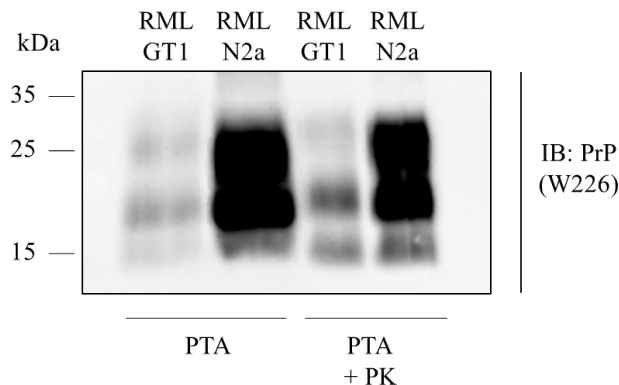
The initial isolation protocol was performed on GT1 cell line, infected both with RML and 22L scrapie-adapted prion strains. After collecting the cell lysate from one 10 cm Petri dish, the total amount of the protein was quantified using BCA protein assay; 500 µg of total protein was used in both cases and 20 µg/mL of PK was added to both samples. After obtaining the pellet from the ultracentrifuge, the samples were loaded on SDS-PAGE and immunoblotted on a membrane, where the presence of PrP<sup>Sc</sup> was confirmed (**Figure 11**). The immunoblot showed a much stronger signal in the case of GT1 infected with 22L, indicating a higher concentration of PrP<sup>Sc</sup>. Nevertheless, 500 µg of total protein was used for glycopeptide analysis for both samples.



**Figure 11.** Immunoblot of GT1 (infected with RML and 22L) cell lysates showing the presence of prions after PK digestion, having the di-, mono- and unglycosylated bands in both samples. In total, 500 µg of protein was used for loading. PrP<sup>Sc</sup> was detected by using W226 as anti-PrP mAb.

After confirming the presence of prions in the sample, in-solution trypsin digestion was used to obtain MoPrP<sup>Sc</sup> glycopeptides. Both samples were used for LC-MS analysis. Unfortunately, only one peptide from PrP (GE<sup>196</sup>NFTETDIK) was detected in the samples. Even though the peptide observed is the one carrying the glycosylation site (N-196), no other peptides or glycopeptides were detected, presumably because the amount of PrP<sup>Sc</sup> was too low in the starting material.

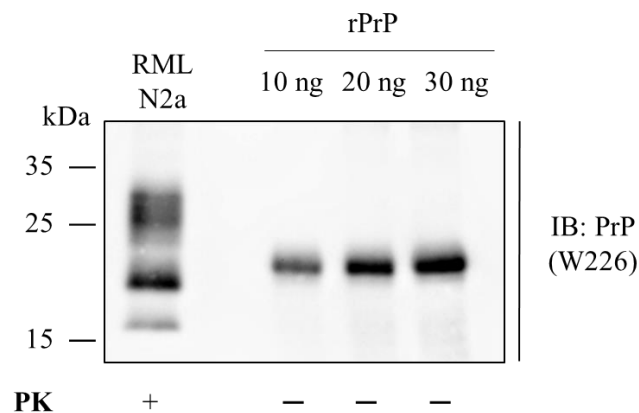
We moved on to test two different cell lines – GT1 and N2a, infected with RML. Our conclusion from the first experiment was that cell lysates from one Petri dish are not sufficient to produce enough protein to perform PrP characterization, therefore we decided to increase 10x the amount of total protein used. To do so, cells from three Petri dishes were collected and used for the protocol as followed. This time in combination with PK digestion, we decided to use PTA precipitation, widely used for PrP<sup>Sc</sup> isolation, since it is known that PTA preferentially promotes the precipitation of PrP<sup>Sc</sup> and not PrP<sup>C</sup> [196]. By performing PTA precipitation together in combination with PK digestion, the concentration of PrP<sup>Sc</sup> is increased (more clearly visible on GT1 RML cell lysates, **Figure 12**). Comparing the two cell lines, it was noticeable that ScN2a cell lysates have a higher concentration of PrP<sup>Sc</sup>. As it was confirmed on previous LC-MS analysis, PrP<sup>Sc</sup> collected from only one Petri dish was not sufficient to perform glycopeptide analysis, and since ScN2a not only have a higher concentration of prions, but also grow much faster than ScGT1 cells, we decided to use them in our further analysis.



**Figure 12.** Immunoblot of GT1 and N2a (infected with RML) cell lysates showing the presence of prions after PTA precipitation alone and PTA precipitation together with PK digestion.

To obtain a higher concentration of the protein, ScN2a cells were grown and collected over a couple of weeks. In the beginning, cell lysates from 4 Petri dishes were collected, but after realizing

the amount would not be enough, cell lysates from 60 Petri dishes (10 cm) were collected for protein isolation. The isolation was repeated as for the previous experiment – PrP<sup>Sc</sup> was first precipitated with PTA, after which PK digestion was performed by adding 20 µg/mL of PK, followed by incubation of 45 min. The pellet was obtained with ultracentrifugation and resuspended in 2X sample loading buffer – 1% of the resuspended pellet was used for immunoblotting, to confirm the presence of PrP<sup>Sc</sup> (**Figure 13**). Different amounts of recombinant PrP (rPrP) were also added on the gel (10, 20 and 30 ng), to approximate the amount of PrP<sup>Sc</sup> present in the samples.



**Figure 13.** Immunoblot of ScN2a cell lysates collected from 60 Petri dishes (10 cm), although only 1% of the final sample was loaded for the Western blot.

The remaining of the pellet was used to load on SDS-PAGE, stain the gel with Coomassie, followed by in-gel trypsin digestion (as described in Materials and methods). To minimize the loss of glycopeptides, the enrichment step was omitted. The pellet obtained after overnight trypsin digestion was reconstituted in H<sub>2</sub>O and ran on LC-MS/MS. The results were analyzed using MaxQuant, and as it is seen from **Table 2**, the prion protein was not the most abundant protein detected, it contributed to less than 5% of the total intensity. In fact, only around 20% of the protein's sequence was covered. Moreover, the trypsin itself was detected with a higher intensity than the prion protein itself, meaning that the trypsin concentration used for the digestion was too high. Even after using 60 Petri dishes (10 cm), the amount of PrP was not adequate to detect glycopeptides.

**Table 2.** MaxQuant results obtained from LC-MS/MS analysis of the band corresponding to PrP mass. Ten protein groups mostly contributing to the total intensity are shown, prion protein is marked in orange

Protein name	Number of peptides	% sequence coverage	Molecular weight / kDa	% intensity
Histone H4	4	34.0	11.37	11.96
Histone H2A	3	30.2	13.99	8.62
Histone H2B	4	27.0	13.99	8.08
Trypsin	3	16.5	24.41	6.92
Vitronectin	3	7.2	54.10	5.16
Major prion protein	4	22.0	27.98	4.51
40S ribosomal protein S8	3	18.8	24.21	4.14
60S ribosomal protein L13	4	19.4	24.31	3.11
Ferritin, two light chains	7	55.7	20.80	2.30
Histone H3.1, H3.2, H3.3	3	19.9	15.33	2.15

\* Sequence coverage represents the percentage of the protein sequence covered by the peptides.

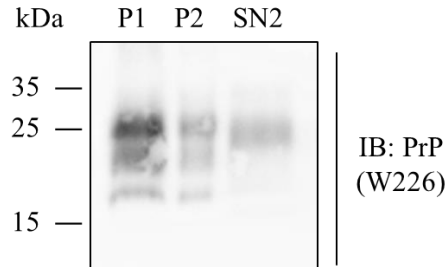
### 3.1.1.2 Using PMCA amplified material

In the initial tests with ScN2a, it has been shown that the necessary amount of the prion protein for glycopeptide analysis is difficult to obtain. Therefore, we decided to take advantage of PMCA, a technique widely used to accelerate the conversion of PrP<sup>C</sup> to PrP<sup>Sc</sup>, since in this way a high amount of PrP<sup>Sc</sup> can be acquired in a short period of time. PMCA seemed like a convenient way to get an increased amount of the starting material, to use it for developing the LC-MS method.

The PMCA sample was received from Milan (IRCCS Istituto Neurologico Carlo Besta), the pellet obtained was from total of 7 mL of PMCA reaction. The pellet, however, was quite large and insoluble. The idea was to load the sample on a gel and use in-gel trypsin digestion to obtain glycopeptides. Unfortunately, even after centrifugation of the total PMCA sample in the ultracentrifuge, the pellet was resuspended in 320  $\mu$ L of H<sub>2</sub>O, making it difficult to load the sample directly on the gel. We performed experiments to see if it would be possible to decrease the pellet.

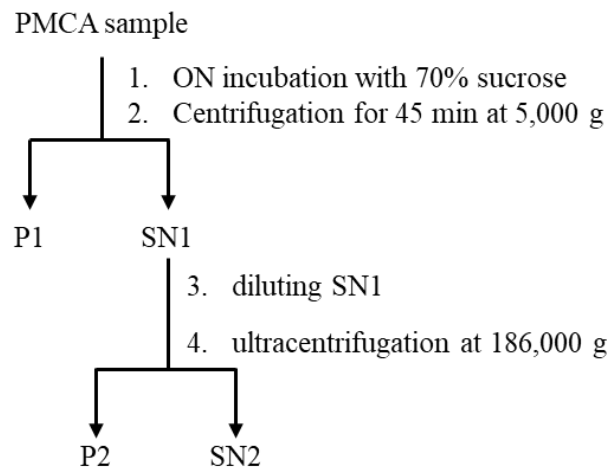
First, only 10  $\mu$ L of the PMCA sample was diluted with 4% sarkosyl and sonicated, since the pellet was not dissolving easily (sonication was performed in each test and each step where the pellet was present). Samples were centrifuged at 5,000 g for 10 min – P1 (pellet) and SN1 (supernatant)

were obtained. SN1 was centrifuged at 186,000 g in an ultracentrifuge – P2 and SN2. Both the pellets and the SN2 were collected and used for immunoblotting to check for loss of PrP<sup>Sc</sup> in the procedure (**Figure 14**). The idea was to keep the majority of PrP in P2 and in this way decrease the initial size of PMCA pellet.



**Figure 14.** Immunoblot of P1, P2 and SN2 left after the first trial with 10  $\mu$ L from total of 320  $\mu$ L PMCA amplified sample.

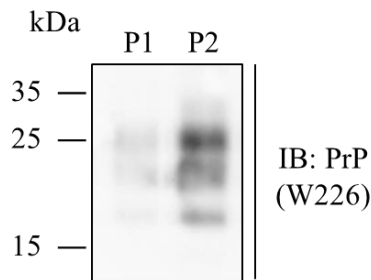
Since P1 had a higher concentration of PrP than P2, next we decided to use differential centrifugation with sucrose, which, together with PTA and sarkosyl, is a method commonly used for PrP<sup>Sc</sup> isolation [197-199]. The idea was to incubate the sample with sucrose, centrifuge it at low speed, so that the PrP is kept in the supernatant, after which the sample would be centrifuged in an ultracentrifuge and PrP<sup>Sc</sup> left in the final pellet. The experiment is similar to the first one performed, but adding the incubation with sucrose, the schematic representation is shown in **Figure 15**.



**Figure 15.** Scheme of the sucrose test performed with PrP<sup>Sc</sup> obtained from PMCA.



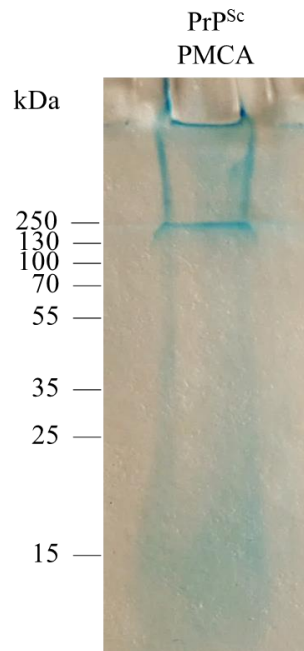
Again, 10  $\mu\text{L}$  of the total sample was used, incubated with 70% sucrose with shaking at 400 rpm overnight at room temperature. The sample was centrifuged again at 5,000 g, but this time prolonging the centrifugation – 45 min instead of 10 min. SN1 was collected and diluted with  $\text{H}_2\text{O}$  so that the concentration of sucrose was decreased 10x (until 7%). Diluted SN1 was ultracentrifuged at 186,000 g for 1 h and P2 was collected and analyzed by immunoblotting. The results are shown in **Figure 16**, and it can be seen that this time, by adding the sucrose, we were able to obtain the majority of  $\text{PrP}^{\text{Sc}}$  in the P2 pellet. Therefore, we decided to use this protocol on all of the PMCA sample.



**Figure 16.** Immunoblot of P1 and P2 from 10  $\mu\text{L}$  of PMCA samples obtained after performing the experiment at Figure 15.

Unfortunately, after upscaling the procedure to the remaining pellet of the PMCA sample, the pellet was still too big. Nevertheless, we managed to resuspend the sample in a smaller volume and load it on a gel, after which it was stained with Coomassie (**Figure 17**). Since the pellet was still too big, there were difficulties with sample loading. We were not able to clearly visualize bands corresponding to  $\text{PrP}^{\text{Sc}}$ , therefore, we decided not to continue with trypsin digestion protocol.

PMCA was used as a method which should have been able to provide a large amount of PrP. However, since the obtained material was not of good purity, we decided not to use further this approach, also because the  $\text{PrP}^{\text{Sc}}$  obtained in this way is from *in vitro* conversion. After these experiments we changed approach, based on differential centrifugation and the use of a density medium.



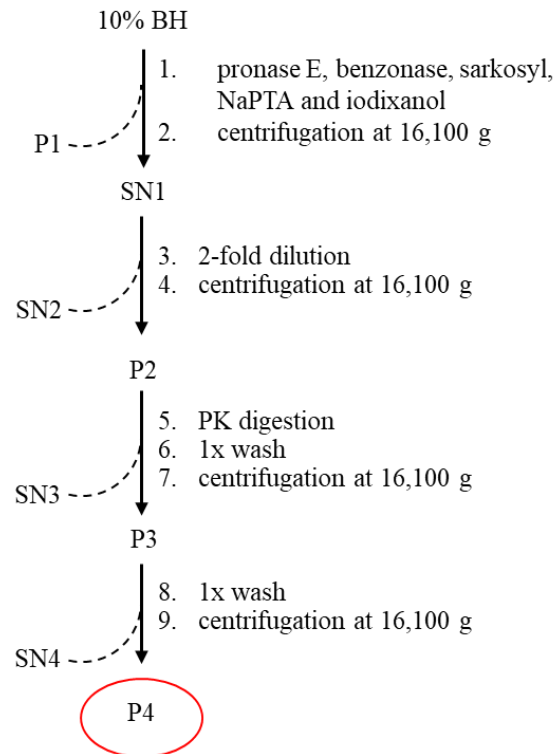
**Figure 17.** Coomassie stained gel of the remaining PMCA sample that was treated with sucrose and centrifugated as described.

### ***3.1.1.3 Protocols based on the use of density medium approach***

As it was described in section 2.2.4, these protocols were based on Wenborn et al. [183], where PrP<sup>Sc</sup> of high purity was managed to be isolated from brain tissue. The steps of the protocol are shown in **Figure 18**, they include main steps used before – use of sarkosyl to solubilize proteins, NaPTA to precipitate PrP<sup>Sc</sup> and PK digestion. The protocol included the use of pronase E, which digests the majority of PrP<sup>C</sup>, and other proteins present in the brain. Benzonase was also added, to degrade nucleic acid and to decrease the viscosity of the sample.

Another important step was the use of a density medium. Previously we tested the use of sucrose, however, we decided to use the density medium used in the paper, iodixanol. Iodixanol was added so that the final concentration was 35% (w/v) in the sample. After the first round of centrifugation at 16,100 g the sample was separated in P1 and SN1. Supernatant SN1, which is the one containing PrP<sup>Sc</sup> was diluted in a 1:1 ratio with an aqueous buffer, so that the concentration of iodixanol was reduced to 17.5%. The diluted SN1 was centrifuged and P2 was collected and treated further with PK.

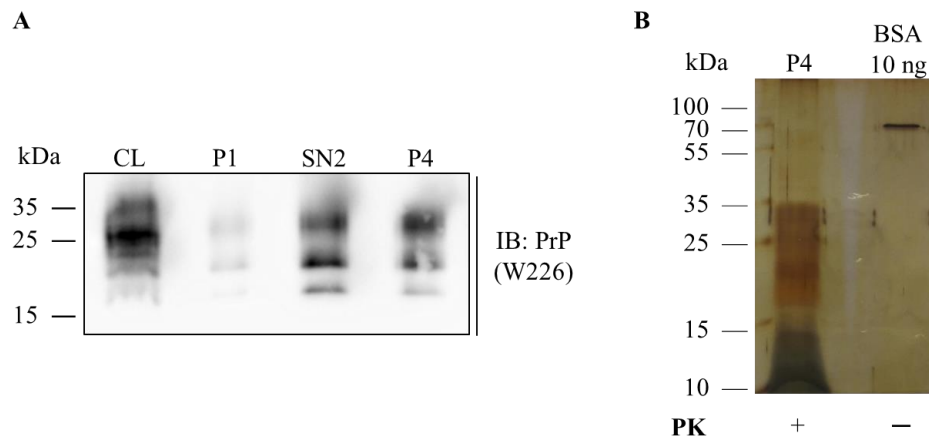
Generally, purification of prions from brain tissue is a major problem, the process is slowed down mainly because of their low abundance in affected tissue. Since the partial purification of prions developed by Prusiner and colleagues [200, 201], many other approaches have been reported [202]. Nonetheless, acquiring prions of high purity still remains an issue in the prion field, due to technical complexities and a need for large quantities of starting material. The aforementioned protocol was chosen since it is a relatively easy and straightforward method for prion isolation and results in highly purified prions. However, the protocol shown in the paper was developed on mammalian brain tissue, and since we lacked brain material, we decided to test this protocol on ScN2a cell lines.



**Figure 18.** Schematic of the purification method, P – pellet, SN – supernatant. Modified from [183].

From preceding tests, we realized that even 60 Petri dishes are not adequate to perform PrP characterization, therefore we decided to upscale the collection of cell lysates. In total, cells from around 750 Petri dishes were collected. Usually cells from around 20 Petri dishes were collected in the same 50 mL tube, lysed, aliquoted and stored at -80 °C until use.

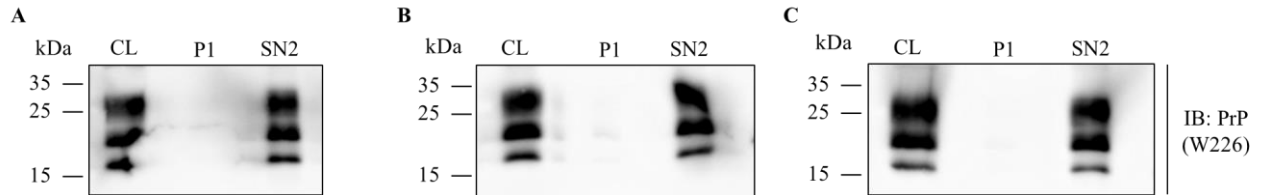
To test this protocol, 100  $\mu$ L of ScN2a cell lysate was used and the steps from **Figure 18** were followed. Since it was not shown in the paper what was the exact loss of PrP<sup>Sc</sup>, we performed an immunoblot containing pellet P1 and supernatant SN2, corresponding to two steps where the samples are discarded (**Figure 19, A**). Indeed, what we observed was that the signal from SN2 was similar to the one coming from P4, the final product, meaning that there is a lot of PrP<sup>Sc</sup> discarded in the process of isolation. Even though cell lysates from around 750 Petri dishes were collected, we wanted to try to adjust the protocol before using all of the sample, in order to have a higher yield of the isolated prion protein. Also, after observing the purity of the sample (**Figure 19, B**), it was difficult to distinguish bands corresponding to PrP<sup>Sc</sup>, meaning that the purity was not high enough. Also, by estimating the amount of the protein, it seemed that a lot less than 10 ng was present in the sample. For this reason, we decided to make some changes to the protocol, starting by changing the dilution ratio and centrifugation speed before obtaining SN2.



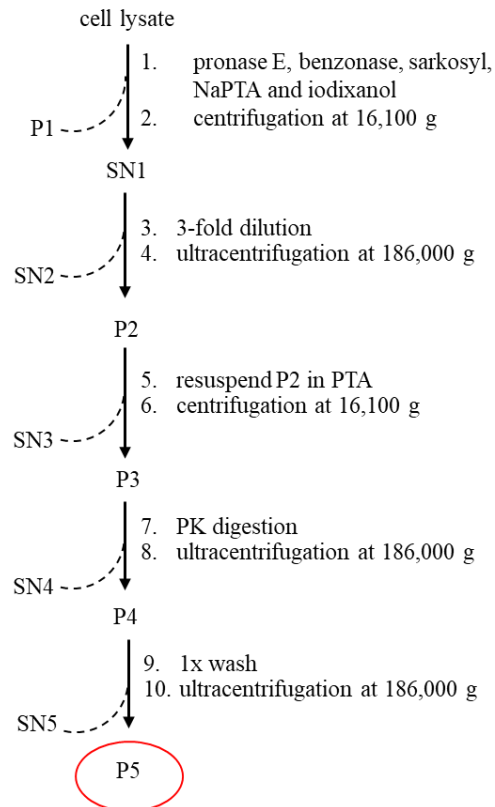
**Figure 19.** Isolation of MoPrP<sup>Sc</sup> from ScN2a (as shown in Figure 18). Immunoblot representing 20% of the 100  $\mu$ L PK-treated cell lysate (CL), P1, SN2 and P4 (**A**). Silver stained gel of PK-treated P4, together with 10 ng BSA, to approximate the amount of PrP<sup>Sc</sup> gained (**B**).

The idea was that by diluting SN1 in a 1:2 ratio, instead of 1:1, and by centrifugation either at 16,100 or 25,000 g, the concentration of PrP<sup>Sc</sup> in SN2 would be decreased. **Figure 20** shows immunoblots from three different conditions – 1:1 dilution + 16,100 g (the standard procedure); 1:2 dilution + 16,100 and 1:2 dilution + 25,000 g. None of the two new conditions (**Figure 20, B and C**) showed improvements, meaning that the amount of PrP<sup>Sc</sup> still present in SN2 was too high and comparable to the amount of protein present in the cell lysate.

Since we did not manage to increase the recovery of PrP<sup>Sc</sup> isolated with this protocol, we decided to perform another test – SN1 would be diluted 3-fold (1:2 ratio), and instead of centrifugation at 16,100 g, we would use the ultracentrifuge, together with an additional treatment with PTA and an extra wash of the pellet (**Figure 21**).

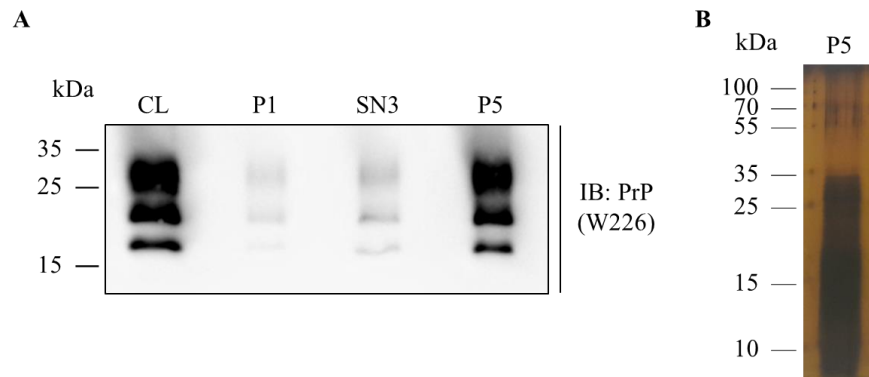


**Figure 20.** Immunoblot representing 5% of 200  $\mu$ L cell lysate, PK-treated cell lysate (CL), P1 and SN2. SN1 was diluted in a 1:1 ratio and centrifuged at 16,100 g (**A**). Dilution in a 1:2 ratio and centrifugation at 16,100 g (**B**). Dilution in a 1:2 ratio and centrifugation at 25,000 g (**C**).



**Figure 21.** Schematic of the adjusted purification method, P – pellet, SN – supernatant.

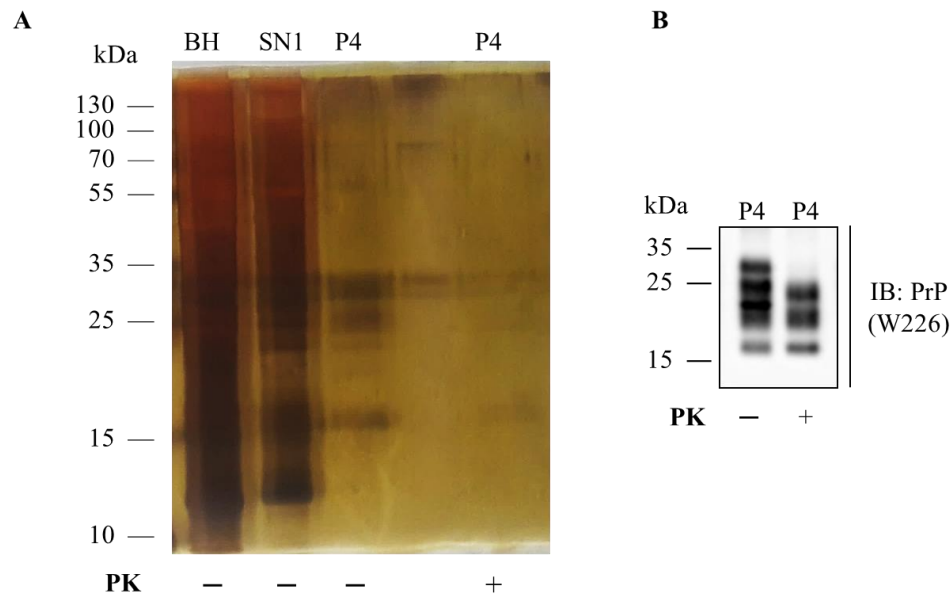
Even though the isolation protocol was not finalized, we decided to try upscaling the collection of cells, so that the protocol would be less time consuming. We lysed cells from 15 Petri dishes in 1 mL of the lysis buffer and took 150  $\mu$ L of those lysates to perform the final protocol mentioned. By observing the results of that new protocol (shown in **Figure 22**), the immunoblot (**A**) showed an increase in the recovery of PrP<sup>Sc</sup>, where the majority of protein was present in the final pellet, P5, instead the supernatant. Although the yield of PrP<sup>Sc</sup> in the final product was high, there was a loss regarding the purity of the protein (as seen on the silver stained gel in **Figure 22, B**).



**Figure 22.** Isolation of MoPrP<sup>Sc</sup> from 200  $\mu$ L of ScN2a by following the protocol as shown in Figure 21. Immunoblot representing 2% of the total sample, PK-treated cell lysate (CL), P1, SN3 and P5 (**A**). Silver stained gel of PK-treated P5 (**B**).

Unfortunately, we were not able to optimize the protocol for isolation of PrP<sup>Sc</sup> from cell lysates in a way that both the amount and purity of the protein were high enough. We concluded that the protocol with the density medium could not be optimized for isolation of PrP<sup>Sc</sup> on cell lines, and since it was actually developed on isolation from mammalian brain tissue, we tested the protocol on CD1 mouse brain infected with RML prion strain.

The initial protocol from **Figure 18** was tested on 10% brain homogenate and the results are shown in a similar fashion as was shown in the paper (**Figure 23**). The 10% brain homogenate, supernatant SN1, and pellet P4 were loaded on the gel (**A**) and silver stained. As it was shown in the paper, comparing the samples from the earlier stages of the procedure and P4, we were able to observe the final three band pattern is visible in P4, also confirmed by immunoblotting (**B**). By using 200  $\mu$ L of brain homogenate (the amount used in the paper), we were able to obtain PrP<sup>Sc</sup> of high purity, showing that the protocol indeed works well for mouse brain tissue.



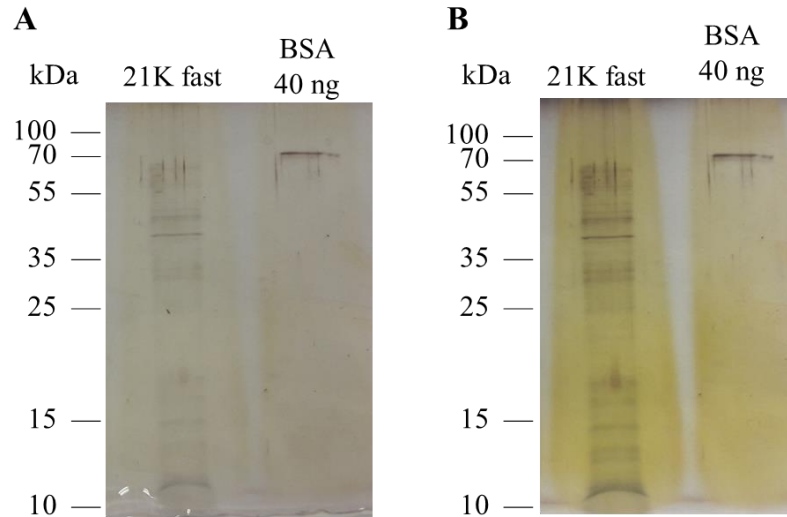
**Figure 23.** Isolation of MoPrP<sup>Sc</sup> from CD1 RML sample (as shown in Figure 18). Silver stained gel with untreated samples: an equivalent of 2  $\mu$ L of 10% brain homogenate (BH) and SN1 was loaded, while P4 and PK-treated P4 were obtained from 200  $\mu$ L of BH and 80% of the final pellet was loaded, while the rest was used for the immunoblot (A). Immunoblot of P4 with and without PK digestion (B).

By comparing the amount of brain tissue used in the paper, where even more than 200 mice brains were used, we concluded that unfortunately we did not have a sufficient amount of mice brain tissue. Fortunately, a collaboration with Prof. Olivier Andréoletti from Toulouse (Ecole Nationale Vétérinaire de Toulouse) was initiated, who kindly provided us with sheep brains infected with different prion strains, therefore we switched to using sheep brain tissue.

### 3.2 Optimizing isolation protocol of ovPrP<sup>Sc</sup>

Sheep brains infected with 21K fast, 21K slow and 19K prion strains were received. Out of those three strains, initial experiments were all done on 21K fast prion strain. We decided to test the protocol based on the density medium approach, since in the paper it was shown to work on mammalian brains. The protocol was followed in the exact same manner as in the paper, 200  $\mu$ L of brain homogenate infected with 21K fast strain was used for isolation. **Figure 24** shows the gel with the final P4 together with 40 ng BSA, at the usual developing time and after prolonging it, in order to have a better visualization of the bands. The protocol was optimized for mammalian brains, but

only for mouse, hamster and human brains. Unfortunately, it seemed that it does not work well when used on sheep brains, as seen from the silver stained gel.



**Figure 24.** Silver stained gel containing 21K fast strain, isolated by following the protocol described in section 2.2.4), together with 40 ng of BSA to approximate the concentration of isolated PrP<sup>Sc</sup>, by the usually shorter developing time (**A**) and longer developing time (**B**).

Until this point our major problem was the lack of a sufficient amount of starting material. Finally, by receiving sheep brains this point was solved. However, the problem of the protein's purity remained, so we tried to improve this protocol by performing immunopurification after the initial steps, and also decided to improve the density medium approach, with some modifications. The immunopurification approach will be presented first.

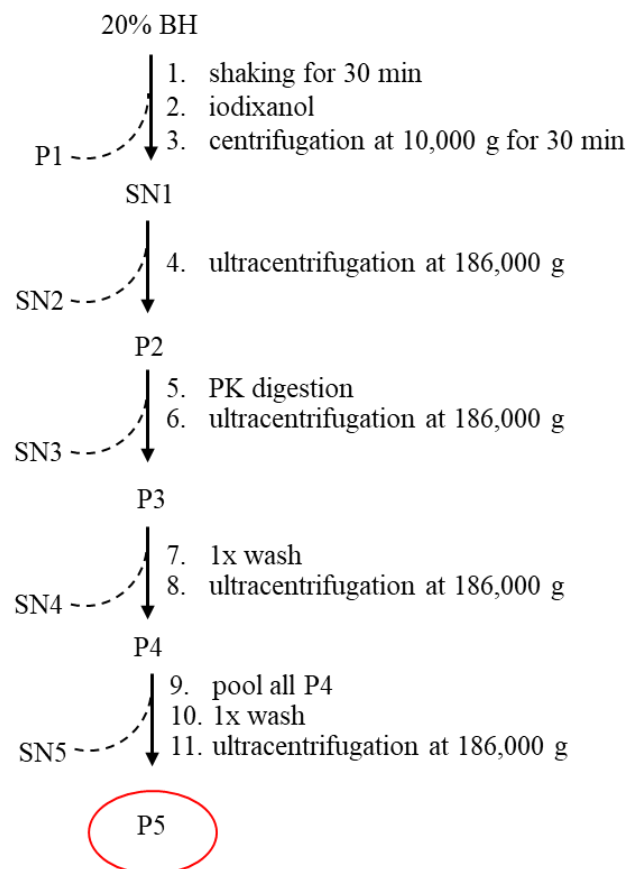
### 3.2.1 Immunopurification approach

For the immunopurification protocols, two mAbs were tested, SAF 61 and EF2, differing by their binding site; whereas EF2 binds at the N-terminus, the epitope for SAF 61 is located in the PK-resistant core (as shown in **Figure 1**).

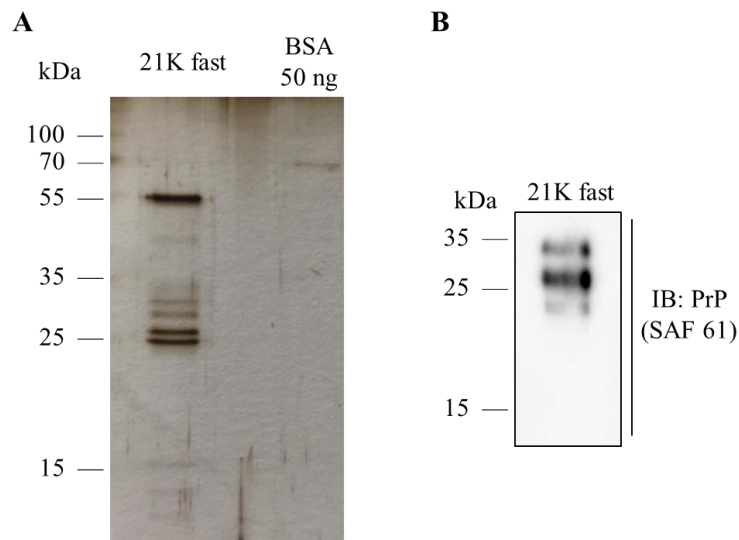
Before the immunoprecipitation, PrP<sup>Sc</sup> was partially purified by centrifugation, PK digestion and iodixanol (shown in **Figure 25**), similarly to the initial protocol from the paper (**Figure 18**). The protocol was, however, performed first by preparing a 20% brain homogenate (BH) instead of 10%, in order to decrease the volume of the starting material and preferably the time needed for isolation. Further on, since we had a total of 500 mL of 20% BH, we immediately upscaled the initial amount



of BH compared to the other samples tested (cell lines and mice brains). For the first test, sarkosyl was added to 5 mL of BH (reaching a final concentration of 4%), the sample was incubated with shaking for 30 min and then further incubated with iodixanol (final concentration of 20%). After vortexing well, the samples were divided into 1.5 mL tubes, centrifuged at 10,000 g for 30 min, after which all the **SN1** were collected and ultracentrifuged at 186,000 g. The pellets (**P2**) were resuspended and treated with 10 µg/mL PK, ultracentrifuged and washed. The **P3** pellets were washed once, after which they were pooled together in one tube and washed again. The final volume of **P5** was 500 µL, and 200 µL was taken for further incubation with SAF 61 mAb and Protein A magnetic beads (performed as described in section 2.2.5.1). After immunoprecipitation, the final pellet was resuspended in 10 µL, for which 9 µL was loaded on a gel and silver stained, while the remaining 1 µL was used for immunoblotting.



**Figure 25.** Scheme of the protocol used for partial purification of ovPrP<sup>Sc</sup> before incubation with mAb.



**Figure 26.** Silver stained gel after immunopurification of 21K fast PrP<sup>Sc</sup> by adding 15  $\mu$ g of SAF 61 directly to the protein and then incubating with Protein A magnetic beads; together with 50 ng of BSA as a way of approximating the concentration (**A**). Immunoblot confirming the presence of PrP<sup>Sc</sup>, which was detected by using SAF 61 as anti-PrP mAb (**B**).

The results of the first trial with SAF 61 are shown in **Figure 26**. The strong signals on the gel, around 25 and 55 kDa come from the mAb (IgG) itself, however, the rest of the bands present correspond to PrP<sup>Sc</sup>, confirmed also by immunoblotting (**A** and **B**). These preliminary results were promising, unfortunately, performing large-scale isolation in this manner would not be feasible, since the amount of the mAb necessary would be too much. There is also the problem of the signal corresponding to mAb, which is stronger than the protein itself and the 25 kDa band is too close to the monoglycosylated band of PrP<sup>Sc</sup>. Upscaling the isolation would lead to a much thicker band, causing problems to cut the band of the protein.

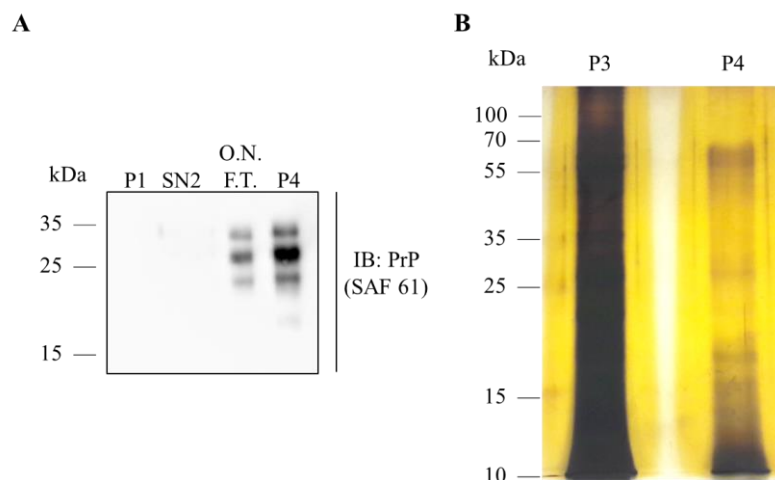
Since the amount of mAb was quite high after isolation, we decided first to couple the mAb to the beads. In this way the mAb would stay coupled to the beads and would not elute together with PrP<sup>Sc</sup>. SAF 61 was first coupled to Protein G beads using Co-Immunoprecipitation Kit. The protocol from **Figure 25** was also adjusted:

1. 4% sarkosyl was added to 20% BH and incubated for 30 min.
2. The sample was incubated for 10 min with benzonase.

3. A final concentration of 20% of iodixanol was added to the sample and after vortexing it well, the samples were divided into a maximum of twelve 1.5 mL tubes (so that they fit in the ultracentrifuge rotor).
4. Samples were centrifuged at 5,000 g for 30 min.
5. **SN1** was diluted 2-fold with 4% sarkosyl and then ultracentrifuged at 186,000 g.
6. **P2** were pooled together, digested with 10  $\mu\text{g}/\text{mL}$  of PK, and ultracentrifuged at 186,000 g.
7. **P3** was resuspended in 500  $\mu\text{L}$  of 1X PBS (containing 0.2% sarkosyl and protease inhibitor).

From the total P3, 200  $\mu\text{L}$  was added to the SAF 61-beads complex following the protocol described in section 2.2.5.2. After an overnight incubation, the protein was eluted with a solution of low pH (glycine HCl, pH 2.5) – 10% of it was used for immunoblotting, and the rest for silver staining. The initial steps of the protocol (before immunopurification) were checked for loss of PrP<sup>Sc</sup> throughout the procedure (**Figure 27, A**). By looking at the immunoblot, we noticed there is a presence of PrP<sup>Sc</sup> in the flow-through, meaning that the major loss of the protein is occurring in the immunoprecipitation step and not before. The sample before immunoprecipitation (P3) and after (P4) were checked with silver staining. P3 sample was obviously not purified at all, while P4 also contained too many bands, but the ones corresponding to the prion protein were quite poorly visible.

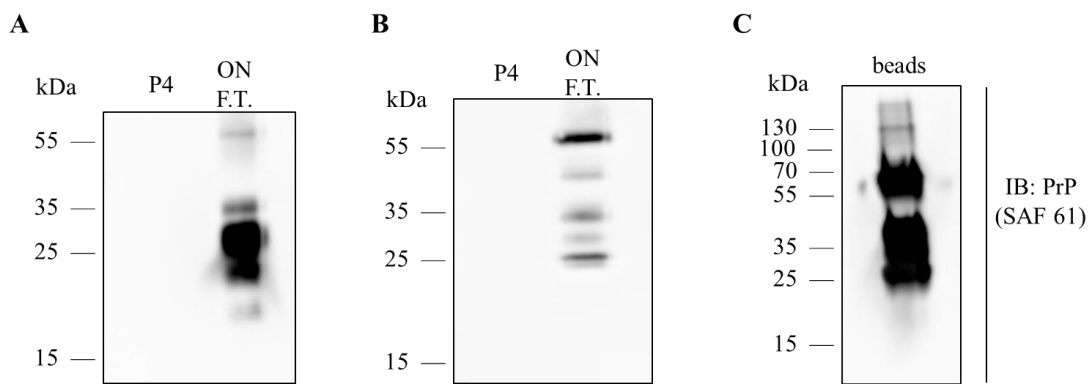
We also decided to test another mAb, an N-terminus antibody (EF2), again coupling it to Protein G beads. To do this, the protocol had to be adjusted, the incubation with mAb-beads needed to be done before PK digestion, since it digests the necessary epitope for EF2.



**Figure 27.** Immunoblot of the initial steps of the protocol: PK-treated P1 and SN2; overnight flow-through (O.N.-F.T.) and P4, obtained after immunopurification (**A**). Silver stained gel of the sample containing PrP<sup>Sc</sup> before (P3) and after (P4) immunoprecipitation (**B**).

The partial purification was performed in the same manner as last protocol but stopping at P2 and pooling the pellets together. This protocol was continued to be performed until 20 g of brain tissue was used. In the case SAF 61 was used, PK digestion was performed on P2 before incubation with the mAb-beads and for EF2 PK digestion was performed after elution of the sample from the beads. Both SAF 61 and EF2 were coupled to Protein G beads and the protein was eluted with solution of glycine HCl, pH 2.5 and the pellet was obtained after ultracentrifugation at 186,000 g. As seen in **Figure 28 (A and B)**, in both cases there is no visible signal for the pellet collected after immunoprecipitation. In both cases there is a strong signal in the flow-through, bands corresponding to PrP<sup>Sc</sup> and IgG are both visible.

There are two possible explanations for this: either PrP<sup>Sc</sup> did not bind to mAbs and just passes the column in the flow-through, or since PrP<sup>Sc</sup> is not a monomeric protein, but a multimer which aggregates, the epitope could be hidden, leading to a low amount of PrP<sup>Sc</sup> that binds to the mAb, and the rest (majority) of PrP<sup>Sc</sup> just passing through the column. So, we decided to check for the presence of PrP<sup>Sc</sup> on the beads coupled with EF2 that were used in the experiment on **Figure 28 (B)** by directly loading on an immunoblot. As it is seen in **Figure 28 (C)**, there is a very strong signal coming from both the protein and the mAb, meaning that there is also a binding of PrP<sup>Sc</sup> to the beads, which could not be eluted by using low pH buffer.

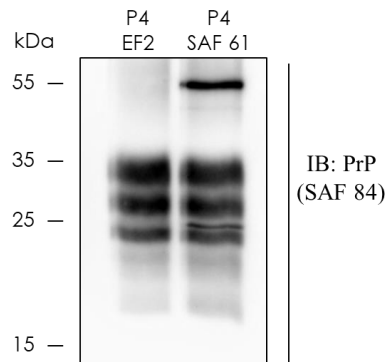


**Figure 28.** Immunoblot of pellets and flow-throughs obtained after immunopurification by coupling Protein G beads with SAF 61 (**A**) and EF2 (**B**). Protein G beads coupled to EF2 were also used to check on an immunoblot (**C**).

Since there was a strong signal of PrP<sup>Sc</sup> when the beads were loaded directly and immunoblotted, we realized that PrP<sup>Sc</sup> cannot be eluted from the mAb-beads complex with a low pH buffer. Therefore, we decided to elute the protein using denaturing conditions (using SDS solution).

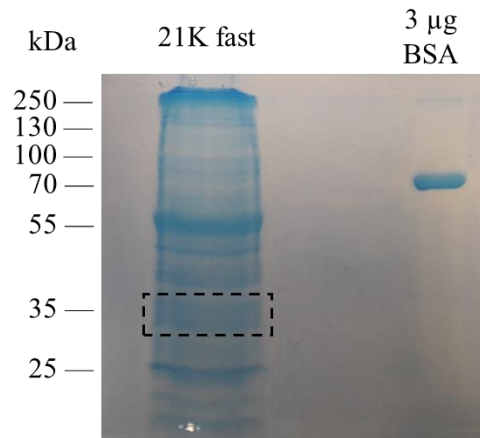
However, by using SDS, PrP<sup>Sc</sup> loses its conformation and propensity to aggregate, hence PK digestion and ultracentrifugation cannot be used to collect PrP<sup>Sc</sup>. Pooled P2 was prepared in the same way as before and instead of treating P4 with PK, thermolysin was used before incubation with EF2, since it digests PrP<sup>C</sup> and leaves PrP<sup>Sc</sup> in its full-length form. Protein was precipitated with acetone and after acquiring the pellets, they were used for immunoblotting. **Figure 29** shows the results obtained and we finally managed to acquire PrP<sup>Sc</sup> by eluting and centrifugation of the final P4 pellet. As it can be seen from the immunoblot, incubation with SAF 61 led to the presence of bands corresponding to IgG, while none were observed when using EF2.

The final results were satisfying, therefore we decided to continue immunoprecipitating the prion protein by using thermolysin digestion and EF2 as the mAb of choice.



**Figure 29.** Immunoblot of pellets obtained after immunopurification by coupling Protein G beads with SAF 61 and EF2, eluting the protein by using SDS, followed by acetone precipitation. PrP<sup>Sc</sup> was detected by using SAF 84 as anti-PrP mAb.

21K fast prion strain was isolated from approximately 160 mL of 20% BH, loaded on gel and stained with Coomassie. As **Figure 30** shows, many proteins actually co-eluted with the prion protein, which could be either due to unspecific binding to EF2 mAb or binding of other proteins to the beads themselves. By using denaturing conditions, all the proteins will co-elute together with the prion protein, leading to a decreased purity of the sample. Nevertheless, by comparing the results with the immunoblot obtained from 21K fast strain (**Figure 29**) we decided to cut out the part that corresponds to the diglycosylated band (marked with the dashed rectangle) and perform an in-gel trypsin digestion. For this first test on ovPrP<sup>Sc</sup> we prepared a solution of 5 ng/ $\mu$ L of trypsin, to avoid having a strong signal from trypsin in the LC-MS. Results of the analysis will be discussed in later sections.



**Figure 30.** Coomassie stained gel isolated from 160 mL of BH infected with 21K fast strain. PrP<sup>Sc</sup> was immunoprecipitated with EF2 and Protein G. BSA was also loaded on the gel (3 μg), to approximate the concentration of isolated PrP<sup>Sc</sup>. The dashed rectangle represents the part cut out from the gel and used for in-gel trypsin digestion.

Even though we were able to isolate PrP<sup>Sc</sup> by immunopurification, it was not purified enough, and the IgG bands were still too strong compared to the prion protein – the 25 kDa is too close to the monoglycosylated band, making it difficult to distinguish those two bands. Immunopurification works well small-scale (as seen in the silver stained gel in **Figure 26**), but upscaling the procedure leads to difficulties in purification and requires large amounts of mAb.

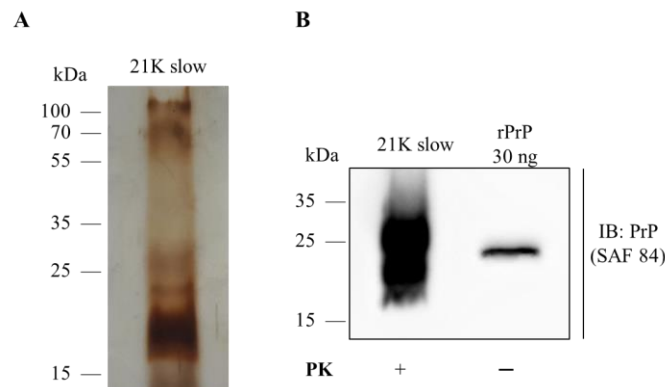
### 3.2.2 Use of a density medium approach

After finishing all the experiments with the immunopurification approach, almost all the 21K fast infected brains were used. Since we were not able to purify the sample enough, we decided to try to optimize the density medium approach. For further experiments, 21K slow prion strain was used, since not a lot of 21K fast infected brains were left. First, the 20% brain homogenate was prepared in 1X PBS containing 4% sarkosyl and protease inhibitor. We used 6 mL of BH and performed the protocol until P2 in the same way we did before immunoprecipitation. The remaining steps of “protocol I” were as follows:

1. To resuspend the pellet easier, instead of using 1X PBS, **P2** was resuspended in 1X RIPA buffer (25 mM Tris HCl pH 8.0, 150 mM NaCl, 1% Nonidet P-40 substitute, 1% sodium deoxycholate), sonicated, incubated with benzonase and ultracentrifuged at 186,000 g.

2. **P3** were sonicated in 1X PBS / 2% sarkosyl / 0.5% PTA, pooled together and incubated with constant shaking for 30 min. Iodixanol was added so that the final concentration was 30%, and after another incubation for 30 min, the samples were centrifuged at 16,100 g for 30 min.
3. **SN4** was diluted until the concentration of iodixanol reached 12%. Samples were incubated with shaking and centrifuged at 30,000 g for 1 h.
4. **P5** was digested with 20  $\mu\text{g/mL}$  of PK for 30 min and ultracentrifuged for 1 h at 186,000 g.
5. **P6** was washed with 0.5% sarkosyl and ultracentrifuged at 186,000 g.
6. **P7** was washed with 2% sarkosyl / 0.5% PTA / 12% iodixanol, incubated with shaking for 30 min and ultracentrifuged at 186,000 g for 1 h.
7. **P8** was washed in the same way and **P9** was obtained.

Results are shown in **Figure 31**, both in a silver stained gel and an immunoblot containing the final pellet (P9). Only 2% of the sample was loaded for immunoblotting, resulting in a very strong signal – comparing it to the 30 ng of rPrP, much more was present in P9. Even though the silver stained gel showed a presence of strong bands below 25 kDa, we were mostly interested in the fact that the bands around 25 kDa, corresponding to both di- and monoglycosylated bands, were nicely visible.



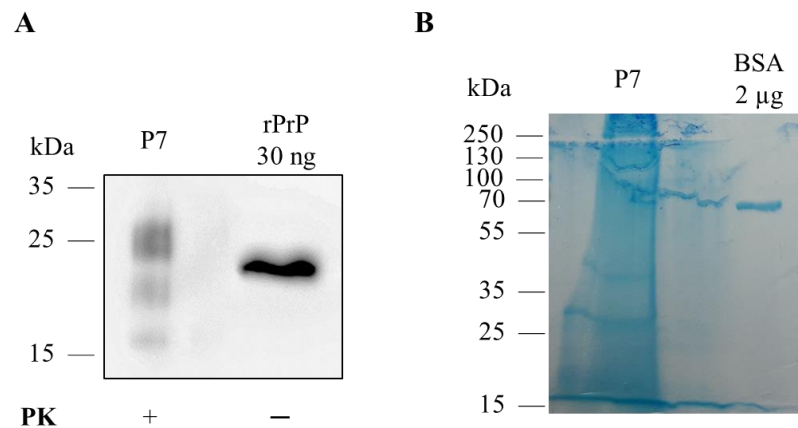
**Figure 31.** Silver stained gel containing the final pellet isolated from sheep brains infected with 21K slow strain by following “protocol I” (A). Corresponding immunoblot with the final pellet, together with 30 ng of rPrP, to approximate the concentration of PrP<sup>Sc</sup> isolated (B).

The next protocols tested were similar to “protocol I”, except that the procedure was upscaled even more – 15 mL of BH was used as a starting point. The “protocol II” went as followed:

1. Iodixanol was added to 15 mL of 20% BH (final concentration of 10%) and centrifuged for 30 min at 4,500 g, after which the SN1 was collected and transferred to 1.5 mL tubes.

2. **SN1** was centrifuged at 5,000 g for 1 h.
3. PTA was added to **SN2** so that the final concentration was 0.5% and the sample was incubated with constant shaking at 500 rpm for 1 h, after which it was centrifuged at 25,000 g for 90 min.
4. **P3** was incubated for 30 min in 2% sarkosyl containing 0.5% PTA and centrifuged again at 25,000 g for 90 min.
5. **P4** was resuspended in 1X RIPA buffer and digested with 20  $\mu\text{g}/\text{mL}$  PK for 30 min.
6. **P5** was obtained after ultracentrifugation at 186,000 g.
7. The pellet was washed two times in 1X RIPA and ultracentrifuged at 186,000 g, until **P7** was obtained.

The final pellet was used for loading on the gel, staining it with Coomassie, and 3% of it was checked on an immunoblot (**Figure 32**). Even if there were problems with gel running, there was a band visible between 25 and 35 kDa (corresponding to the diglycosylated band), which we decided to cut and do an in-gel trypsin digestion, again by using a 5  $\text{ng}/\mu\text{L}$  solution of trypsin.

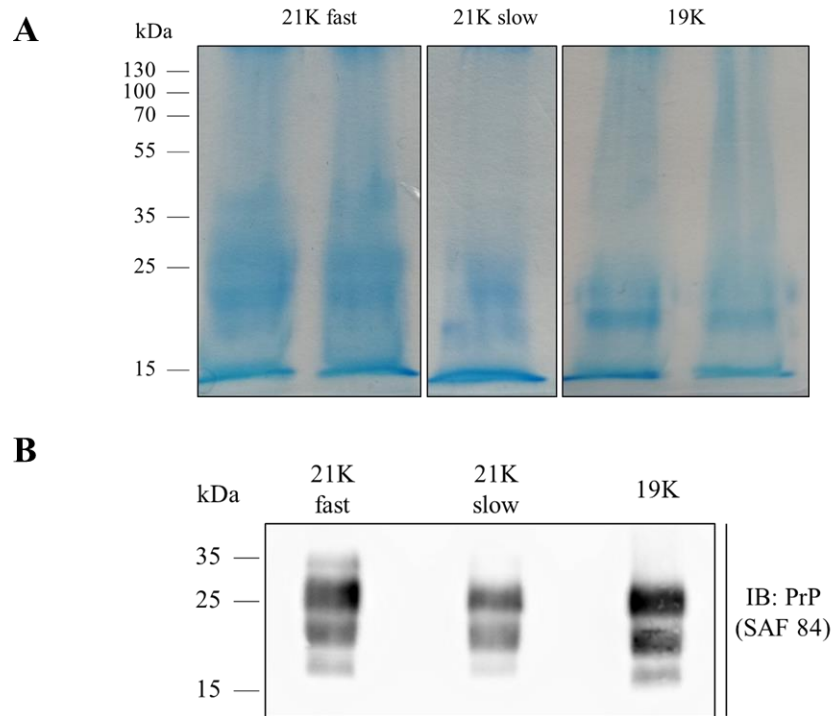


**Figure 32.** Immunoblot containing the final pellet isolated from sheep brains infected with 21K slow strain by following “protocol II”, together with 30 ng of rPrP (**A**). Coomassie stained gel with PrPSc isolated from 130 mL of 20% BH (**B**).

Both 21K fast and 21K slow strain were isolated, run on a gel and used for in-gel trypsin digestion. Since “protocol II” was less time-consuming, we decided this was our protocol of choice. All of 19K and the remaining of 21K fast and 21K slow strain were isolated using “protocol II”, and loaded on a gel, shown in **Figure 33** (**A**). All three strains had visible three-band patterns (for 21K slow strain it was a slightly weaker signal, since less starting material was used than for the other



two strains) and the presence of PrP<sup>Sc</sup> was confirmed with immunoblotting (**Figure 33, B**). All diglycosylated bands were cut and used for in-gel trypsin digestion and after drying the glycopeptides in the vacuum centrifuge, the two samples for 21K fast and the two for 19K were pooled together and used for analysis.



**Figure 33.** Coomassie stained gel containing PrP<sup>Sc</sup> isolated from sheep brains infected with all three strains, 21K fast, and 19K strain by following “protocol II” and the remaining of 21K slow from “protocol I” (**A**). Corresponding immunoblot of all three strains (**B**).

### 3.3 LC-MS/MS analysis of different ovPrP<sup>Sc</sup> strains

Diglycosylated gel bands used for in-gel trypsin digestion were from immunopurification (**Figure 30**), or the density medium approach (**Figure 32, Figure 33**). After overnight incubation with trypsin, dried glycopeptides were reconstituted in 20 $\mu$ L of H<sub>2</sub>O. For LC-MS analysis, 2  $\mu$ L were loaded (10% of the total sample). Proteomic analysis revealed that the relative intensity (normalized by total intensity) of the prion protein in the sample increases. For immunopurified 21K fast strain it was around 13%, for 21K slow strain after “protocol I” 58%, and for “protocol II” isolated 21K fast and 19K strain it was around 60%. From this we concluded that the density medium approach seems to be better for our large-scale PrP<sup>Sc</sup> isolation than the immunopurification one. “Protocol I”

and “protocol II” are based on the same approach, the only difference is that “protocol II” works faster for larger amount of the starting material. Therefore, “protocol II” should be used for large-scale isolation of PrP<sup>Sc</sup> from infected ovine brain tissue.

The accession number corresponding to the sheep prion protein (Q712V9) was entered in PeptideMass and theoretical masses of tryptic digests were calculated. The sheep prion protein carries two glycosylation sites, which are:

- N-184, located on YPNQVYYRPVDQYSNQNNFVHDCV<sup>184</sup>NITVK, a tryptic peptide of 3573.6735 Da (the mass of the peptide is larger by 57 Da, because the cysteine residue was treated with iodoacetamide).
- and N-200, located on GE<sup>200</sup>NFTETDIK, a smaller tryptic peptide of 1152.5299 Da. The peptides will further be referred to as simply N-184 and N-200.

After overnight trypsin digestion, no additional cleanup procedure was performed, and the sample was loaded directly on LC-MS (10% of the total sample). Analyzing these results, only one of the glycosylated peptides was observed, N-184. Since glycopeptide ionization is suppressed by peptides, HILIC enrichment was performed for further glycopeptide purification. Interestingly, after the enrichment, the peptide containing N-184 site was no longer observed. The reason could be due to the diversity in the peptides themselves, since N-184 peptide is more hydrophobic than the N-200 peptide, this could lead to its loss during the enrichment procedure. Unfortunately, there was not enough samples left to test the conditions for HILIC enrichment, in order to obtain both glycopeptides in one analytical run. Because of different response factors of the two glycosylated peptides, the relative quantification is performed within one glycosylation site – the N-184 peptide with direct injection of the sample obtained after trypsin digestion and N-200 peptide after HILIC enrichment.

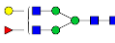






The analytical run for each analysis was 90 min. Because of differences in the peptide’s hydrophobicity, the glycosylated peptides elute at different retention times: N-200 glycopeptides from approximately 19 to 26 min, while N-184 glycopeptides from 33 to 36 min. The signals corresponding to glycopeptides were identified at the MS level. Also, the observed isotopic distribution of each glycopeptide was compared to the theoretical distribution (using <https://www.protpi.ch/Calculator/PeptideTool#Results>). An additional parameter used for glycopeptide verification was the value of the monoisotopic peak, so that the difference of the






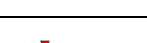





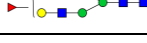




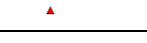


observed and theoretical  $m/z$  value was below 20 ppm. If possible, MS/MS data was used as the final verification step of the glycan composition. The glycan portion was identified by searching the low molecular glycan-specific marker ions. Signals corresponding to the peptide portion were identified by searching values of peptides' b and y ions; theoretical values obtained by a fragment calculator (<http://db.systemsbio.net:8080/proteomicsToolkit/FragIonServlet.html>). Another confirmation was the presence of fragments corresponding to the peptide containing one (or two) GlcNAc residue, peptide with one GlcNAc and Fuc residue, confirming core fucose, and so on.

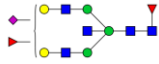
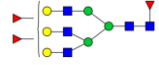



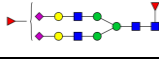
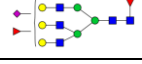
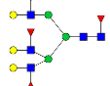
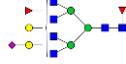
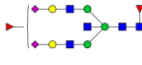
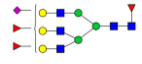
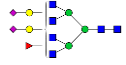
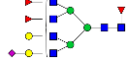
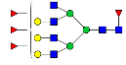




### 3.3.1 Analysis of N-184 glycosylation site



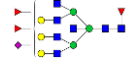
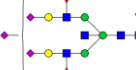

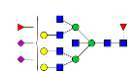
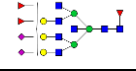
A list of  $m/z$  values was obtained as described in Materials and methods. The  $m/z$  values were converted to a peak list of singly charged species, which were then searched against GlycoMod. In total, 51 glycan compositions were detected in all three strains at the N-184 glycosylation site. The list of all the glycan composition, together with their proposed structures can be seen in **Table 3**.

**Table 3.** List of all the proposed glycan structures on N-184 glycosylation site detected specifically for each strain. H – hexose, N – *N*-acetylhexosamine, F – fucose and S – *N*-acetylneuraminic acid (sialic acid).

#	Glycan composition	Proposed structure	Theoretical $m/z$ [M+H] <sup>+</sup>	Detected		
				21K fast	21K slow	19K
1	H4N4F1		5181.2675	+	+	+
2	H3N5F1		5222.2941	+	+	+
3	H5N3F2		5286.2988	+	+	+
4	H4N4F2		5327.3254	+	+	+
5	H5N4F1		5343.3203	+	+	+
6	H4N5F1		5384.3469	+	+	+
7	H5N3S1F1		5431.3363	+	+	+

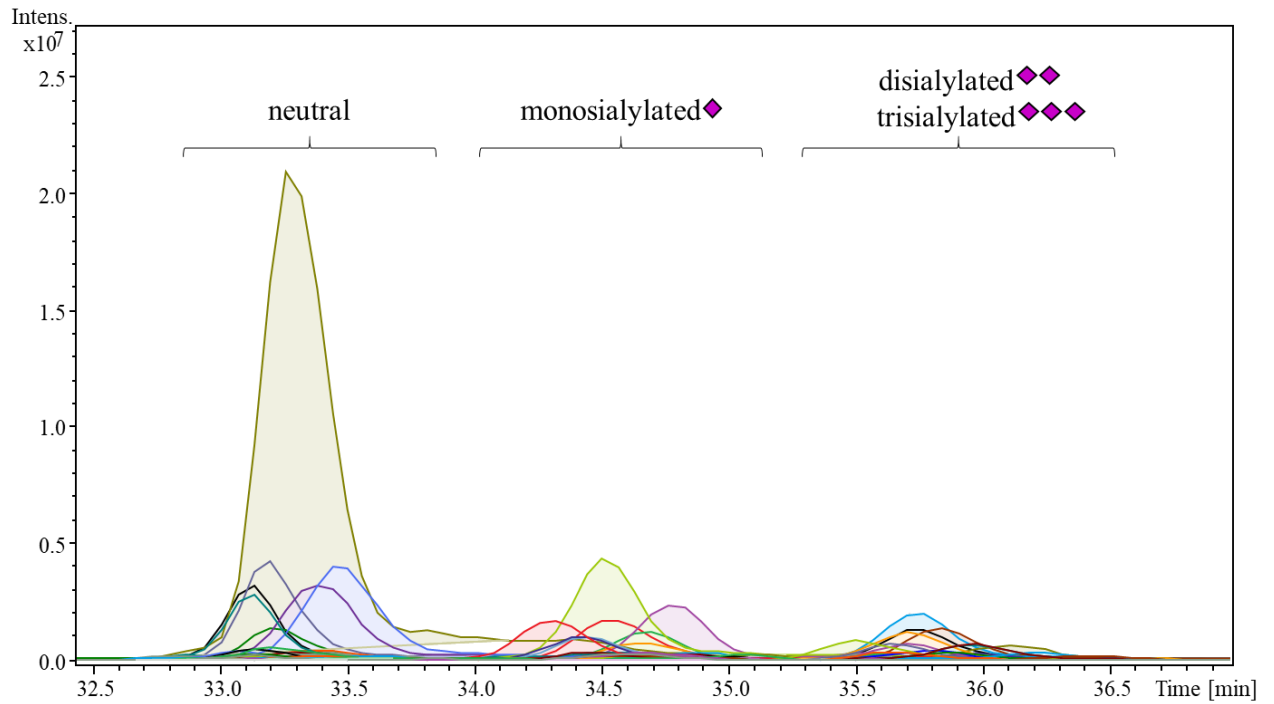
8	H4N4S1F1		5472.3629	+	+	+
9	H5N4F2		5489.3782	+	+	+
10	H4N5F2		5530.4048	+	+	+
11	H4N6F1		5587.4263	/	/	+
12	H5N4S1F1		5634.4157	+	+	+
13	H5N4F3		5635.4361	+	+	+
14	H4N5S1F1		5675.4423	+	+	+
15	H5N5F2		5692.4576	+	+	+
16	H4N6F2		5733.4842	+	+	+
17	H5N4S1F2		5780.4736	+	+	+
18	H6N4F3		5797.4889	+	+	+
19	H4N5S1F2		5821.5002	+	+	+
20	H5N5S1F1		5837.4951	+	/	/
21	H5N5F3		5838.5155	+	+	+
22	H4N6S1F1		5878.5217	+	+	+
23	H5N6F2		5895.5370	+	+	+
24	H6N4S1F2		5942.5264	+	+	+
25	H7N4F3		5959.5417	+	+	/
26	H4N5S2F1		5966.5377	+	+	+

27	H5N5S1F2		5983.5530	+	+	+
28	H6N5F3		6000.5683	+	+	+
29	H5N3S3F1		6013.5271	+	/	+
30	H5N6S1F1		6040.5745	+	+	+
31	H5N6F3		6041.5949	+	+	+
32	H5N4S2F2		6071.5690	+	+	+
33	H6N5S1F2		6145.6058	+	+	+
34	H6N5F4		6146.6262	+	+	+
35	H5N6S1F2		6186.6324	+	+	+
36	H5N5S2F2		6274.6484	+	+	+
37	H6N5S1F3		6291.6637	+	+	+
38	H5N6S2F1		6331.6699	+	+	+
39	H5N6S1F3		6332.6903	+	+	+
40	H6N6F4		6349.7056	+	+	+
41	H5N7S1F2		6389.7118	+	+	+
42	H5N6S2F2		6477.7278	+	+	+
43	H6N6S1F3		6494.7431	+	+	+
44	H5N5S3F2		6565.7438	+	+	+

45	H6N6S2F2		6639.7806	+	+	+
46	H5N7S2F2		6680.8072	+	+	+
47	H6N7S1F3		6697.8225	+	+	+
48	H5N5S3F3		6711.8017	/	/	+
49	H6N6S2F3		6785.8385	+	+	+
50	H6N7S2F2		6842.8600	+	+	+
51	H6N7S2F3		6988.9179	+	+	+

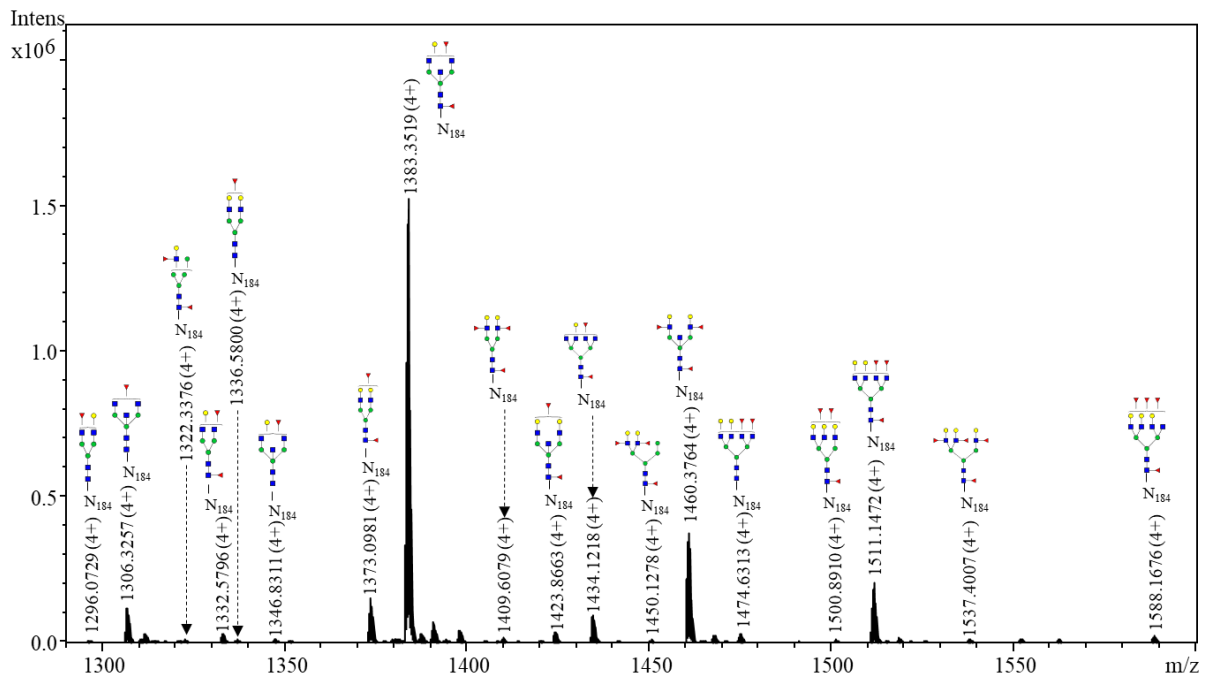
As it was mentioned before, the N-184 glycopeptides elute from 33 to 36 min. **Figure 34** represents EICs for different 21K fast PrP<sup>Sc</sup> glycopeptides. It is observed that the neutral and charged glycopeptides elute in separate retention time frames : neutral ones elute first and were detected in the range from 33 – 33.8, followed by monosialylated structures from 34 – 35.1, and finally, disialylated (together with one trisialylated glycoform) from 35.5 – 36.2 min.

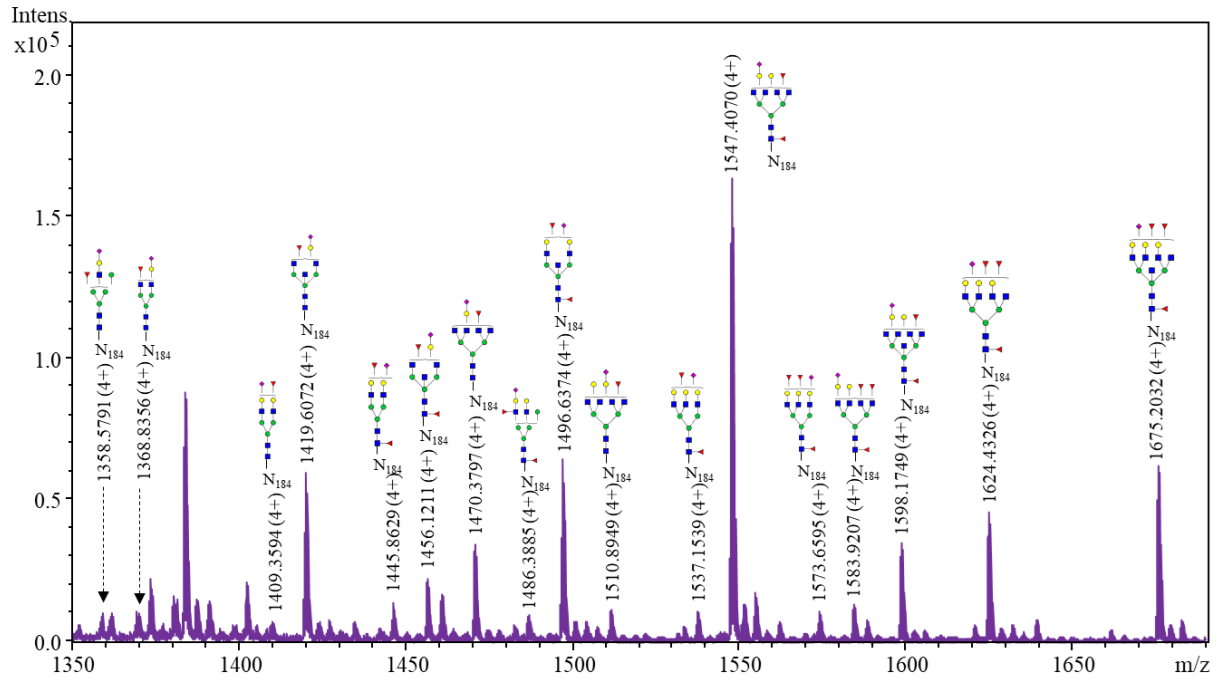
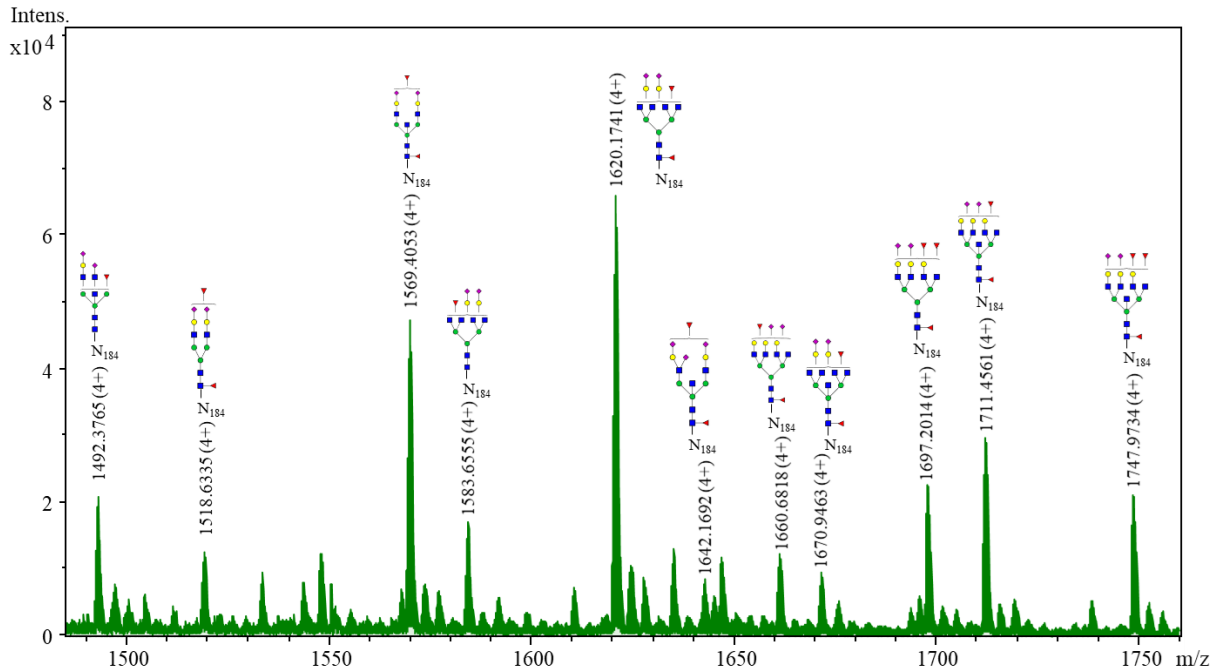
**Figure 35 (A–C)** represents averaged full MS with the assigned N-184 glycopeptides. The  $m/z$  values for these glycopeptides were generally in both 4+ and 5+ charged state (4+ charged state illustrated on the MS spectra) and thus both  $m/z$  values were used for generating the EIC. In the case of more abundant glycopeptides, additionally 3+ charged state was also observed and therefore used for generating EIC. For some glycopeptides of lower intensities, only the 4+ state was observed, and was the only one used for the EIC. All the structures detected were fucosylated (at least one fucose residue was present), 8 of them were biantennary, 3 triantennary, 13 tetraantennary, while 16 of them had bisecting GlcNAc. Only 4 hybrid structures were detected, while the rest were complex structures and no high mannose structures were detected.



**Figure 34.** Extracted ion chromatograms of 46 detected N-184 glycopeptides, mutual for all three strains, with different retention times for neutral, mono- and di-/trisialylated structures.

**A**



**B****C**

**Figure 35.** Assigned glycoforms in MS with the N-184 peptide backbone. Neutral (A), monosialylated (B), and disialylated (+ one trisialylated) glycoforms (C) were detected in different retention times.

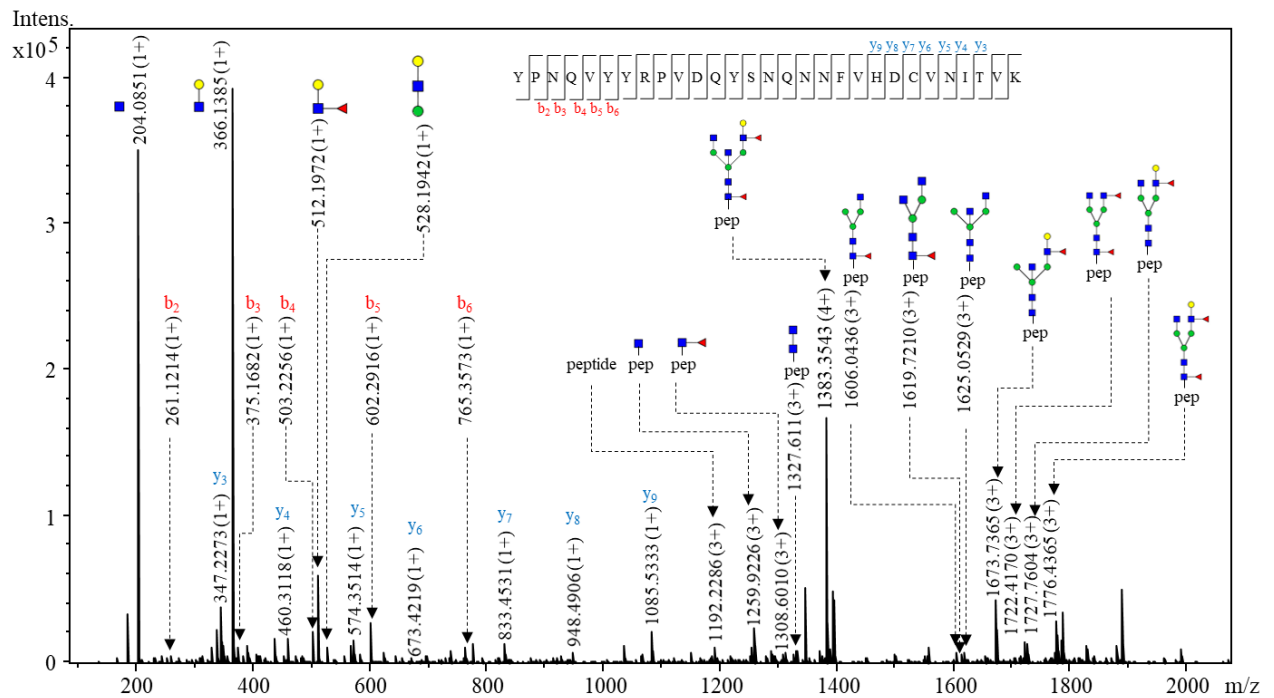


Out of the 51 detected structures, 21 of them were confirmed by MS/MS spectra. The “quick” search was usually done by checking if the MS/MS spectrum contained the  $m/z$  value of the peptide fragment itself, which in the case of N-184 peptide, was the  $y$  ion with  $m/z$  value of 1192.2247 (3+). The other confirmation of the peptide portion was the fragment from the peptide carrying GlcNAc residue, usually with a higher intensity than the peptide itself, with  $m/z$  value of 1259.9178 (3+). The amino acid sequence was confirmed with the presence of mainly  $y$  ions ( $y_3 - y_9$ ), but in some cases also  $b$  ions were detected ( $b_2 - b_6$ ), as seen on **Figure 36**. After confirming that the glycopeptide is in fact a prion glycopeptide, the glycan structural features were annotated by searching the main glycan diagnostic ions,  $m/z$  values of:

- 204.08 (1+) representing one *N*-acetylhexosamine (HexNAc) residue,
- 366.13 (1+) representing HexNAc + Hex residue,
- 512.19 (1+) in case outer-arm fucose was present (Hex + HexNAc + Fuc residue), and
- 657.22 (+1) in case of sialylation, corresponding to the HexNAc + Hex + NeuAc residue.

N-glycan structures can be annotated from the MS/MS spectrum even if information regarding some fragments is missing, because of known biosynthetic pathways in the N-glycan formation [115]. As it can be seen from the MS/MS spectrum of the N-184 peptide containing N-glycan with a composition of H4N5F2 (**Figure 36**), it is a neutral structure, containing one agalactosyl antennae, carrying two fucose residues, one core and another outer-arm fucose. No sialic acids were found on the glycopeptide, since the fragment of  $m/z$  value 657.22 (1+) was not detected. Another interesting feature of this structure was the presence of bisecting GlcNAc, even though of low intensity,  $m/z$  value of 1619.72 (3+) indicates this. This structure was found as the major N-glycan also on mouse PrP<sup>Sc</sup> [162]. It is important to emphasize, however, that all the structures reported here are considered as proposed, since the MS/MS data obtained in positive mode cannot reveal all glycan structural features.

One of the most interesting glycans found on this glycosylation site was H5N5S3F2, suggested to contain 6-sialyl-LewisX (6sLeX) structure, where NeuAc residue is directly attached to the GlcNAc residue, proposed because of the presence of the fragment with  $m/z$  value 495.18 (1+), corresponding to HexNAc + NeuAc. This structure was not observed previously in the study on mouse PrP<sup>Sc</sup>, however, it is known to be present in the brain [203-205].



**Figure 36.** Example of N-184 glycopeptide whose structure was confirmed by MS/MS, the precursor ion with  $m/z$  value of 1383.3543 (+4) is shown. Fragments of glycan-specific marker ions are represented, together with b and y ions confirming the amino acid sequence and fragments of the peptide backbone with the N-glycan H4N5F2.





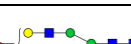





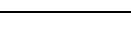
### 3.3.1.1 Quantitative analysis of N-184 glycosylation site from different prion strains

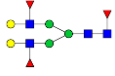
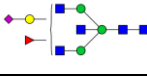



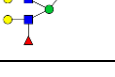

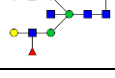




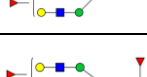
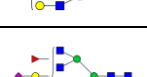

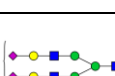
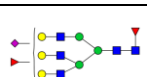

Out of the total 51 proposed structures, the minimal set of mutual ones was 46, hence, these were used for further quantification and comparison. The composition of the remaining five N-glycans not used for quantification are: H5N5S1F1 detected in 21K fast strain; H7N4F3 in 21K slow strain; and H4N6F1, H5N5S3F3 and H5N3S3F1 in 19K strain, all the compositions with relative abundances below 1%. Therefore, it cannot be claimed that these structures are not present in other strains, since their abundance is low, it is possible they were not detected simply because their signals were too low. Out of the mutual structures, 18 of them are neutral (39.13%) and 28 are sialylated structures (60.87%). Most of the sialylated structures are monosialylated, 17 of the total N-glycans (36.95%), 10 of them are disialylated (21.74%) and only one structure is trisialylated.

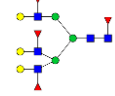
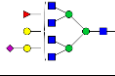


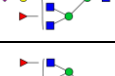






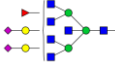
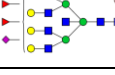




The EICs were integrated in DataAnalysis, from which absolute peak areas for each glycopeptide were obtained. Relative abundance for each glycopeptide was normalized by total area; peak area of each glycopeptide in each sample was divided by total area of the sample (values seen

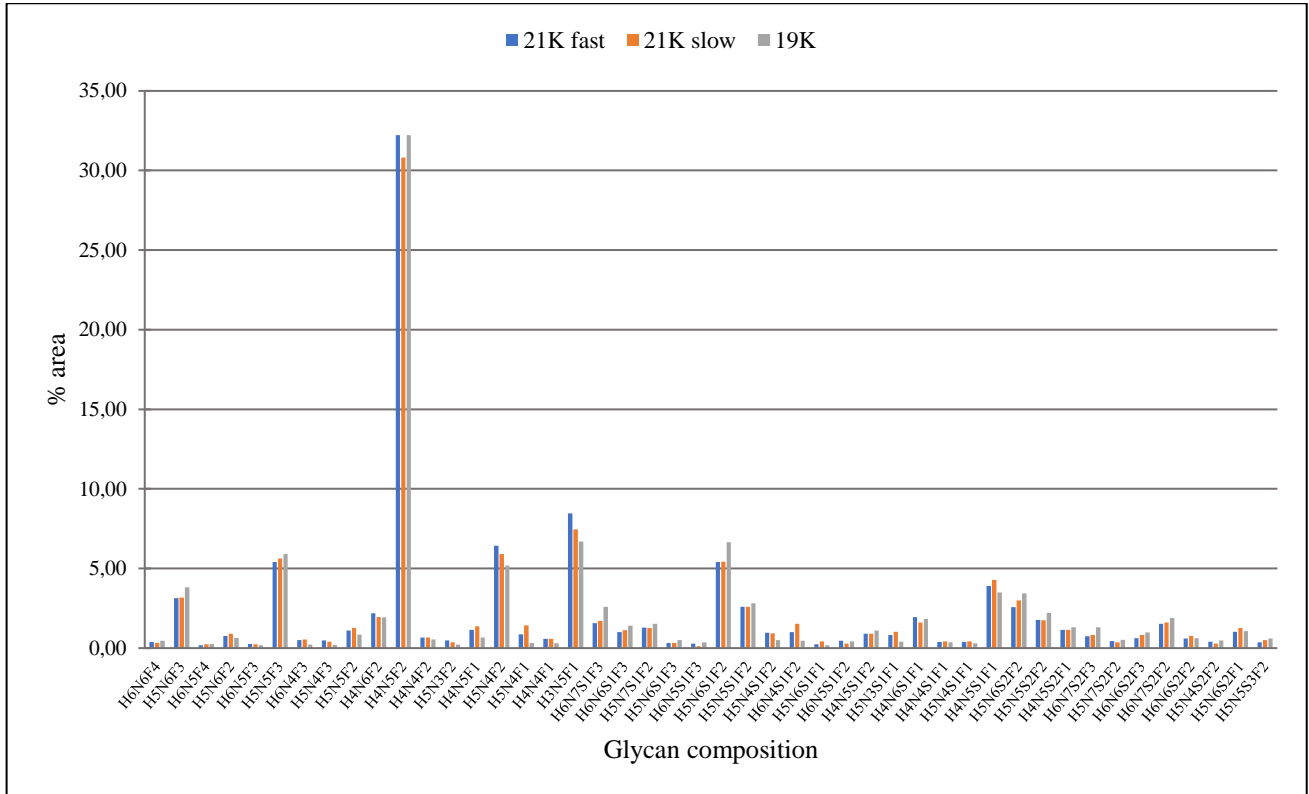
in **Table 4**). This was done for the mutual 46 structures in each strain. The most abundant structure (H4N5F2) was found to be the same for all three strains, contributing to around 30%. The next most abundant glycoforms are: H3N5F1 (6.7 – 8.4%), H5N5F3 (5.4 – 5.9%) – both with bisecting GlcNAc, H5N4F2 (5.2 – 6.4%) – a neutral glycan structure, and H5N6S1F2 (5.4 – 6.6%) – monosialylated, while the abundance of all the other glycopeptides was below 5% (shown in the table). The similarities between 21K fast, 21K slow and 19K prion strains can be visualized better with the bar representation of percentages of relative area, seen on **Figure 37**, where no major differences were detected.

**Table 4.** List of the proposed glycan structures on N-184 glycosylation site, mutual for all three strains; together with the glycan composition and their relative abundance. Major glycan structure marked in bold. H – hexose, N – *N*-acetylhexosamine, F – fucose and S – *N*-acetylneuraminic acid (sialic acid).

#	Glycan composition	Proposed structure	Theoretical m/z [M+H] <sup>+</sup>	21K fast	21K slow	19K
				%area		
1	H4N4F1		5181.2675	0.57	0.58	0.31
2	H3N5F1		5222.2941	8.47	7.46	6.69
3	H5N3F2		5286.2988	0.49	0.37	0.23
4	H4N4F2		5327.3254	0.67	0.67	0.55
5	H5N4F1		5343.3203	0.86	1.42	0.33
6	H4N5F1		5384.3469	1.15	1.38	0.67
7	H5N3S1F1		5431.3363	0.83	1.02	0.41
8	H4N4S1F1		5472.3629	0.39	0.42	0.36
9	H5N4F2		5489.3782	6.44	5.92	5.18
<b>10</b>	<b>H4N5F2</b>		5530.4048	<b>32.21</b>	<b>30.81</b>	<b>32.21</b>
11	H5N4S1F1		5634.4157	0.37	0.42	0.31

12	H5N4F3		5635.4361	0.49	0.39	0.21
13	H4N5S1F1		5675.4423	3.89	4.29	3.49
14	H5N5F2		5692.4576	1.11	1.26	0.85
15	H4N6F2		5733.4842	2.19	1.96	1.93
16	H5N4S1F2		5780.4736	0.96	0.92	0.51
17	H6N4F3		5797.4889	0.51	0.55	0.22
18	H4N5S1F2		5821.5002	0.90	0.90	1.10
19	H5N5F3		5838.5155	5.42	5.63	5.91
20	H4N6S1F1		5878.5217	1.94	1.62	1.84
21	H5N6F2		5895.5370	0.77	0.90	0.64
22	H6N4S1F2		5942.5264	1.01	1.52	0.47
23	H4N5S2F1		5966.5377	1.14	1.14	1.31
24	H5N5S1F2		5983.5530	2.59	2.59	2.81
25	H6N5F3		6000.5683	0.26	0.25	0.19
26	H5N6S1F1		6040.5745	0.25	0.43	0.18
27	H5N6F3		6041.5949	3.13	3.18	3.82
28	H5N4S2F2		6071.5690	0.41	0.27	0.47
29	H6N5S1F2		6145.6058	0.47	0.27	0.43

30	H6N5F4		6146.6262	0.18	0.23	0.26
31	H5N6S1F2		6186.6324	5.41	5.42	6.65
32	H5N5S2F2		6274.6484	1.76	1.76	2.20
33	H6N5S1F3		6291.6637	0.28	0.13	0.36
34	H5N6S2F1		6331.6699	1.02	1.26	1.06
35	H5N6S1F3		6332.6903	0.32	0.33	0.51
36	H6N6F4		6349.7056	0.37	0.33	0.46
37	H5N7S1F2		6389.7118	1.29	1.27	1.53
38	H5N6S2F2		6477.7278	2.58	2.99	3.43
39	H6N6S1F3		6494.7431	1.00	1.13	1.41
40	H5N5S3F2		6565.7438	0.37	0.50	0.61
41	H6N6S2F2		6639.7806	0.60	0.76	0.63
42	H5N7S2F2		6680.8072	0.45	0.36	0.52
43	H6N7S1F3		6697.8225	1.56	1.72	2.60
44	H6N6S2F3		6785.8385	0.63	0.82	0.98
45	H6N7S2F2		6842.8600	1.54	1.60	1.88
46	H6N7S2F3		6988.9179	0.74	0.83	1.30



**Figure 37.** Bar representation of relative abundance of N-glycans on N-184 peptide expressed as percentage of total normalized area. Total of 46 N-glycan structures were quantitatively compared between 21K fast, 21K slow and 19K prion strains.

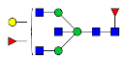
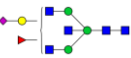


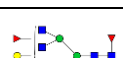



### 3.3.2 Analysis of N-200 glycosylation site

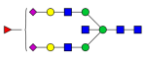















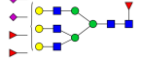
For the analysis of N-184 glycopeptides, 10% of the total sample amount after trypsin digestion was used, which was enough for detection. However, N-200 glycopeptides were detected only after performing HILIC enrichment. Since the amount of isolated PrP<sup>Sc</sup> was approximated simply by observing the Coomassie stained gel, it was not possible to know for certainty what amount was used for HILIC. Generally, around 30-50% of the total sample was used for enrichment, in order to save as much as possible of the sample, in case the analysis had to be repeated.

The first sample tested for HILIC was the immunopurified 21K fast PrP<sup>Sc</sup>. Since this was a preliminary test for sheep PrP<sup>Sc</sup> glycopeptide analysis, we decided to use all the remaining sample, to be sure the glycopeptides would be detected. In total, 72 glycan structures were found for the immunopurified 21K fast PrP<sup>Sc</sup>. The HILIC enrichment was tested again on samples isolated with “protocol I” (21K slow strain, ) and “protocol II” (all three strains). In the case of 21K slow prion


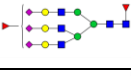

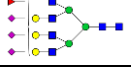
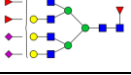
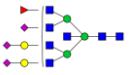
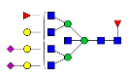
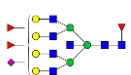

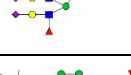


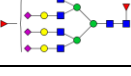
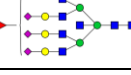
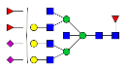
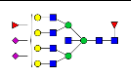
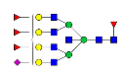
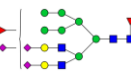
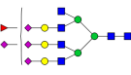
strain, 43 glycopeptides were detected, whereas for 19K strain, 42 glycopeptides were detected. The reason for a higher number of glycoforms detected with the immunopurified PrP<sup>Sc</sup> could be the isolation method, or the amount of brain tissue used. Even though attempts were made to improve the HILIC enrichment procedure and therefore detection of N-200 glycopeptides, we were not able to get a higher number of detected glycopeptides for 21K slow and 19K prion strains. Also, since the first enrichment procedure of 21K fast strain was just a trial, it was tested on a different instrument, which uses CE sprayer, instead of the CaptiveSpray used for all the other analysis, which could also contribute to the difference. All the N-glycan compositions, together with their proposed structures, detected specifically for each prion strain can be seen in **Table 5**. Out of the 72 structures detected on 21K fast strain, 67 of them are sialylated: 14 are monosialylated, 16 disialylated, 18 trisialylated, 12 tetrasialylated and 7 pentasialylated.


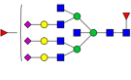
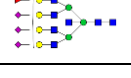
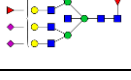
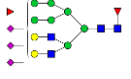
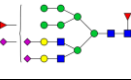
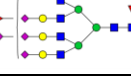
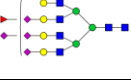
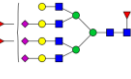
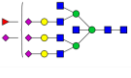
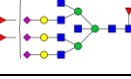
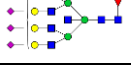
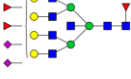
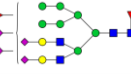
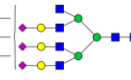
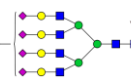
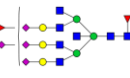
**Table 5.** List of all the proposed glycan structures on N-200 glycosylation site detected specifically for each strain. H – hexose, N – *N*-acetylhexosamine, F – fucose and S – *N*-acetylneuraminic acid (sialic acid).

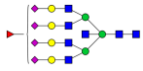
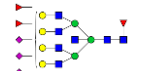
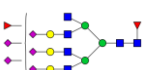





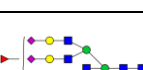


#	Glycan composition	Proposed structure	Theoretical m/z [M+H] <sup>+</sup>	Detected		
				21K fast	21K slow	19K
1	H4N52		3109.2612	+	+	+
2	H4N5S1F1		3254.2987	+	+	/
3	H5N5F3		3417.3719	+	+	+
4	H4N6S1F1		3457.3781	+	+	+
5	H5N6F2		3474.3934	+	+	+
6	H5N5S1F2		3562.4094	+	+	+
7	H5N6S1F1		3619.4309	+	+	/
8	H8N3S1F2		3642.4090	+	+	/

9	H5N5S2F1		3707.4469	+	+	/
10	H5N6S1F2		3765.4888	+	+	+
11	H6N6F3		3782.5041	+	+	+
12	H5N6S2F1		3910.5263	+	+	+
13	H6N6S1F2		3927.5416	+	+	+
14	H5N7S1F2		3968.5682	+	+	+
15	H6N7F3		3985.5835	+	/	+
16	H5N6S2F2		4056.5842	+	+	+
17	H6N6S1F3		4073.5995	+	+	+
18	H5N7S2F1		4113.6057	+	+	+
19	H6N7S1F2		4130.6210	+	+	+
20	H8N4S2F2		4136.5838	+	/	/
21	H9N4S1F3		4153.5991	+	/	/
22	H6N5S2F3		4161.6155	+	+	+
23	H5N6S3F1		4201.6217	+	+	+
24	H6N6S2F2		4218.6370	+	+	+
25	H6N7S2F1		4275.6585	+	+	/



26	H6N7S1F3		4276.6789	+	+	+
27	H6N5S3F2		4306.6530	+	+	+
28	H5N6S3F2		4347.6796	+	+	+
29	H6N6S3F1		4363.6745	+	+	/
30	H6N6S2F3		4364.6949	+	+	+
31	H5N7S3F1		4404.7011	+	+	+
32	H6N7S2F2		4421.7164	+	+	+
33	H7N7S1F3		4438.7317	+	+	+
34	H9N4S2F3		4444.6945	+	+	+
35	H7N5S3F2		4468.6915	+	/	/
36	H9N5S2F2		4501.7160	+	/	/
37	H6N6S3F2		4509.7324	+	+	+
38	H6N7S3F1		4566.7539	+	+	+
39	H6N7S2F3		4567.7743	+	+	+
40	H7N7S2F2		4583.7692	+	+	/
41	H7N7S1F4		4584.7896	+	+	+
42	H9N4S3F2		4589.7320	+	/	/
43	H6N6S4F1		4654.7699	+	/	/
44	H6N6S3F3		4655.7903	+	+	+

45	H5N7S4F1		4695.7965	+	/	/
46	H6N7S3F2		4712.8118	+	+	+
47	H7N7S3F1		4728.8067	+	/	/
48	H7N7S2F3		4729.8271	+	+	+
49	H9N4S3F3		4735.7899	+	/	+
50	H9N5S3F2		4792.8114	+	/	/
51	H6N6S4F2		4800.8278	+	+	/
52	H7N6S4F1		4816.8227	+	/	/
53	H7N6S3F3		4817.8431	+	/	+
54	H6N7S4F1		4857.8493	+	/	+
55	H6N7S3F3		4858.8697	+	/	+
56	H7N7S3F2		4874.8646	+	+	+
57	H7N7S2F4		4875.8850	+	+	+
58	H9N4S4F2		4880.8274	+	/	/
59	H6N6S5F1		4945.8653	+	/	+
60	H7N6S4F2		4962.8806	+	/	/
61	H6N7S4F2		5003.9072	+	/	+

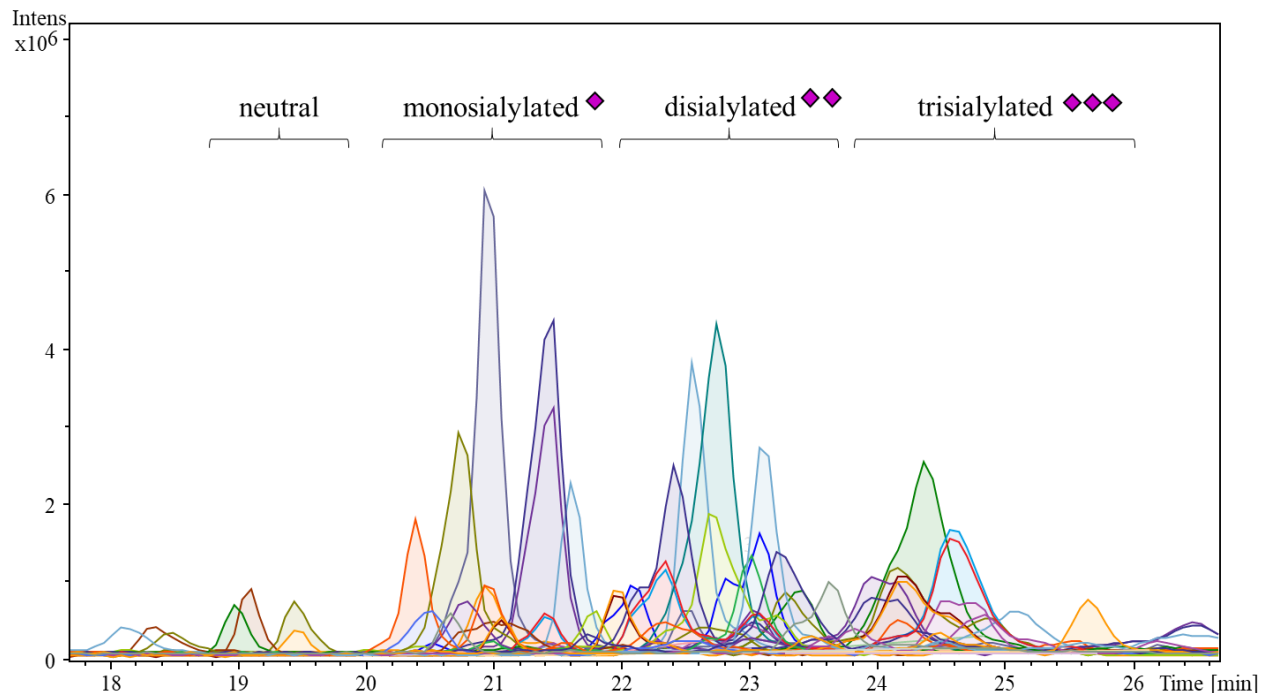
62	H7N7S4F1		5019.9021	+	/	/
63	H7N7S3F3		5020.9225	+	+	+
64	H6N6S5F2		5091.9232	+	/	/
65	H7N6S5F1		5107.9181	+	/	/
66	H7N6S4F3		5108.9385	+	/	/
67	H6N7S5F1		5148.9447	+	/	/
68	H7N7S4F2		5165.9600	+	/	/
69	H6N7S5F2		5295.0026	+	/	/
70	H7N7S5F1		5310.9975	+	/	/
71	H7N7S4F3		5312.0179	+	/	/
72	H7N7S5F2		5457.0554	+	/	/

All 42 and 43 structures detected on 19K strain and 21K slow, respectively, were also present in those 72 structures from 21K fast strain, however, the minimal set of mutual structures was 35. Since all the 21K slow and 19K PrP<sup>Sc</sup> glycopeptides were detected also in 21K fast sample, the possibility that the remaining glycopeptides are present in other strains cannot be excluded. It is possible they were not detected because of the lower amount of starting material or the isolation protocol itself. Since none of the remaining 37 glycopeptides were major structures, with relative abundances less than 3%, the mutual 35 glycopeptides were used for further quantification and comparison.

The N-200 glycopeptides elute from 19 to 26 min, **Figure 38** represents EICs from 21K fast strain, only of the 35 mutual glycopeptides. The different glycoforms are again characterized by

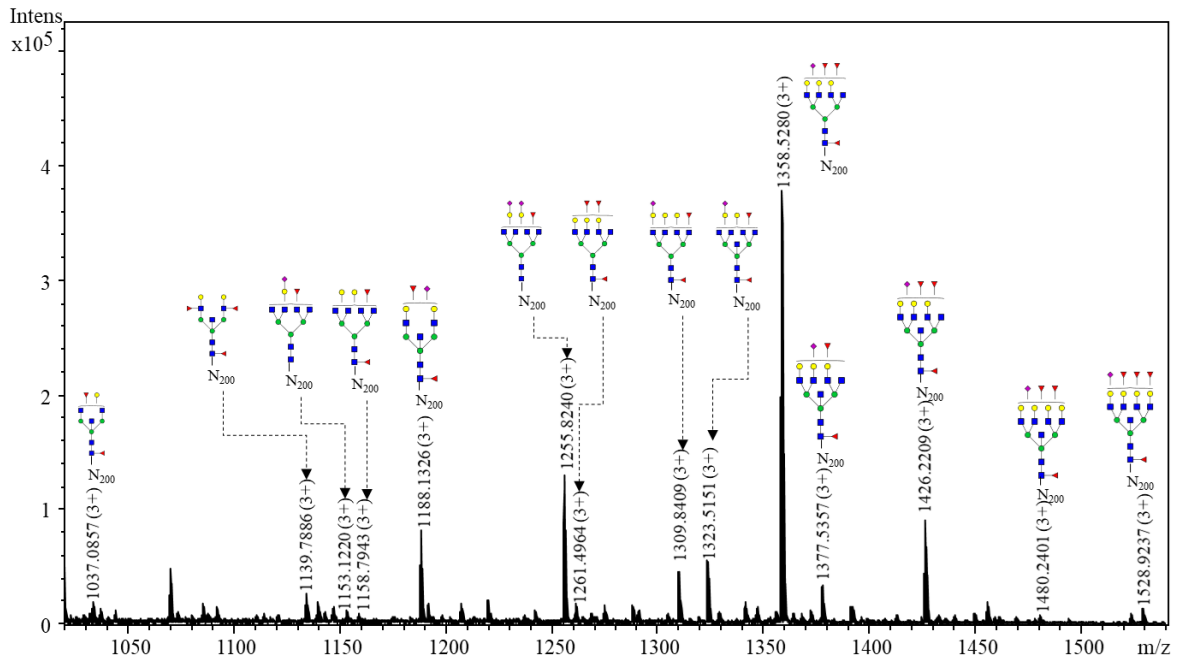
elution at different retention times; neutral glycopeptides elute in a range from 18.8 – 19.6, followed by sialylated structures: monosialylated from 20 – 21.8, disialylated from 22 – 23.6 min, and trisialylated from 23.8 – 25 min. The exact separation of sialylated glycoforms is a bit difficult to determine, since the chromatograms of these structures overlap. This is due to the fact that structures with NeuAc residues usually elute in two (or even three) peaks, caused by isomers in which NeuAc residues can be localized on different antennas [206].

The averaged MS with the observed N-200 glycopeptides are shown on **Figure 39 (A and B)**. These glycopeptides were generally found in 3+ and 4+ charged states (3+ charged state was used for illustration on the spectra) and again as for N-184 glycopeptides, all the charged states detected for each glycopeptide were used for generating the EIC. From the 35 mutual structures, again all the structures were fucosylated (with at least one fucose residue), no biantennary structures were found, 2 were triantennary, 14 were tetraantennary, and 18 had bisecting GlcNAc. Only one hybrid structure was detected, while the rest were complex N-glycan structures and again no high mannose ones were detected.

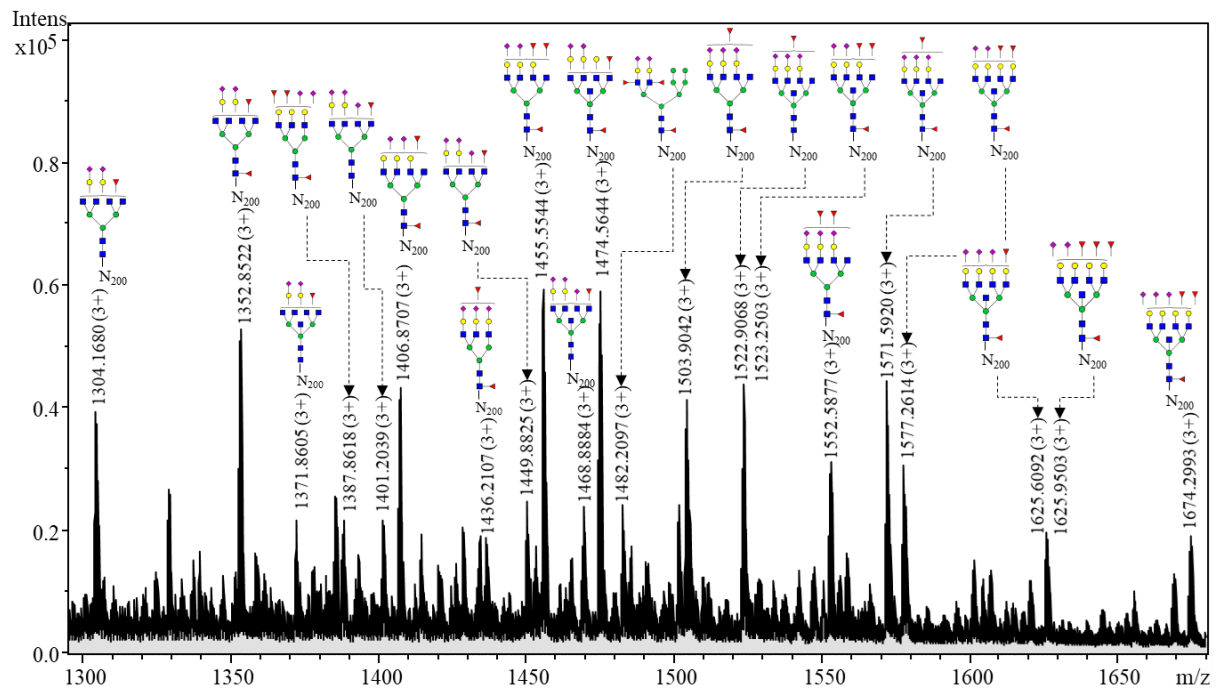


**Figure 38.** Extracted ion chromatograms of 35 detected N-200 glycopeptides, mutual for all three strains, with different retention times for neutral, mono-, di- and trisialylated structures.

A



B



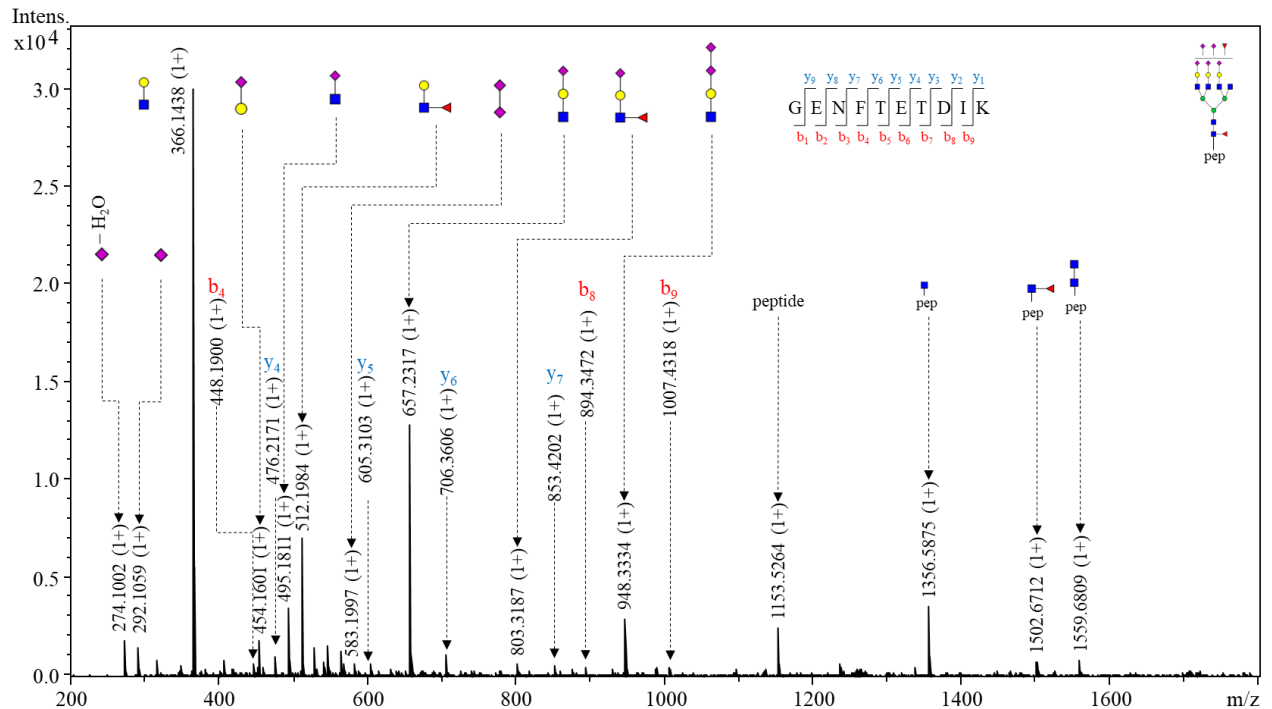
**Figure 39.** Assigned glycoforms in MS with the N-200 peptide backbone: neutral and monosialylated (A), disialylated and trisialylated glycoforms (B).

---

From the total 72 structures, 65 of them were confirmed with a corresponding MS/MS spectrum. The peptide portion was confirmed by the presence of a signal with  $m/z$  value of 1153.52 (1+), the y ion of the N-200 peptide (GE<sup>200</sup>NFTETDIK), together with 1356.58 (1+) representing the peptide carrying one GlcNAc residue. In the case of core fucosylation, this was indicated by the presence of 1559.68 (1+), representing the peptide + GlcNAc + Fuc fragment. The amino acid sequence was confirmed with the presence of mainly y ions (in some cases also b ions were detected).

The glycan structure features were annotated again with the main glycan-specific markers. However, in the tetrasialylated and pentasialylated glycopeptides, two interesting features were found – again the same structure found already on N-184 glycopeptides, 6sLeC, together with an additional one, disialic acids. **Figure 40** represents an MS/MS spectrum of a glycopeptide with glycan composition H6N6S5F2, where both features were detected. The presence of 6sLeC is indicated with the  $m/z$  value of 495.18 (1+), corresponding to the HexNAc + NeuAc fragment. The presence of disialic acids is indicated by two fragments with  $m/z$  values of 583.19 (1+), corresponding to NeuAc + NeuAc fragment and 948.33 (1+), corresponding to NeuAc + NeuAc + Gal + GlcNAc fragment. The presence of disialic acids, like 6sLeC, has previously been found in the brain [207].

The signals above  $m/z$  value of 2000 were too low to be annotated in most MS/MS spectra, presumably because the collision energy was too high for the N-200 peptide.



**Figure 40.** Example of N-200 glycopeptide whose structure was confirmed by MS/MS, the precursor ion with  $m/z$  value of 1697.9579 (+3) is shown. Fragments of glycan-specific marker ions are represented, together with b and y ions confirming the amino acid sequence and fragments of the peptide backbone with the N-glycan H6N6S5F2 (full glycopeptide structure shown).

### 3.3.2.1 Quantitative analysis of N-200 glycosylation site from different prion strains











The proposed mutual glycan structures found on N-200 glycosylation site are shown in **Table 6**, of the total 35 glycan structures found, only 4 are neutral (11.43%) and 31 are sialylated (88.57%), 10 are monosialylated, 11 disialylated and 10 trisialylated.

The integration in DataAnalysis was performed in the same manner as for N-184, and the relative abundance for each glycopeptide in each strain is seen in **Table 6**. The most abundant structure for 21K fast and 19K prion strain was the glycan with a composition of H6N7S2F2 (7.81% and 9.65%, respectively), which is the second most abundant for 21K slow strain (7.57%), where the most abundant one is H5N6S1F2 (8.63%). In total, the abundance was above 5% for only 5 glycan structures (for 21K fast and 19K strains, and for 6 structures in the case of 21K slow strain). The abundance was below 1% for total of 8 glycan structures (in the case of 21K fast and 21K slow strain, and 9 structures in the case of 19K strain). The 12 most abundant structures (in a range of 7.8 – 3.5%) were the same for all the strains, just with a slightly different order. However, it is difficult

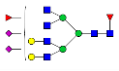
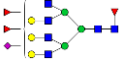




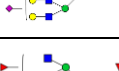
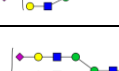




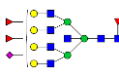
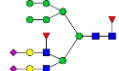
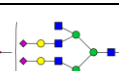


to claim that these differences are due to strain differences or due to the integration, since for certain signals it was difficult to determine the beginning and the end of the peak.






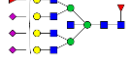
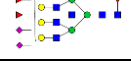

The relative abundances for all N-200 glycan structures are shown with bar representation on **Figure 41**. Even though the small differences in certain glycan structures can be seen, they are around 1–2% and therefore, we can suggest that there are no major differences in the glycan composition of N-200 glycosylation site between strains.

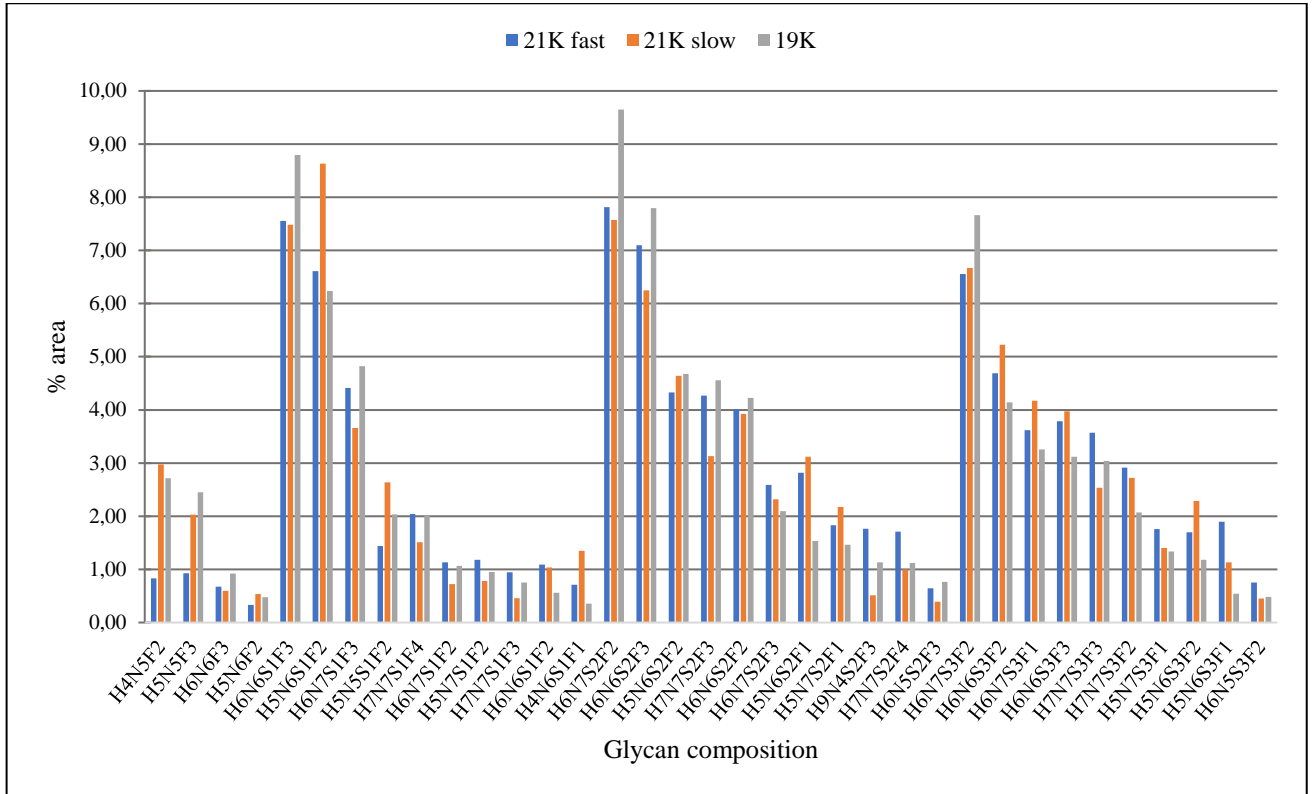
**Table 6.** List of the proposed glycan structures on N-200 glycosylation site, mutual for all three strains; together with the glycan composition and their relative abundance. Major glycan structure marked in bold. H – hexose, N – *N*-acetylhexosamine, F – fucose and S – *N*-acetylneuraminic acid (sialic acid).

#	Glycan composition	Proposed structure	Theoretical m/z [M+H] <sup>+</sup>	21K fast	21K slow	19K
				%area		
1	H4N5F2		3109.2612	0.83	2.98	2.71
2	H5N5F3		3417.3719	0.93	2.03	2.45
3	H4N6S1F1		3457.3781	0.71	1.35	0.35
4	H5N6F2		3474.3934	0.33	0.54	0.47
5	H5N5S1F2		3562.4094	1.44	2.64	2.03
6	H5N6S1F2		3765.4888	6.61	8.63	6.23
7	H6N6F3		3782.5041	0.68	0.60	0.92
8	H5N6S2F1		3910.5263	2.82	3.12	1.54
9	H6N6S1F2		3927.5416	1.09	1.04	0.56
10	H5N7S1F2		3968.5682	1.18	0.78	0.95



11	H5N6S2F2		4056.5842	4.33	4.64	4.68
12	H6N6S1F3		4073.5995	7.56	7.48	8.79
13	H5N7S2F1		4113.6057	1.83	2.17	1.46
14	H6N7S1F2		4130.6210	1.13	0.73	1.06
15	H6N5S2F3		4161.6155	0.64	0.39	0.76
16	H5N6S3F1		4201.6217	1.90	1.13	0.54
17	H6N6S2F2		4218.6370	4.01	3.93	4.23
18	H6N7S1F3		4276.6789	4.41	3.66	4.82
19	H6N5S3F2		4306.6530	0.75	0.45	0.48
20	H5N6S3F2		4347.6796	1.70	2.29	1.18
21	H6N6S2F3		4364.6949	7.10	6.25	7.80
22	H5N7S3F1		4404.7011	1.76	1.40	1.34
23	H6N7S2F2		4421.7164	7.81	7.57	9.65
24	H7N7S1F3		4438.7317	0.94	0.46	0.75
25	H9N4S2F3		4444.6945	1.77	0.51	1.13
26	H6N6S3F2		4509.7324	4.69	5.23	4.14
27	H6N7S3F1		4566.7539	3.62	4.17	3.26

28	H6N7S2F3		4567.7743	2.59	2.32	2.09
29	H7N7S1F4		4584.7896	2.04	1.51	2.02
30	H6N6S3F3		4655.7903	3.79	3.97	3.12
31	H6N7S3F2		4712.8118	6.56	6.67	7.66
32	H7N7S2F3		4729.8271	4.27	3.13	4.56
33	H7N7S3F2		4874.8646	2.91	2.72	2.07
34	H7N7S2F4		4875.8850	1.71	1.00	1.12
35	H7N7S3F3		5020.9225	3.57	2.53	3.04



**Figure 41.** Bar representation of relative abundance of N-glycans on N-200 peptide expressed as percentage of total normalized area. Total of 35 N-glycan structures were quantitatively compared between 21K fast, 21K slow and 19K prion strains.

---

## CHAPTER IV

### 4 DISCUSSION

There are many mysteries revolving around the prion protein and prion diseases. Prion diseases occur when PrP<sup>C</sup> changes its conformation to PrP<sup>Sc</sup>, leading to aggregation, neuronal death and eventually, fatal neurodegeneration. Although the exact mechanism still remains unknown, the widely accepted explanation is the “protein-only” hypothesis, which states that the prion protein is the main cause responsible for prion diseases. Additional complications arise from the fact that within the same species, the infectious prion protein exists in a large variety of strains [208]. From a biochemical point of view, strains differ in their resistance to PK, glycosylation profiles and electrophoretic mobility. The differences in their glycosylation profiles are characterized by the size and abundance of each PrP<sup>Sc</sup> band (di-, mono- and unglycosylated). Only a small number of studies have determined exact glycan structures attached on the PrP<sup>Sc</sup>, isolated from hamsters [152, 160] and mice [162]. One other study investigated the differences between PrP<sup>C</sup> and PrP<sup>Sc</sup> glycans [161]. However, no studies determining the exact glycan composition of different strains has been done before.

In this study, for the first time, glycan composition of different sheep PrP<sup>Sc</sup> strains has been determined, and the results will be discussed in this section. However, the isolation and purification of a large amount of prion protein step has been shown as a major bottleneck of this study, and therefore, both parts will be discussed separately.

#### 4.1 Developing a protocol for large-scale isolation and purification of PrP<sup>Sc</sup>

In the past, it has been shown that the prion protein is rather difficult to isolate and purify, due to its resistance to proteases, insolubility and propensity to aggregate. However, since defining it as a protein with a molecular weight of 27 to 30 kDa (therefore termed PrP<sup>27-30</sup>) in 1982, done by Prusiner and his colleagues [200, 209], many different methods for isolation and purification have

---

been developed and tested. One of them includes immunopurification [210, 211], but the more used and explored one usually includes differential centrifugation steps, enzymes such as PK, the use of sarkosyl and ways of precipitation PrP<sup>Sc</sup> either with NaCl or PTA [183, 212-214]. The main problem with prion protein isolation is the co-purification of other proteins, the major contaminants being: ferritin (both heavy and light chain), calcium/calmodulin-dependent protein kinase alpha type II, apolipoprotein E, tubulin and myelin proteolipid protein [215-217]. In all of the methods, brain homogenates are usually used as starting material.

The first approach we decided to test was the use of cell lines, since we had easy access, unlimited amount of cells and it seemed like a convenient way to use them for developing the LC-MS method. Cell lines are widely used as experimental models of prion diseases. They are able to replicate PrP<sup>Sc</sup> in a stable and continuous way, as well as the protein's infectivity [218, 219]. The most commonly used are mouse neuroblastoma cell lines (N2a). Together with those, we tested mouse hypothalamic cell lines (GT1), both infected with two different mouse-adapted scrapie strains, 22L and RML. Cell lines are usually used for studying the biosynthesis [220, 221], function of the prion protein [222], and for example, therapeutic studies [223]. In fact, no studies have been reported using them for large-scale isolation of prion protein.

Even though in this study many efforts have been put into optimizing the isolation from cell lines, we have shown that, unfortunately, this was not feasible. The prion protein gained from one Petri dish was merely a test of the protocol and the PK digestion alone proved as an inadequate method for isolating a pure sample containing PrP<sup>Sc</sup>. The number of Petri dishes was increased to 60, from which the prion protein was isolated with PTA precipitation, followed by PK digestion. Again, PrP<sup>Sc</sup> isolated from cell lysates of total 60 Petri dishes had its limitations – even though the presence of the prion protein was confirmed, co-purified proteins contributed much more to the total signal intensity than the prion protein. Nevertheless, we decided to continue using cell lines by increasing the number of collected cells and began lysing cells in a period of 2–3 months. Eventually we collected cell lysates from over 700 Petri dishes. Many variations to the protocol were tested, both the protocol based on density medium and immunopurification (results not shown in this thesis because they did not result in the isolation of PrP<sup>Sc</sup>), and we have shown that none of the protocols worked in large-scale isolation from cell lines. Not only did many concerns occur while isolating PrP<sup>Sc</sup> from cells, like the purity and amount of the PrP<sup>Sc</sup>, but also, to collect cells from such a high number of Petri dishes is time consuming and requires a lot of medium for cell growth.

---

The next approach tested was the use of PMCA amplified PrP<sup>Sc</sup>, which was thought to be an even more convenient and easier way to obtain high-titre of the prion protein in a short amount of time, unlike the time-consuming collection of cell lysates. However, the PMCA had its limitations, mainly the pellet present after finishing the amplification, which in the end was shown to be a problem while sample loading on the gel. Finally, after all the protocols tested, together on cell lines and mice brain tissue, we concluded that isolation *ex vivo* is a much more suitable way of isolating high-titre PrP<sup>Sc</sup>.

Therefore, we put all of our focus and efforts on isolation from brain tissue. For optimization of the isolation protocol, together with LC-MS method optimization, we required much more than 1 g of mice brain tissue. Since all of the mice brains were used for optimizing the isolation protocol, there was no more sample left. The lack of mice brains was solved by starting a collaboration with Prof. Olivier Andréoletti, who provided us with sheep brains infected with different prion strains. For two out of three strains, in total 200 g of brain tissue from different animals was received, which proved to be enough for both the isolation and final analysis. Initial isolation protocol was performed by immunopurification, however, due to bindings to the Protein G beads of proteins co-purifying with the prion protein, the use of this approach for further isolation was discarded. Testing the protocol with the density medium approach showed to be a much more promising one. The differences between these two protocols were visible merely from corresponding Coomassie stained gels, but also from MaxQuant analysis – after isolation with the density medium approach, the contaminants had lower intensities than the prion protein itself, while vice versa was in the case of immunopurified PrP<sup>Sc</sup>.

We concluded that the density medium approach resulted with a much purer sample, although both approaches were practicable for glycopeptide analysis. Since the use of a density medium approach was the one which resulted with a purer sample, this one would be recommended for further experiments requiring high-titre prions.

## 4.2 Determining the glycan composition of different prion strains

It is of great importance to comprehend the strain phenomenon, not only from a scientific point of view, but also because it imposes a public health risk, since prions are known to adapt, leading to transmission between species [90, 96], which could generate even more infectious

---

material with new and unknown characteristics. The existence of prion strains was difficult to explain in the beginning, because this signifies that a protein with the same amino acid sequence is able to cause a wide range of diseases which are, as mentioned previously, characterized by diverse clinical signs, incubation periods, lesion profiles and biochemical properties [208]. The existence of strains, however, has been shown also in other neurodegenerative diseases, which progress in a prion-like way, such as A $\beta$  in AD [224], tau in tauopathies [225], and  $\alpha$ -synuclein in PD [226].

After solving the major bottleneck and finally isolating and purifying the PrP<sup>Sc</sup> from sheep brains, the glycopeptide analysis was performed. On both sites, all detected N-glycans were fucosylated, and the majority of structures also had bisecting GlcNAc. The possibility of these structures being triantennary cannot be excluded, since structural isomers cannot be differed only from MS characterization. The majority of structures also carried sialic acid residues, although the N-200 glycosylation site was shown to be heavily sialylated, in comparison to N-184 site, reported also on equivalent mouse PrP<sup>Sc</sup> glycosylation sites, N-180 and N-196 [162]. The site-specific analysis showed a major difference between glycan structures on the two glycosylation sites, since from the total of 123 structures detected on both sites, only 17 were found to be glycans with the same composition.

Previously it has been shown that sialic acid has a major role in prion diseases, since it controls the rate of prion amplification, the species barrier, infectivity and the ratio of PrP<sup>Sc</sup> glycoforms [169]. Additionally, not only is the N-200 glycosylation site more sialylated than N-184, but what is more interesting are the sialylated structures. The analysis of N-200 glycosylation site revealed a feature not found on the N-184 site – the occurrence of structures with disialic acids, in general common for both N- and O-glycans [207, 227, 228]. The two most common linkages reported in sialic acids are  $\alpha$ 2-3 and  $\alpha$ 2-6, however, in order for disialic structures to occur, the two sialic acid residues need to be  $\alpha$ 2-8 linked, meaning that  $\alpha$ 2-8 sialyltransferase is active [229]. Even though polysialic acid residues (carrying 8 to 12 sialic acids) have been known to exist in mammalian brains, not many glycoproteins carrying this type of structure have been reported, except for the well-studied neural cell adhesion molecule (NCAM) [230], for which the prion protein is known to interact with, although the functionality of this interaction is still being investigated [231, 232]. Since glycoproteins carrying polysialic acids usually have not been detected in adult brains, it has been attributed to occur in developing (embryonic) brains [233]. However, much less attention has been given to disialic acid residues until finally advances in analytical techniques could allow

---

identification of even more proteins with this feature, yet their function remains to be investigated further.

Prion strains occur in almost all species susceptible to prion diseases and their variation has been a topic of many studies. The source of strain variation lies in the fact that they can generate in a spontaneous way or adapt and change through interspecies transmission [208, 234], but also because of PrP polymorphisms, present in most species, such as mice [235, 236], sheep, goats [91, 237], and humans [77, 238]. Methionine or valine at position 129 is the polymorphism responsible for susceptibility, incubation time and pathology of human prion diseases and strain diversity in humans [159]. However, with just methionine at this position, different PrP strains have been reported [208], meaning that there are other factors contributing to the extent of strain diversity.

It was long believed that these differences occur because of distinct conformational states that PrP<sup>Sc</sup> can acquire [234]. One of the possible explanations was that post-translational modifications are the ones affecting strain properties and PrP infectivity, however, conflicting results have been reported. Cancellotti et al. performed experiments by intracerebrally infecting wild type mice with different PrP strains obtained from transgenic mice with mutations in one (first or second) or both glycosylation sites. For some strains, their properties were maintained in the infected host, but in other cases they were changed, leading to the emergence of new strains. They concluded that glycans are not essential for prion replication, although there were cases where strain properties were changed, glycosylation status of the host seems to affect the prion replication. However, strain properties do not depend on the host PrP and can therefore be modified by changes in post-translational modifications [179]. Further on, a study done by Wiseman et al. demonstrated that by infecting transgenic mice carrying mutations at glycosylation sites, there is a difference in susceptibility to different prion strains. The absence of the first (N-180) or both of the glycosylation sites resulted in almost a complete resistance of the host to the disease, while the absence of glycosylation at the second site (N-196) facilitated the transmission of the disease to the host. This suggested that prion transmission in different species is influenced by glycosylation status of host PrP<sup>C</sup> [239]. Infecting mice intraperitoneally, however, leads to different results. The lack of glycans actually slows down or even prevents the disease, suggesting glycosylation of host PrP has a role in the prion replication in the peripheral tissue or prion transport to the CNS [240].

The major point to address in this thesis was whether the glycans influence strain properties. In a study from 2016, cell-based PMCA was used on different species and PrP with mutations in the



---

glycosylation sites. They showed that in the un- and monoglycosylated mutants PrP<sup>C</sup> was efficiently converted to PrP<sup>Sc</sup>. Neither PrP<sup>C</sup> nor PrP<sup>Sc</sup> glycoforms alter the formation rate of prions or have an influence on strain properties, meaning that their characteristics are encoded in the protein backbone [241]. The same effect was observed also in human prion studies, by enhancing the amplification rate of human prions in PMCA with partially or completely unglycosylated PrP<sup>C</sup>. The proposed mechanisms explaining the effect PrP<sup>C</sup> glycosylation has in PMCA is interpreted through the stabilizing effect glycans have on the protein's structure, rendering the protein more resistant to misfolding, or the glycan interfering in PrP<sup>C</sup> and PrP<sup>Sc</sup> interaction [242]. This can be related to another study done with PMCA on desialylated PrP<sup>C</sup>, where the researchers proposed that the PrP<sup>Sc</sup> amplification is increased when sialic acid is removed, thereby removing the electrostatic repulsion between the glycan structures [169].

In conclusion, after testing many different approaches, we were able to develop a protocol for large-scale isolation of different sheep PrP<sup>Sc</sup> strains. Even though the isolation was performed by obtaining an N-glycan pool (by using different animals and brain regions), we were also able to develop an LC-MS/MS method for glycopeptide analysis. This is the first time glycopeptide analysis has been performed on sheep PrP<sup>Sc</sup>, but moreover, the first time glycan composition on different prion strains has been compared. The first major result observed is the different glycan composition found on the two glycosylation sites. The other major point observed in this thesis is the fact that the three different prion strains analyzed do not show any major differences in their glycan composition; which could suggest that strain properties are encoded in the protein backbone, instead in the glycan structures. Due to the many issues regarding prion protein isolation, it was not possible to perform replicates, in order to confirm the initial data. Further experiments should be performed. However, from all the studies done on prion protein glycosylation, it has been shown that glycans are not necessary for transmitting prion infection, and that the host PrP<sup>C</sup> has an important role in determining the glycosylation of the newly formed PrP<sup>Sc</sup> and that changes in its glycosylation has an impact in prion conversion in a strain-specific way [243, 244]. Also, it is known that glycosylation significantly varies in different cell types and different brain regions [245]. This leads to the hypothesis that prion strains preferentially accumulate in cells in distinct brain regions where the specific PrP<sup>C</sup> glycoforms are contained [246].

For future studies, it would be interesting to analyze only the monoglycosylated band of PrP<sup>Sc</sup>, to see whether the preference for a certain glycosylation site is strain specific and if the glycan

composition differs in the same manner as for the diglycosylated band; to investigate PrP<sup>Sc</sup> glycan structures from specific brain regions, and possibly to expand the analysis on strains from different species to see if the glycosylation strain similarities are species independent.

---

## BIBLIOGRAPHY

1. Prusiner, S. B., *Neurodegenerative diseases and prions*. The New England Journal of Medicine, 2001. **344**: p. 1516-1526.
2. Gitler, A. D., Dhillon, P., and Shorter, J., *Neurodegenerative disease: models, mechanisms, and a new hope*. Dis Model Mech, 2017. **10**(5): p. 499-502.
3. Soto, C. and Satani, N., *The intricate mechanisms of neurodegeneration in prion diseases*. Trends Mol Med, 2011. **17**(1): p. 14-24.
4. Glenner, G. G. and Wong, C. W., *Alzheimer's disease: initial report of the purification and characterization of a novel cerebrovascular amyloid protein*. Biochem. Biophys. Res. Commun., 1984. **120**: p. 885-890.
5. Grundke-Iqbal, I., et al., *Microtubule-associated protein tau. A component of Alzheimer paired helical filaments*. J Biol Chem, 1986. **261**: p. 6084-6089.
6. Polymeropoulos, M. H., *Mutation in the  $\alpha$ -Synuclein Gene Identified in Families with Parkinson's Disease*. Science, 1997. **276**(5321): p. 2045-2047.
7. Group, T. H. s. D. C. R., *A novel gene containing a trinucleotide repeat that is expanded and unstable on Huntington's disease chromosomes*. Cell, 1993. **72**: p. 971-963.
8. Rosen, D. R., et al., *Mutations in Cu/Zn superoxide dismutase gene are associated with familial amyotrophic lateral sclerosis*. Nature, 1993. **362**: p. 59-62.
9. Neumann, M., et al., *Ubiquitinated TDP-43 in frontotemporal lobar degeneration and amyotrophic lateral sclerosis*. Science, 2006. **314**(5796): p. 130-133.
10. Prusiner, S. B., *Novel proteinaceous infectious particles cause scrapie*. Science, 1982. **216**: p. 136-144.
11. Gammon, K., *Brain windfall: Diseases such as Alzheimer's and Parkinson's are rising up the research agenda, partly because of ageing populations*. Nature, 2014. **515**: p. 299-300.
12. Safar, J. G., *Molecular pathogenesis of sporadic prion diseases in man*. Prion, 2012. **6**(2): p. 108-115.
13. Brown, P. and Bradley, R., *1755 and all that: a historical primer of transmissible spongiform encephalopathy*. BMJ, 1998. **317**: p. 19-26.
14. Appleby, B. S. and Lyketsos, C. G., *Rapidly progressive dementias and the treatment of human prion diseases*. Expert Opin Pharmacother, 2011. **12**(1): p. 1-12.
15. Gajdusek, D. C., Gibbs, C., and Alpers, M., *Experimental transmission of a kuru-like syndrome to chimpanzees*. Nature, 1996. **209**(5025): p. 794-796.
16. Johnson, R. T. and Gibbs, C. J., *Creutzfeldt-Jakob Disease and Related Transmissible Spongiform Encephalopathies*. New England Journal of Medicine, 1998. **339**(27): p. 1994-2004.
17. Masters, C. L., Gajdusek, D. C., and Gibbs, C., *Creutzfeldt-Jakob disease virus isolations from the Gerstmann-Sträussler-Scheinker syndrome*. Brain, 1981. **104**: p. 559-588.
18. Medori, R., et al., *Fatal familial insomnia, a prion disease with a mutation at codon 178 of the prion protein gene*. N Engl J Med, 1992. **326**(7): p. 444-449.
19. Wells, G. A., et al., *A novel progressive spongiform encephalopathy in cattle*. Vet Rec, 1987. **121**(18): p. 419-420.
20. Detwiler, L. A., *Scrapie*. Rev Sci Tech, 1992. **11**(2): p. 491-537.
21. Williams, E. S. and Young, S., *Spongiform Encephalopathy of Rocky Mountain Elk*. Journal of Wildlife Diseases, 1982. **18**(4): p. 465-471.

22. Hartsough, G. R. and Burger, D., *Encephalopathy of mink. I. epizootiologic and clinical observations*. The Journal of Infectious Diseases. **115**(4): p. 387-392.
23. Budka, H., *Neuropathology of prion diseases*. British Medical Bulletin, 2003. **66**: p. 121-130.
24. Kübler, E., Oesch, B., and Raeber, A. J., *Diagnosis of prion diseases*. British Medical Bulletin, 2003. **66**: p. 267-279.
25. Green, A. J. E., *RT-QuIC: a new test for sporadic CJD*. Pract Neurol, 2019. **19**(1): p. 49-55.
26. Bolognesi, M. L. and Legname, G., *Approaches for discovering anti-prion compounds: lessons learned and challenges ahead*. Expert Opin Drug Discov, 2015. **10**(4): p. 389-397.
27. Mathiason, C. K., *Scrapie, CWD, and Transmissible Mink Encephalopathy*. Prog Mol Biol Transl Sci, 2017. **150**: p. 267-292.
28. Goldman, W., et al., *PrP genotype and agent effects in scrapie: change in allelic interaction with different isolates of agent in sheep, a natural host of scrapie*. Journal of General Virology, 1994. **75**: p. 989-995.
29. Groschup, M. H., et al., *Classic Scrapie in Sheep with the ARR/ARR Prion Genotype in Germany and France*. Emerging Infectious Diseases, 2007. **13**(8): p. 1201-1207.
30. Benestad, S. L., et al., *Cases of scrapie with unusual features in Norway and designation of a new type, Nor98*. Veterinary Record, 2003. **153**: p. 202-208.
31. Luhken, G., et al., *Epidemiological and genetical differences between classical and atypical scrapie cases*. Vet Res, 2007. **38**(1): p. 65-80.
32. Curcio, L., et al., *Review: A review on classical and atypical scrapie in caprine: Prion protein gene polymorphisms and their role in the disease*. Animal, 2016. **10**(10): p. 1585-1593.
33. Gibbs, C. J., Jr. and Gajdusek, D. C., *Transmission of scrapie to the cynomolgus monkey (Macaca fascicularis)*. Nature, 1972. **236**: p. 73-74.
34. Comoy, E. E., et al., *Transmission of scrapie prions to primate after an extended silent incubation period*. Sci Rep, 2015. **5**: p. 11573.
35. Cassard, H., et al., *Evidence for zoonotic potential of ovine scrapie prions*. Nature Communications, 2014. **5**(1): p. 5821.
36. Acevedo-Morantes, C. Y. and Wille, H., *The structure of human prions: from biology to structural models-considerations and pitfalls*. Viruses, 2014. **6**(10): p. 3875-3892.
37. Linden, R., et al., *Physiology of the prion protein*. Physiol Rev, 2008. **88**(2): p. 673-728.
38. Haire, L. F., et al., *The Crystal Structure of the Globular Domain of Sheep Prion Protein*. Journal of Molecular Biology, 2004. **336**: p. 1175-1183.
39. Martin, R., et al., *Polymorphism of the Prion Protein in Mammals: A Phylogenetic Approach*. Recent Patents on DNA & Gene Sequences, 2009. **3**(1): p. 63-71.
40. Chakrabarti, O., Ashok, A., and Hegde, R. S., *Prion protein biosynthesis and its emerging role in neurodegeneration*. Trends Biochem Sci, 2009. **34**(6): p. 287-295.
41. Chen, K. C., et al., *Microsecond unfolding kinetics of sheep prion protein reveals an intermediate that correlates with susceptibility to classical scrapie*. Biophys J, 2011. **101**(5): p. 1221-1230.
42. Hegde, R. S., et al., *A transmembrane form of the prion protein in neurodegenerative disease*. Science, 1998. **279**(5352): p. 827-834.
43. Minikel, E. V. *Prion protein N-linked glycosylation: review and assessment of therapeutic potential*. 2013; Available from: <http://www.cureffi.org/2013/05/05/prion-protein-n-linked-glycosylation-review-and-assessment-of-therapeutic-potential/>.
44. Sunyach, C., et al., *The mechanism of internalization of glycosylphosphatidylinositol-anchored prion protein*. EMBO J, 2003. **22**(14): p. 3591-3601.

45. Taylor, D. R. and Hooper, N. M., *The low-density lipoprotein receptor-related protein 1 (LRP1) mediates the endocytosis of the cellular prion protein*. *Biochem J*, 2007. **402**(1): p. 17-23.
46. Peters, P. J., et al., *Trafficking of prion proteins through a caveolae-mediated endosomal pathway*. *J Cell Biol*, 2003. **162**(4): p. 703-717.
47. Altmepfen, H. C., et al., *Proteolytic processing of the prion protein in health and disease*. *Am J Neurodegener Dis*, 2012. **1**(1): p. 15-31.
48. Collinge, J., et al., *Prion protein is necessary for normal synaptic function*. *Nature*, 1994. **370**(6487): p. 295-297.
49. Criado, J. R., et al., *Mice devoid of prion protein have cognitive deficits that are rescued by reconstitution of PrP in neurons*. *Neurobiology of Disease*, 2005. **19**(1): p. 255-265.
50. Beraldo, F. H., et al., *Metabotropic glutamate receptors transduce signals for neurite outgrowth after binding of the prion protein to laminin  $\gamma$ 1 chain*. *The FASEB Journal*, 2011. **25**(1): p. 265-279.
51. Santuccione, A., et al., *Prion protein recruits its neuronal receptor NCAM to lipid rafts to activate p59fyn and to enhance neurite outgrowth*. *J Cell Biol*, 2005. **169**(2): p. 341-354.
52. Mitteregger, G., et al., *The Role of the Octarepeat Region in Neuroprotective Function of the Cellular Prion Protein*. *Brain Pathology*, 2007. **17**(2): p. 174-183.
53. Bremer, J., et al., *Axonal prion protein is required for peripheral myelin maintenance*. *Nature Neuroscience*, 2010. **13**: p. 310.
54. Barmada, S., et al., *GFP-tagged prion protein is correctly localized and functionally active in the brains of transgenic mice*. *Neurobiology of Disease*, 2004. **16**(3): p. 527-537.
55. Lima, F. R. S., et al., *Cellular prion protein expression in astrocytes modulates neuronal survival and differentiation*. *Journal of Neurochemistry*, 2007. **103**(6): p. 2164-2176.
56. Bertuchi, F. R., et al., *PrPC displays an essential protective role from oxidative stress in an astrocyte cell line derived from PrPC knockout mice*. *Biochemical and Biophysical Research Communications*, 2012. **418**(1): p. 27-32.
57. Kleene, R., et al., *Prion Protein Regulates Glutamate-Dependent Lactate Transport of Astrocytes*. *The Journal of Neuroscience*, 2007. **27**(45): p. 12331-12340.
58. Brown, D. R., et al., *The cellular prion protein binds copper in vivo*. *Nature*, 1997. **390**(6661): p. 684-687.
59. Gasperini, L., et al., *In Absence of the Cellular Prion Protein, Alterations in Copper Metabolism and Copper-Dependent Oxidase Activity Affect Iron Distribution*. *Frontiers in Neuroscience*, 2016. **10**(437).
60. Watt, N. T., et al., *Prion protein facilitates uptake of zinc into neuronal cells*. *Nature Communications*, 2012. **3**: p. 1134.
61. Giachin, G., et al., *The non-octarepeat copper binding site of the prion protein is a key regulator of prion conversion*. *Scientific Reports*, 2015. **5**: p. 15253.
62. Gasperini, L., et al., *Prion Protein and Copper Cooperatively Protect Neurons by Modulating NMDA Receptor Through S-nitrosylation*. *Antioxidants & Redox Signaling*, 2015. **22**(9): p. 772-784.
63. Aguzzi, A. and O'Connor, T., *Protein aggregation diseases: pathogenicity and therapeutic perspectives*. *Nature Reviews Drug Discovery*, 2010. **9**: p. 237.
64. DeMarco, M. L. and Daggett, V., *From conversion to aggregation: protofibril formation of the prion protein*. *Proc Natl Acad Sci U S A*, 2004. **101**(8): p. 2293-2298.
65. Govaerts, C., et al., *Evidence for assembly of prions with left-handed beta-helices into trimers*. *Proc Natl Acad Sci U S A*, 2004. **101**(22): p. 8342-8347.

- 
66. Cobb, N. J., et al., *Molecular architecture of human prion protein amyloid: a parallel, in-register beta-structure*. Proc Natl Acad Sci U S A, 2007. **104**(48): p. 18946-18951.
  67. Gremer, L., et al., *Fibril structure of amyloid- $\beta$ (1-42) by cryo-electron microscopy*. Science (New York, N.Y.), 2017. **358**(6359): p. 116-119.
  68. Spagnolli, G., et al., *Full Atomistic Model of Prion Structure and Conversion*. bioRxiv, 2018: p. 505271.
  69. Parchi, P., et al., *Genetic influence on the structural variations of the abnormal prion protein*. Proc Natl Acad Sci U S A, 2000. **97**(18): p. 10168-10172.
  70. Friedlander, G., et al., *Protease-Sensitive Scrapie Prion Protein in Aggregates of Heterogeneous Sizes*. Biochemistry, 2002. **41**(42): p. 12868-12875.
  71. Thackray, A. M., Hopkins, L., and Bujdoso, R., *Proteinase K-sensitive disease-associated ovine prion protein revealed by conformation-dependent immunoassay*. Biochem J, 2007. **401**(2): p. 475-483.
  72. Gambetti, P., et al., *A novel human disease with abnormal prion protein sensitive to protease*. Ann Neurol, 2008. **63**(6): p. 697-708.
  73. Owen, J. P., et al., *Use of thermolysin in the diagnosis of prion diseases*. Molecular Biotechnology, 2007. **35**(2): p. 161-170.
  74. Cronier, S., et al., *Detection and characterization of proteinase K-sensitive disease-related prion protein with thermolysin*. Biochem J, 2008. **416**(2): p. 297-305.
  75. Griffith, J. S., *Nature of the Scrapie Agent: Self-replication and Scrapie*. Nature, 1967. **215**(5105): p. 1043-1044.
  76. Prusiner, S. B., *Molecular biology of prion diseases*. Science, 1991. **252**(5012): p. 1515-1522.
  77. Collinge, J., *Prion Diseases of Humans and Animals: Their Causes and Molecular Basis*. Annual Review of Neuroscience, 2001. **24**(1): p. 519-550.
  78. Hope, J., et al., *The major polypeptide of scrapie-associated fibrils (SAF) has the same size, charge distribution and N-terminal protein sequence as predicted for the normal brain protein (PrP)*. The EMBO journal, 1986. **5**(10): p. 2591-2597.
  79. Büeler, H., et al., *Mice devoid of PrP are resistant to scrapie*. Cell, 1993. **73**(7): p. 1339-1347.
  80. Race, R. E., Fadness, L. H., and Chesebro, B., *Characterization of Scrapie Infection in Mouse Neuroblastoma Cells*. Journal of General Virology, 1987. **68**(5): p. 1391-1399.
  81. Legname, G., et al., *Synthetic Mammalian Prions*. Science, 2004. **305**(5684): p. 673-676.
  82. Saborio, G. P., Permanne, B., and Soto, C., *Sensitive detection of pathological prion protein by cyclic amplification of protein misfolding*. Nature, 2001. **411**(6839): p. 810-813.
  83. Castilla, J., et al., *In Vitro Generation of Infectious Scrapie Prions*. Cell, 2005. **121**(2): p. 195-206.
  84. Cohen, F. E., et al., *Structural clues to prion replication*. Science, 1994. **264**(5158): p. 530-531.
  85. Jarrett, J. T. and Lansbury, P. T., Jr., *Seeding "one-dimensional crystallization" of amyloid: A pathogenic mechanism in Alzheimer's disease and scrapie?* Cell, 1993. **73**(6): p. 1055-1058.
  86. Aguzzi, A., Montrasio, F., and Kaeser, P. S., *Prions: health scare and biological challenge*. Nature Reviews Molecular Cell Biology, 2001. **2**(2): p. 118-126.
  87. Pattison, I. H. and Millson, G. C., *Scrapie Produced Experimentally in Goats With Special Reference To the Clinical Syndrome*. Journal of Comparative Pathology and Therapeutics, 1961. **71**: p. 101-IN110.

- 
88. Fraser, H., et al., *Transmission of bovine spongiform encephalopathy and scrapie to mice*. Journal of General Virology, 1992. **73**(8): p. 1891-1897.
  89. Bruce, M., et al., *Transmission of bovine spongiform encephalopathy and scrapie to mice: strain variation and the species barrier*. Philosophical Transactions of the Royal Society of London. Series B: Biological Sciences, 1994. **343**(1306): p. 405-411.
  90. Bessen, R. A. and Marsh, R. F., *Identification of two biologically distinct strains of transmissible mink encephalopathy in hamsters*. Journal of General Virology, 1992. **73**(2): p. 329-334.
  91. Bruce, M. E., *Scrapie strain variation and mutation*. British Medical Bulletin, 1993. **49**(4): p. 822-838.
  92. Fraser, H., *Diversity in the neuropathology of scrapie-like diseases in animals*. British Medical Bulletin, 1993. **49**(4): p. 792-809.
  93. Bruce, M. E., *TSE strain variation*. British Medical Bulletin, 2003. **66**: p. 99-108.
  94. Collinge, J., *Molecular neurology of prion disease*. Journal of Neurology, Neurosurgery & Psychiatry, 2005. **76**(7): p. 906-919.
  95. Moore, R.-A., Vorberg, I., and Priola, S.-A. *Species barriers in prion diseases — brief review*. 2005. Vienna: Springer Vienna.
  96. Bartz, J. C., et al., *Adaptation and Selection of Prion Protein Strain Conformations following Interspecies Transmission of Transmissible Mink Encephalopathy*. Journal of Virology, 2000. **74**(12): p. 5542-5547.
  97. Chen, S. G. and Gambetti, P., *A Journey through the Species Barrier*. Neuron, 2002. **34**(6): p. 854-856.
  98. Vanik, D. L., Surewicz, K. A., and Surewicz, W. K., *Molecular Basis of Barriers for Interspecies Transmissibility of Mammalian Prions*. Molecular Cell, 2004. **14**(1): p. 139-145.
  99. Otero, A., et al., *An Amino Acid Substitution Found in Animals with Low Susceptibility to Prion Diseases Confers a Protective Dominant-Negative Effect in Prion-Infected Transgenic Mice*. Molecular Neurobiology, 2018. **55**(7): p. 6182-6192.
  100. Smith, P. G. and Bradley, R., *Bovine spongiform encephalopathy (BSE) and its epidemiology*. British Medical Bulletin, 2003. **66**(1): p. 185-198.
  101. Wall, B. A., et al., *Evidence for more cost-effective surveillance options for bovine spongiform encephalopathy (BSE) and scrapie in Great Britain*. Euro Surveill, 2017. **22**(32): p. 30594.
  102. Hamir, A. N., et al., *Experimental Transmission of Chronic Wasting Disease Agent from Mule Deer to Cattle by the Intracerebral Route*. Journal of Veterinary Diagnostic Investigation, 2005. **17**(3): p. 276-281.
  103. Marsh, R. F., et al., *Interspecies transmission of chronic wasting disease prions to squirrel monkeys (*Saimiri sciureus*)*. Journal of virology, 2005. **79**(21): p. 13794-13796.
  104. Han, L. and Costello, C. E., *Mass spectrometry of glycans*. Biochemistry (Mosc), 2013. **78**(7): p. 710-720.
  105. Lauc, G., et al., *Complex genetic regulation of protein glycosylation*. Molecular BioSystems, 2010. **6**(2): p. 329-335.
  106. Ohtsubo, K. and Marth, J. D., *Glycosylation in Cellular Mechanisms of Health and Disease*. Cell, 2006. **126**(5): p. 855-867.
  107. Mitra, N., et al., *N-linked oligosaccharides as outfitters for glycoprotein folding, form and function*. Trends in Biochemical Sciences, 2006. **31**(3): p. 156-163.
  108. Hanson, S. R., et al., *The core trisaccharide of an N-linked glycoprotein intrinsically accelerates folding and enhances stability*. Proc Natl Acad Sci U S A, 2009. **106**(9): p. 3131-3136.

- 
109. Sareneva, T., et al., *N-glycosylation of human interferon-gamma: glycans at Asn-25 are critical for protease resistance*. *Biochem J*, 1995. **308** ( Pt 1)(Pt 1): p. 9-14.
  110. Weinbaum, S., Tarbell, J. M., and Damiano, E. R., *The Structure and Function of the Endothelial Glycocalyx Layer*. *Annual Review of Biomedical Engineering*, 2007. **9**(1): p. 121-167.
  111. Varki, A., et al., *Essentials of Glycobiology. 3rd edition*. 2015-2017: Cold Spring Harbor (NY): Cold Spring Harbor Laboratory Press.
  112. Reily, C., et al., *Glycosylation in health and disease*. *Nat Rev Nephrol*, 2019. **15**(6): p. 346-366.
  113. Alberts, B., et al., *Molecular Biology of the Cell. 4th edition*. 2002: New York: Garland Science.
  114. Iozzo, R. V. and Schaefer, L., *Proteoglycan form and function: A comprehensive nomenclature of proteoglycans*. *Matrix Biol*, 2015. **42**: p. 11-55.
  115. Stanley, P., Schachter, H., and Taniguchi, N., *N-Glycans*, in *Essentials of Glycobiology. 2nd edition*, Varki, A., et al., Editors. 2009, Cold Spring Harbor (NY): Cold Spring Harbor Laboratory Press.
  116. Moremen, K. W., Tiemeyer, M., and Nairn, A. V., *Vertebrate protein glycosylation: diversity, synthesis and function*. *Nat Rev Mol Cell Biol*, 2012. **13**(7): p. 448-462.
  117. Bieberich, E., *Synthesis, Processing, and Function of N-glycans in N-glycoproteins*. *Adv Neurobiol*, 2014. **9**: p. 47-70.
  118. Quellhorst, G. J., et al., *Identification of Schizosaccharomyces pombe Prenol as Dolichol-16,17*. *Biochemical and Biophysical Research Communications*, 1998. **244**(2): p. 546-550.
  119. Rip, J. W., et al., *Distribution, metabolism and function of dolichol and polyprenols*. *Progress in Lipid Research*, 1985. **24**(4): p. 269-309.
  120. Burda, P. and Aebi, M., *The dolichol pathway of N-linked glycosylation*. *Biochimica et Biophysica Acta (BBA) - General Subjects*, 1999. **1426**(2): p. 239-257.
  121. Sanyal, S., Frank, C. G., and Menon, A. K., *Distinct flippases translocate glycerophospholipids and oligosaccharide diphosphate dolichols across the endoplasmic reticulum*. *Biochemistry*, 2008. **47**(30): p. 7937-7946.
  122. Ruiz-Canada, C., Kelleher, D. J., and Gilmore, R., *Cotranslational and posttranslational N-glycosylation of polypeptides by distinct mammalian OST isoforms*. *Cell*, 2009. **136**(2): p. 272-283.
  123. Harada, Y., et al., *Oligosaccharyltransferase directly binds to ribosome at a location near the translocon-binding site*. *Proc Natl Acad Sci U S A*, 2009. **106**(17): p. 6945-6949.
  124. Hettkamp, H., Legler, G., and Bause, E., *Purification by affinity chromatography of glucosidase I, an endoplasmic reticulum hydrolase involved in the processing of asparagine-linked oligosaccharides*. *European Journal of Biochemistry*, 1984. **142**(1): p. 85-90.
  125. Brada, D. and Dubach, U. C., *Isolation of a homogeneous glucosidase II from pig kidney microsomes*. *European Journal of Biochemistry*, 1984. **141**(1): p. 149-156.
  126. Caramelo, J. J. and Parodi, A. J., *Getting in and out from calnexin/calreticulin cycles*. *J Biol Chem*, 2008. **283**(16): p. 10221-10225.
  127. Gonzalez, D. S., et al., *Identification, Expression, and Characterization of a cDNA Encoding Human Endoplasmic Reticulum Mannosidase I, the Enzyme That Catalyzes the First Mannose Trimming Step in Mammalian Asn-linked Oligosaccharide Biosynthesis*. *Journal of Biological Chemistry*, 1999. **274**(30): p. 21375-21386.
  128. Oda, Y., et al., *EDEM As an Acceptor of Terminally Misfolded Glycoproteins Released from Calnexin*. *Science*, 2003. **299**(5611): p. 1394-1397.
  129. Stanley, P., *Golgi glycosylation*. *Cold Spring Harb Perspect Biol*, 2011. **3**(4): p. a005199.



130. Geyer, H. and Geyer, R., *Strategies for analysis of glycoprotein glycosylation*. Biochimica et Biophysica Acta (BBA) - Proteins and Proteomics, 2006. **1764**(12): p. 1853-1869.
131. Mariño, K., et al., *A systematic approach to protein glycosylation analysis: a path through the maze*. Nature Chemical Biology, 2010. **6**: p. 713.
132. Prime, S. and Merry, T., *Exoglycosidase Sequencing of N-Linked Glycans by the Reagent Array Analysis Method (RAAM)*, in *Glycoanalysis Protocols*, Hounsell, Elizabeth F., Editor. 1998, Humana Press: Totowa, NJ. p. 53-69.
133. Ali, L., et al., *Structural Identification of O-Linked Oligosaccharides Using Exoglycosidases and MSn Together with UniCarb-DB Fragment Spectra Comparison*. Metabolites, 2012. **2**(4): p. 648-666.
134. Moradian, A., et al., *The top-down, middle-down, and bottom-up mass spectrometry approaches for characterization of histone variants and their post-translational modifications*. PROTEOMICS, 2014. **14**(4-5): p. 489-497.
135. Aebersold, R. and Goodlett, D. R., *Mass Spectrometry in Proteomics*. Chemical Reviews, 2001. **101**(2): p. 269-296.
136. Miah, S., et al., *Advancement of mass spectrometry-based proteomics technologies to explore triple negative breast cancer*. Molecular bioSystems, 2016. **13**(1): p. 42-55.
137. Zhu, Z. and Desaire, H., *Carbohydrates on Proteins: Site-Specific Glycosylation Analysis by Mass Spectrometry*. Annual Review of Analytical Chemistry, 2015. **8**(1): p. 463-483.
138. Wang, X., et al., *A Novel Quantitative Mass Spectrometry Platform for Determining Protein O-GlcNAcylation Dynamics*. Mol Cell Proteomics, 2016. **15**(7): p. 2462-2475.
139. McLachlin, D. T. and Chait, B. T., *Analysis of phosphorylated proteins and peptides by mass spectrometry*. Current Opinion in Chemical Biology, 2001. **5**(5): p. 591-602.
140. Thaysen-Andersen, M., Packer, N. H., and Schulz, B. L., *Maturing Glycoproteomics Technologies Provide Unique Structural Insights into the N-glycoproteome and Its Regulation in Health and Disease*. Mol Cell Proteomics, 2016. **15**(6): p. 1773-1790.
141. Chen, W., Smeekens, J. M., and Wu, R., *Systematic and site-specific analysis of N-sialoglycosylated proteins on the cell surface by integrating click chemistry and MS-based proteomics*. Chem Sci, 2015. **6**(8): p. 4681-4689.
- 142.Unione, L., et al., *Glycoprofile Analysis of an Intact Glycoprotein As Inferred by NMR Spectroscopy*. ACS Central Science, 2019. **5**(9): p. 1554-1561.
143. Cummings, R. D., *Use of lectins in analysis of glycoconjugates*, in *Methods in Enzymology*. 1994, Academic Press. p. 66-86.
144. Cao, L., et al., *Global site-specific analysis of glycoprotein N-glycan processing*. Nature Protocols, 2018. **13**: p. 1196.
145. Tretter, V., Altmann, F., and März, L., *Peptide-N4-(N-acetyl-β-glucosaminyl)asparagine amidase F cannot release glycans with fucose attached α1 → 3 to the asparagine-linked N-acetylglucosamine residue*. European Journal of Biochemistry, 1991. **199**(3): p. 647-652.
146. O'Neill, R. A., *Enzymatic release of oligosaccharides from glycoproteins for chromatographic and electrophoretic analysis*. Journal of Chromatography A, 1996. **720**(1): p. 201-215.
147. Bigge, J. C., et al., *Nonselective and Efficient Fluorescent Labeling of Glycans Using 2-Amino Benzamide and Anthranilic Acid*. Analytical Biochemistry, 1995. **230**(2): p. 229-238.
148. Anumula, K. R. and Dhume, S. T., *High resolution and high sensitivity methods for oligosaccharide mapping and characterization by normal phase high performance liquid chromatography following derivatization with highly fluorescent anthranilic acid*. Glycobiology, 1998. **8**(7): p. 685-694.

149. Takegawa, Y., et al., *Separation of isomeric 2-aminopyridine derivatized N-glycans and N-glycopeptides of human serum immunoglobulin G by using a zwitterionic type of hydrophilic-interaction chromatography*. Journal of Chromatography A, 2006. **1113**(1): p. 177-181.
150. Klapoetke, S., et al., *The evaluation of a novel approach for the profiling and identification of N-linked glycan with a procainamide tag by HPLC with fluorescent and mass spectrometric detection*. Journal of Pharmaceutical and Biomedical Analysis, 2010. **53**(3): p. 315-324.
151. Callewaert, N., et al., *Ultrasensitive profiling and sequencing of N-linked oligosaccharides using standard DNA-sequencing equipment*. Glycobiology, 2001. **11**(4): p. 275-281.
152. Haraguchi, T., et al., *Asparagine-linked glycosylation of the scrapie and cellular prion proteins*. Archives of Biochemistry and Biophysics, 1989. **274**(1): p. 1-13.
153. Rogers, M., et al., *Intracellular accumulation of the cellular prion protein after mutagenesis of its Asn linked glycosylation sites*. Glycobiology, 1990. **1**(1): p. 101-109.
154. DeArmond, S. J., et al., *Selective Neuronal Targeting in Prion Disease*. Neuron, 1997. **19**(6): p. 1337-1348.
155. Korth, C., Kaneko, K., and Prusiner, S. B., *Expression of unglycosylated mutated prion protein facilitates PrP<sup>Sc</sup> formation in neuroblastoma cells infected with different prion strains*. Journal of General Virology, 2000. **81**(10): p. 2555-2563.
156. Neuendorf, E., et al., *Glycosylation Deficiency at Either One of the Two Glycan Attachment Sites of Cellular Prion Protein Preserves Susceptibility to Bovine Spongiform Encephalopathy and Scrapie Infections*. Journal of Biological Chemistry, 2004. **279**(51): p. 53306-53316.
157. Capellari, S., et al., *The Thr183Ala Mutation, Not the Loss of the First Glycosylation Site, Alters the Physical Properties of the Prion Protein*. Journal of Alzheimer's disease : JAD, 2000. **2**: p. 27-35.
158. Cancellotti, E., et al., *Altered Glycosylated PrP Proteins Can Have Different Neuronal Trafficking in Brain but Do Not Acquire Scrapie-like Properties*. Journal of Biological Chemistry, 2005. **280**(52): p. 42909-42918.
159. Cancellotti, E., et al., *The role of host PrP in Transmissible Spongiform Encephalopathies*. Biochimica et Biophysica Acta (BBA) - Molecular Basis of Disease, 2007. **1772**(6): p. 673-680.
160. Endo, T., et al., *Diversity of oligosaccharide structures linked to asparagines of the scrapie prion protein*. Biochemistry, 1989. **28**(21): p. 8380-8388.
161. Rudd, P. M., et al., *Glycosylation differences between the normal and pathogenic prion protein isoforms*. Proc Natl Acad Sci U S A, 1999. **96**(23): p. 13044-13049.
162. Stimson, E., et al., *Site-Specific Characterization of the N-Linked Glycans of Murine Prion Protein by High-Performance Liquid Chromatography/Electrospray Mass Spectrometry and Exoglycosidase Digestions*. Biochemistry, 1999. **38**(15): p. 4885-4895.
163. Baskakov, I. V. and Katorcha, E., *Multifaceted Role of Sialylation in Prion Diseases*. Frontiers in Neuroscience, 2016. **10**(358).
164. Varki, A. and Gagneux, P., *Multifarious roles of sialic acids in immunity*. Ann N Y Acad Sci, 2012. **1253**(1): p. 16-36.
165. Suzuki, A., *Genetic basis for the lack of N-glycolylneuraminic acid expression in human tissues and its implication to human evolution*. Proc Jpn Acad Ser B Phys Biol Sci, 2006. **82**(3): p. 93-103.
166. Davies, L. R. and Varki, A., *Why Is N-Glycolylneuraminic Acid Rare in the Vertebrate Brain?* Top Curr Chem, 2015. **366**: p. 31-54.

- 
167. Rösner, H., *Gangliosides, sialoglycoproteins and acetylcholinesterase of the developing mouse brain*. Wilhelm Roux's archives of developmental biology, 1977. **183**(4): p. 325-335.
  168. Requena, J. R. and Wille, H., *The structure of the infectious prion protein*. Prion, 2014. **8**(1): p. 60-66.
  169. Katorcha, E., et al., *Sialylation of Prion Protein Controls the Rate of Prion Amplification, the Cross-Species Barrier, the Ratio of PrP<sup>Sc</sup> Glycoform and Prion Infectivity*. PLoS Pathog, 2014. **10**(9): p. e1004366.
  170. Katorcha, E., et al., *Sialylation of the prion protein glycans controls prion replication rate and glycoform ratio*. Scientific Reports, 2015. **5**: p. 16912.
  171. Varki, A., *Sialic acids in human health and disease*. Trends in Molecular Medicine, 2008. **14**(8): p. 351-360.
  172. Varki, A., *Letter to the Glyco-Forum: Since there are PAMPs and DAMPs, there must be SAMPs? Glycan "self-associated molecular patterns" dampen innate immunity, but pathogens can mimic them*. Glycobiology, 2011. **21**(9): p. 1121-1124.
  173. Linnartz-Gerlach, B., et al., *Sialylation of neurites inhibits complement-mediated macrophage removal in a human macrophage-neuron Co-Culture System*. Glia, 2016. **64**(1): p. 35-47.
  174. Linnartz, B., et al., *Sialic Acid on the Neuronal Glycocalyx Prevents Complement C1 Binding and Complement Receptor-3-Mediated Removal by Microglia*. The Journal of Neuroscience, 2012. **32**(3): p. 946-952.
  175. Katorcha, E., et al., *Reversible off and on switching of prion infectivity via removing and reinstalling prion sialylation*. Scientific Reports, 2016. **6**: p. 33119.
  176. Srivastava, S., et al., *Sialylation Controls Prion Fate in Vivo*. Journal of Biological Chemistry, 2017. **292**(6): p. 2359-2368.
  177. Bessen, R. A., et al., *Non-genetic propagation of strain-specific properties of scrapie prion protein*. Nature, 1995. **375**(6533): p. 698-700.
  178. Piro, J. R., et al., *Prion protein glycosylation is not required for strain-specific neurotropism*. Journal of virology, 2009. **83**(11): p. 5321-5328.
  179. Cancellotti, E., et al., *Post-translational changes to PrP alter transmissible spongiform encephalopathy strain properties*. EMBO J, 2013. **32**(5): p. 756-769.
  180. Baskakov, I. V., Katorcha, E., and Makarava, N., *Prion Strain-Specific Structure and Pathology: A View from the Perspective of Glycobiology*. Viruses, 2018. **10**(12): p. 723.
  181. Vliegenthart, J. F. G., *The impact of defining glycan structures*. Perspectives in Science, 2017. **11**: p. 3-10.
  182. D'Castro, L., et al., *Isolation of Proteinase K-Sensitive Prions Using Pronase E and Phosphotungstic Acid*. PLOS ONE, 2010. **5**(12): p. e15679.
  183. Wenborn, A., et al., *A novel and rapid method for obtaining high titre intact prion strains from mammalian brain*. Scientific Reports, 2015. **5**: p. 10062.
  184. Shevchenko, A., et al., *Mass Spectrometric Sequencing of Proteins from Silver-Stained Polyacrylamide Gels*. Analytical Chemistry, 1996. **68**(5): p. 850-858.
  185. Shevchenko, A., et al., *In-gel digestion for mass spectrometric characterization of proteins and proteomes*. Nature Protocols, 2006. **1**(6): p. 2856-2860.
  186. Gundry, R. L., et al., *Preparation of proteins and peptides for mass spectrometry analysis in a bottom-up proteomics workflow*. Curr Protoc Mol Biol, 2009. **Chapter 10**: p. Unit10.25-Unit10.25.
  187. Suttapitugsakul, S., et al., *Evaluation and optimization of reduction and alkylation methods to maximize peptide identification with MS-based proteomics*. Molecular bioSystems, 2017. **13**(12): p. 2574-2582.

- 
188. *In-Solution Trypsin Digestion*. 2018; Available from: <http://www.kumc.edu/mspc/protocols/in-solution-trypsin-digestion.html>.
189. Wilkins, M. R., et al., *Detailed peptide characterization using PEPTIDEMASS – a World-Wide-Web-accessible tool*. ELECTROPHORESIS, 1997. **18**(3-4): p. 403-408.
190. Artimo, P., et al., *ExpASY: SIB bioinformatics resource portal*. Nucleic Acids Research, 2012. **40**(W1): p. W597-W603.
191. Cox, J. and Mann, M., *MaxQuant enables high peptide identification rates, individualized p.p.b.-range mass accuracies and proteome-wide protein quantification*. Nature Biotechnology, 2008. **26**(12): p. 1367-1372.
192. Carr, S. A., Huddleston, M. J., and Bean, M. F., *Selective identification and differentiation of N- and O-linked oligosaccharides in glycoproteins by liquid chromatography-mass spectrometry*. Protein Sci, 1993. **2**(2): p. 183-196.
193. Ceroni, A., et al., *GlycoWorkbench: A Tool for the Computer-Assisted Annotation of Mass Spectra of Glycans*. Journal of Proteome Research, 2008. **7**(4): p. 1650-1659.
194. Cooper, C. A., Gasteiger, E., and Packer, N. H., *GlycoMod – A software tool for determining glycosylation compositions from mass spectrometric data*. PROTEOMICS, 2001. **1**(2): p. 340-349.
195. Alocci, D., et al., *GlyConnect: Glycoproteomics Goes Visual, Interactive, and Analytical*. Journal of Proteome Research, 2019. **18**(2): p. 664-677.
196. Safar, J., et al., *Eight prion strains have PrPSc molecules with different conformations*. Nature Medicine, 1998. **4**(10): p. 1157-1165.
197. Somerville, R. A., Merz, P. A., and Carp, R. I., *Partial Copurification of Scrapie-Associated Fibrils and Scrapie Infectivity*. Intervirology, 1986. **25**(1): p. 48-55.
198. Bossers, A., et al., *Scrapie susceptibility-linked polymorphisms modulate the in vitro conversion of sheep prion protein to protease-resistant forms*. Proc Natl Acad Sci U S A, 1997. **94**(10): p. 4931-4936.
199. Choi, Y.-G., et al., *Semi-purification procedures of prions from a prion-infected brain using sucrose has no influence on the nonenzymatic glycation of the disease-associated prion isoform*, in *Biological Chemistry*. 2016. p. 125.
200. Bolton, D., McKinley, M., and Prusiner, S., *Identification of a protein that purifies with the scrapie prion*. Science, 1982. **218**(4579): p. 1309-1311.
201. McKinley, M. P., Bolton, D. C., and Prusiner, S. B., *A protease-resistant protein is a structural component of the Scrapie prion*. Cell, 1983. **35**(1): p. 57-62.
202. Bolton, D. C. and Bendheim, P. E., *Purification of Scrapie Agents: How Far Have We Come?*, in *Transmissible Spongiform Encephalopathies: Scrapie, BSE and Related Human Disorders*, Chesebro, Bruce W., Editor. 1991, Springer Berlin Heidelberg: Berlin, Heidelberg. p. 39-55.
203. Handa-Narumi, M., et al., *Branched Sialylated N-glycans Are Accumulated in Brain Synaptosomes and Interact with Siglec-H*. Cell Structure and Function, 2018. **43**(2): p. 141-152.
204. Ishii, A., et al., *Developmental changes in the expression of glycogenes and the content of N-glycans in the mouse cerebral cortex*. Glycobiology, 2006. **17**(3): p. 261-276.
205. Torii, T., et al., *Determination of major sialylated N-glycans and identification of branched sialylated N-glycans that dynamically change their content during development in the mouse cerebral cortex*. Glycoconjugate Journal, 2014. **31**(9): p. 671-683.
206. Kozlik, P., Goldman, R., and Sanda, M., *Hydrophilic interaction liquid chromatography in the separation of glycopeptides and their isomers*. Anal Bioanal Chem, 2018. **410**(20): p. 5001-5008.

- 
207. Sato, C. and Kitajima, K., *Disialic, oligosialic and polysialic acids: distribution, functions and related disease*. The Journal of Biochemistry, 2013. **154**(2): p. 115-136.
  208. Morales, R., *Prion strains in mammals: Different conformations leading to disease*. PLoS Pathog, 2017. **13**(7): p. e1006323-e1006323.
  209. Prusiner, S. B., et al., *Further purification and characterization of scrapie prions*. Biochemistry, 1982. **21**(26): p. 6942-6950.
  210. Gabizon, R., et al., *Immunoaffinity purification and neutralization of scrapie prion infectivity*. Proc Natl Acad Sci U S A, 1988. **85**(18): p. 6617-6621.
  211. Biasini, E., et al., *Immunopurification of Pathological Prion Protein Aggregates*. PLOS ONE, 2009. **4**(11): p. e7816.
  212. Diringer, H., et al., *Towards Purification of the Scrapie Agent*. European Journal of Biochemistry, 1983. **134**(3): p. 555-560.
  213. Diringer, H., et al., *Scrapie infectivity, fibrils and low molecular weight protein*. Nature, 1983. **306**(5942): p. 476-478.
  214. Polymenidou, M., et al., *A short purification process for quantitative isolation of PrP<sup>Sc</sup> from naturally occurring and experimental transmissible spongiform encephalopathies*. BMC Infect Dis, 2002. **2**: p. 23-23.
  215. Giorgi, A., et al., *Proteomic profiling of PrP<sup>27-30</sup>-enriched preparations extracted from the brain of hamsters with experimental scrapie*. PROTEOMICS, 2009. **9**(15): p. 3802-3814.
  216. Moore, R. A., et al., *Comparative profiling of highly enriched 22L and Chandler mouse scrapie prion protein preparations*. Proteomics, 2010. **10**(15): p. 2858-2869.
  217. Moore, R. A., et al., *Identification and removal of proteins that co-purify with infectious prion protein improves the analysis of its secondary structure*. Proteomics, 2011. **11**(19): p. 3853-3865.
  218. Solassol, J., Crozet, C., and Lehmann, S., *Prion propagation in cultured cells*. British Medical Bulletin, 2003. **66**(1): p. 87-97.
  219. Bosque, P. J. and Prusiner, S. B., *Cultured Cell Sublines Highly Susceptible to Prion Infection*. Journal of Virology, 2000. **74**(9): p. 4377-4386.
  220. Caughey, B., et al., *Prion protein biosynthesis in scrapie-infected and uninfected neuroblastoma cells*. Journal of virology, 1989. **63**(1): p. 175-181.
  221. Taraboulos, A., et al., *Synthesis and trafficking of prion proteins in cultured cells*. Molecular Biology of the Cell, 1992. **3**(8): p. 851-863.
  222. Bedecs, K., *Cell Culture Models to Unravel Prion Protein Function and Aberrancies in Prion Diseases*, in *Prion Protein Protocols*, Hill, Andrew F., Editor. 2008, Humana Press: Totowa, NJ. p. 1-20.
  223. Brown, P., *Drug therapy in human and experimental transmissible spongiform encephalopathy*. Neurology, 2002. **58**(12): p. 1720-1725.
  224. Petkova, A. T., et al., *Self-Propagating, Molecular-Level Polymorphism in Alzheimer's  $\beta$ -Amyloid Fibrils*. Science, 2005. **307**(5707): p. 262-265.
  225. Sanders, D. W., et al., *Distinct tau prion strains propagate in cells and mice and define different tauopathies*. Neuron, 2014. **82**(6): p. 1271-1288.
  226. Guo, J. L., et al., *Distinct  $\alpha$ -synuclein strains differentially promote tau inclusions in neurons*. Cell, 2013. **154**(1): p. 103-117.
  227. FINNE, J., et al., *The Disialosyl Group of Glycoproteins*. European Journal of Biochemistry, 1977. **77**(2): p. 319-323.
  228. Inoue, S. and Iwasaki, M., *Isolation of a novel glycoprotein from the eggs of rainbow trout: Occurrence of disialosyl groups on all carbohydrate chains*. Biochemical and Biophysical Research Communications, 1978. **83**(3): p. 1018-1023.

- 
229. Sato, C., et al., *Frequent Occurrence of Pre-existing  $\alpha 2 \rightarrow 8$ -Linked Disialic and Oligosialic Acids with Chain Lengths Up to 7 Sia Residues in Mammalian Brain Glycoproteins: prevalence revealed by highly sensitive chemical methods and anti-di-, oligo-, and poly-sia antibodies specific for defined chain lengths*. Journal of Biological Chemistry, 2000. **275**(20): p. 15422-15431.
230. Finne, J., *Occurrence of unique polysialosyl carbohydrate units in glycoproteins of developing brain*. Journal of Biological Chemistry, 1982. **257**(20): p. 11966-11970.
231. Slapšak, U., et al., *The N Terminus of the Prion Protein Mediates Functional Interactions with the Neuronal Cell Adhesion Molecule (NCAM) Fibronectin Domain*. Journal of Biological Chemistry, 2016. **291**(42): p. 21857-21868.
232. Mehrabian, M., Hildebrandt, H., and Schmitt-Ulms, G., *NCAM1 Polysialylation: The Prion Protein's Elusive Reason for Being?* ASN Neuro, 2016. **8**(6): p. 1759091416679074.
233. Ong, E., et al., *Developmental regulation of polysialic acid synthesis in mouse directed by two polysialyltransferases, PST and STX*. Glycobiology, 1998. **8**(4): p. 415-424.
234. Morales, R., Abid, K., and Soto, C., *The prion strain phenomenon: molecular basis and unprecedented features*. Biochim Biophys Acta, 2007. **1772**(6): p. 681-691.
235. Fraser, H. and Dickinson, A. G., *Scrapie in mice: Agent-strain differences in the distribution and intensity of grey matter vacuolation*. Journal of Comparative Pathology, 1973. **83**(1): p. 29-40.
236. Carp, R. I., et al., *Genetic Control of Scrapie: Incubation Period and Plaque Formation in I Mice*. Journal of General Virology, 1987. **68**(2): p. 401-407.
237. Baylis, M. and Goldmann, W., *The Genetics of Scrapie in Sheep and Goats*. Current Molecular Medicine, 2004. **4**(4): p. 385-396.
238. Parchi, P., et al., *Classification of sporadic Creutzfeldt-Jakob disease based on molecular and phenotypic analysis of 300 subjects*. Ann Neurol, 1999. **46**(2): p. 224-233.
239. Wiseman, F. K., et al., *The glycosylation status of PrPC is a key factor in determining transmissible spongiform encephalopathy transmission between species*. Journal of virology, 2015. **89**(9): p. 4738-4747.
240. Cancellotti, E., et al., *Glycosylation of PrPC determines timing of neuroinvasion and targeting in the brain following transmissible spongiform encephalopathy infection by a peripheral route*. Journal of virology, 2010. **84**(7): p. 3464-3475.
241. Moudjou, M., et al., *Glycoform-independent prion conversion by highly efficient, cell-based, protein misfolding cyclic amplification*. Scientific reports, 2016. **6**: p. 29116-29116.
242. Camacho, M. V., et al., *Role of prion protein glycosylation in replication of human prions by protein misfolding cyclic amplification*. Laboratory Investigation, 2019. **99**(11): p. 1741-1748.
243. Tuzi, N. L., et al., *Host PrP glycosylation: a major factor determining the outcome of prion infection*. PLoS Biol, 2008. **6**(4): p. e100-e100.
244. Nishina, K. A., et al., *The Stoichiometry of Host PrPC Glycoforms Modulates the Efficiency of PrPSc Formation in Vitro*. Biochemistry, 2006. **45**(47): p. 14129-14139.
245. Scott, H. and Panin, V. M., *N-glycosylation in regulation of the nervous system*. Adv Neurobiol, 2014. **9**: p. 367-394.
246. Beringue, V., et al., *Regional heterogeneity of cellular prion protein isoforms in the mouse brain*. Brain, 2003. **126**(9): p. 2065-2073.